AD-A042 769 RADIATION RESEARCH ASSOCIATES INC FORT WORTH TEX F/G 4/1
MONTE CARLO STUDIES ON THE TIME-DEPENDENT TRANSPORT OF OPTICAL --ETC(U)
MAR 77 D G COLLINS, M B WELLS F08606-74-C-0011
UNCLASSIFIED RRA-T7608-VOL-2 AFTAC-TR-77-6-VOL-2 NL

1 OF 2
ADA042 769

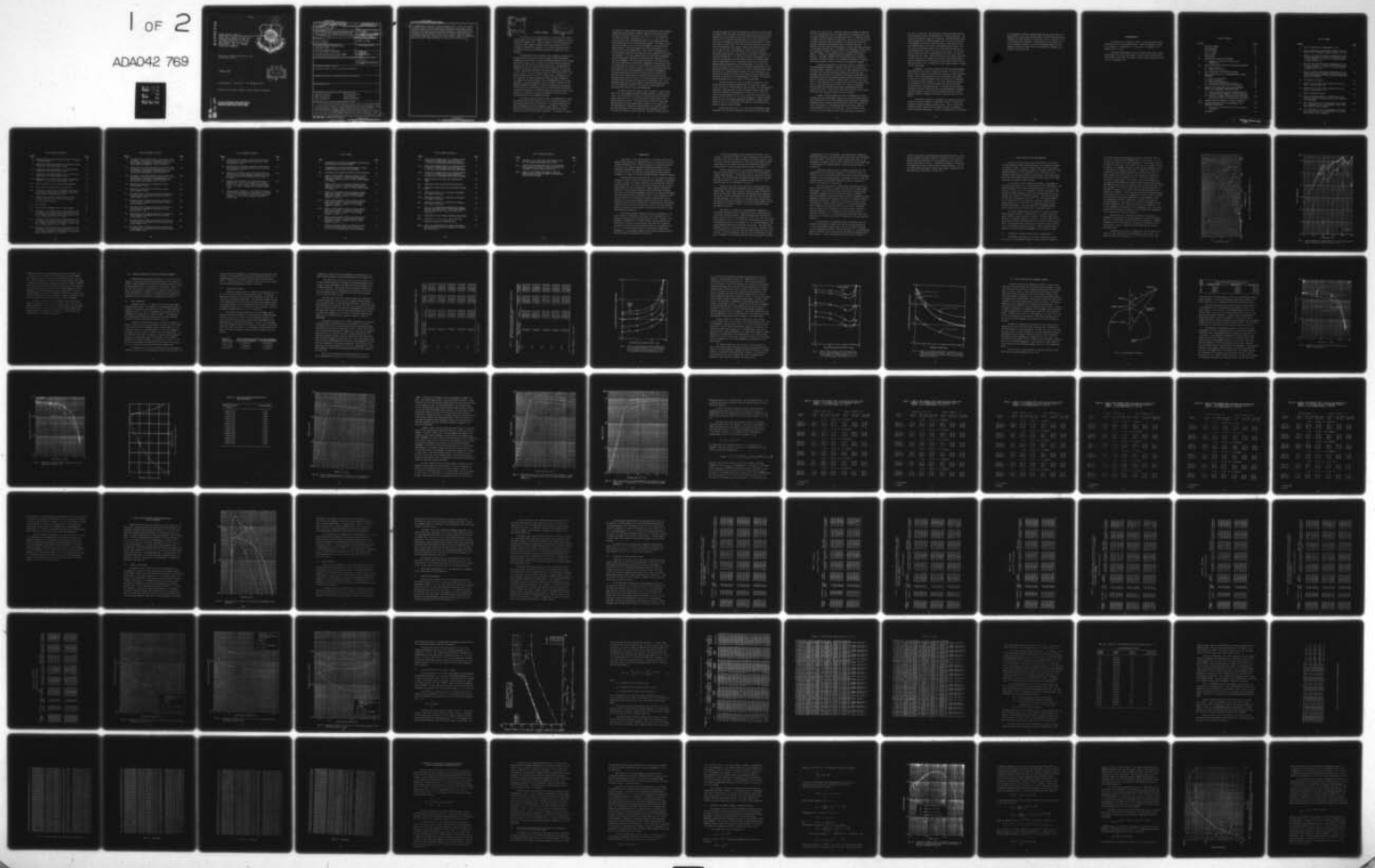

12

B.S.

AFTAC-TR-77-6, VOL II

MONTE CARLO STUDIES ON THE TIME-DEPENDENT TRANSPORT OF OPTICAL AND INFRARED RADIATION IN THE ATMOSPHERE: VOL. II, THERMAL RADIATION TRANSPORT

Radiation Research Associates, Inc.
Fort Worth, Texas

VI AD-E010 801L

1 MARCH 1977

Final Report, 1 July 1975 - 30 September 1976

Approved for public release; distribution unlimited.

AIR FORCE TECHNICAL APPLICATIONS CENTER
HEADQUARTERS UNITED STATES AIR FORCE
PATRICK AIR FORCE BASE, FLORIDA 32925

UNCLASSIFIED

SECURITY CLASSIFICATION OF THIS PAGE (When Data Entered)

REPORT DOCUMENTATION PAGE

READ INSTRUCTIONS BEFORE COMPLETING FORM

1. REPORT NUMBER: AFTAC-TR-77-6 Vol II	2. GOVT ACCESSION NO.
3. RECIPIENT'S CATALOG NUMBER	
4. TITLE (and Subtitle): MONTE CARLO STUDIES ON THE TIME-DEPENDENT TRANSPORT OF OPTICAL AND INFRARED RADIATION IN THE ATMOSPHERE, Vol II. Thermal Radiation Transport.	5. TYPE OF REPORT & PERIOD COVERED: Final Report. 1 July 1975 — 30 September 1976.
	6. PERFORMING ORG. REPORT NUMBER: RRA-T7608, Vol II
7. AUTHOR(s): Dave G. Collins, Michael B. Wells	8. CONTRACT OR GRANT NUMBER(s): F08606-74-C-0011
9. PERFORMING ORGANIZATION NAME AND ADDRESS: RADIATION RESEARCH ASSOCIATES, INC. 3550 Hulen Street Fort Worth, Texas 76107	10. PROGRAM ELEMENT, PROJECT, TASK AREA & WORK UNIT NUMBERS
11. CONTROLLING OFFICE NAME AND ADDRESS: AIR FORCE TECHNICAL APPLICATIONS CENTER Patrick Air Force Base, Florida 32925	12. REPORT DATE: 1 March 1977
	13. NUMBER OF PAGES: 143
14. MONITORING AGENCY NAME & ADDRESS (if different from Controlling Office)	15. SECURITY CLASS. (of this report): Unclassified
	15a. DECLASSIFICATION/DOWNGRADING SCHEDULE

16. DISTRIBUTION STATEMENT (of this Report)

Approved for public release, distribution unlimited.

17. DISTRIBUTION STATEMENT (of the abstract entered in Block 20, if different from Report)

18. SUPPLEMENTARY NOTES

19. KEY WORDS (Continue on reverse side if necessary and identify by block number)

Monte Carlo methods	Infrared absorption
Radiation transport	Mie scattering
Cloud transmission	Rayleigh scattering
Model atmospheres	Optical radiation

20. ABSTRACT (Continue on reverse side if necessary and identify by block number)

This report describes modifications that were made to the POLO procedures to treat infrared absorption by the gaseous molecules in the atmosphere. Also described are the results of studies performed with the POLO procedure to compute time-dependent scattered light fluxes at satellite receivers for 1) 0.4278-, 0.75-, and 1.07-μm wavelength anisotropic point sources; 2) 0.4278-, 0.5-, 0.6-, 0.75-, and 1.07-μm wavelength point isotropic sources in a 40-km meteorological range atmosphere; 3) point isotropic sources emitting in the → next page.

DD FORM 1 JAN 73 1473 EDITION OF 1 NOV 65 IS OBSOLETE

294300

UNCLASSIFIED

SECURITY CLASSIFICATION OF THIS PAGE (When Data Entered)

cont

2.7-μm wavelength band; and 4) point isotropic 0.4278-, 0.75-, and 1.07-μm wavelength sources in model atmospheres containing a cloud layer. Three computer codes are described which were developed for convoluting the POLO-calculated wavelength- and time-dependent atmospheric scattering data with wavelength- and time-dependent source data for thermal radiation sources. A calculational method is described that can be used to compute the Legendre polynomial coefficients required in discrete ordinates codes for defining the phase function for light scattering by aerosols and cloud particles.

EXECUTIVE SUMMARY

This report is the second volume of a two-volume final report prepared under Contract No. F08606-74-C-0011 for the period 1 July 1975 through 30 September 1976. The work reported on involved making modifications to the computer programs previously developed for use in studying the atmospheric transport of the thermal radiation produced by nuclear sources and in performing parametric studies with these programs.

The POLO Monte Carlo procedure, which computes the transport of thermal radiation from point sources through an altitude-dependent atmosphere, was modified to utilize the gaseous absorption cross section data for CO_2, H_2O, O_3, N_2O, CO, CH_4, and O_2 that had been compiled by McClatchey at the Air Force Geophysics Laboratory. The AFGL gaseous absorption cross section data are available on magnetic tape for use in POLO. The gaseous absorption cross section data have a resolution of $\Delta\nu = 20$ cm^{-1} at 5 cm^{-1} spacing between 10 cm^{-1} and 13155 cm^{-1}. The modified POLO procedure was used to compute direct transmission data at a satellite for sources positioned within two model atmospheres for comparison with data computed with the LOWTRAN3 code for the same atmosphere. The good comparison obtained between the results of the POLO and LOWTRAN calculations for the two different model atmospheres verified that the calculational method used in POLO properly accounts for gaseous absorption. In addition, POLO can be used to compute transmissions less than 0.001, which is the smallest value that can be computed with use of the LOWTRAN3 procedure.

The POLO procedure was used to study the transmission of infrared radiation from point isotropic sources to satellite positions for wavelengths between 2.6525 and 3.0030 μm. The gaseous absorption in that wavelength band is due principally to H_2O and CO_2. The transmission calculations were made with the POLO procedure for both a tropical and a mid-latitude summer atmosphere. The satellite altitude

was taken to be 35800 km and detectors were positioned at polar position angles (polar angle between a radial through the source and a radial through the satellite's position) of 0, 30, 60, 78, and 82 degrees. The source altitudes considered were 0.1, 0.5, 2, 5, and 10 km. The point isotropic source strength was taken to be one photon uniformly distributed across the source wavelength interval. The detector filter function was taken to be 1.0 for all wavelengths in the source wavelength interval. From the results of the POLO calculations, it was found that for source heights above 3 km the direct transmission for the mid-latitude atmosphere was higher than that computed for the tropical atmosphere. For source heights below 3 km the direct transmission for the mid-latitude atmosphere was less than that computed for the tropical atmosphere. When the ground albedo was 0.0, the fraction of the total transmittance contributed by atmospheric scattering was found to increase with an increase in the satellite polar position angle and with a decrease in the source altitude. When the ground albedo was 0.8, the fraction of the total transmittance contributed by atmospheric scattering and ground reflection decreases with an increase in the satellite polar position angle for angles up to about 65° and then increases with a further increase in the satellite polar position angle. The POLO calculations show, for point sources emitting in the 2.7 μm wavelength band, that the air-scattered and ground-reflected radiation can be an important component of the radiation field measured by satellite-borne sensors in that wavelength band.

The POLO procedure was used to study the effect of source anisotropy on the time-dependent thermal radiation signal at satellite positions. The calculations were run for a satellite altitude of 20187 km, source altitudes of 0.5, 3, and 10 km and for several receiver look angles between 0° and 90°. The sources were positioned in model atmospheres having sea-level meteorological ranges of 3, 10, and 25 km. The time-dependent transmission data generated with the POLO procedure was convoluted with source data generated with the RADFLO code for a 2-KT event and detector response data for a wide-band silicon detector.

The POLY procedure was used in performing the convolution calculations. The times at which the power is one-half and one-tenth of that at first maximum for the unattenuated source power time distribution was determined to be 51.72 microseconds and 39.09 microseconds, respectively. The effect of atmospheric scattering and ground reflection is to shift these times to later times. Not only did the anisotropy of the source affect the magnitude of the optical signal at the detector position, but the time at which first maximum is reached was also shifted to later times when the source was peaked in the backward direction. The source anisotrophy has a small effect on the times of one-half and one-tenth maximum power. For small look angles, the peaking of the source in the backward direction shifts the time of one-half maximum power by approximately 0.85 microseconds and the time of one-tenth maximum power by approximately 0.52 microseconds. For the 90° look angle, the average shift in the time of one-half maximum power is 2.66 microseconds and the average shift in the time of one-tenth first maximum power is 1.13 microseconds. However, for those cases where the source was at 500 meters altitude, the shift in time of one-half maximum power is as much as 7.48 microseconds and the shift in the time of one-tenth maximum power is as much as 3.78 microseconds.

The POLO procedure was used to extend the atmospheric transmission data base previously generated for meteorological ranges of 3, 10, and 25 km to a meteorolgoical range of 40 km. The time-dependent atmospheric scattering data for the 40-km meteorological range atmosphere was computed for wavelengths of 0.4278, 0.5, 0.6, 0.75, and 1.07 μm, source altitudes of 0.1, 0.5, 3, and 10 km and receiver look angles of 0, 30, 45, 60, 70, 75, 80, and 90 degrees. Curve-fit coefficients for use in the TMTAU program were generated for ground albedo values of 0.0, 0.2, 0.5, and 0.8. The curve-fit coefficient data are stored on Tape No. 001706 at AFTAC.

The POLO data for the 3-, 10-, and 25-km meteorological range atmosphere were previously computed for only three source wavelengths,

0.4278, 0.75, and 1.07 μm. A procedure denoted as POLICE was developed for use in generating curve-fit coefficients for wavelengths other than the three wavelengths used in the POLO calculations. A modified version of TMTAU, denoted as TMTRF01 was developed to use curve-fit coefficients for more than three source wavelengths in evaluating the convolution integral giving the time-dependent power at receiver positions. In addition, the POLY procedure was modified to accept source data generated by the RADFLO procedure and to interpolate the atmospheric transport data over wavelength to obtain transport data at the wavelengths used in RADFLO to compute the wavelength and time dependence of the source emission. The TMTAU, TMTRF01, and POLY procedures were checked out against an analytic solution of the convolution integral to illustrate that these procedures correctly evaluate the convolution integral.

A study was performed with the POLO procedure to determine if the time-dependent atmospheric transport data for a given satellite altitude could be converted to give data for other satellite altitudes. The results of the POLO calculations showed that direct and time-dependent scattered fluxes for satellite altitudes between 20186.8 km and 93621.626 km could be obtained from data previously generated with POLO for a satellite altitude of 35800 km with an error of less than 1.0%. It was found that the correction factors for converting the POLO data for a satellite altitude of 35800 km to satellite altitudes between 20186.8 km and 93621.626km varied significantly with the receiver look angle. There was no significant variation in the correction factor for a given look angle with source height.

A number of POLO problems were run to investigate the effect of clouds on the time-dependent response at a satellite-borne receiver. POLO problems were run for 10-km meteorological range Haze C atmosphere containing either a 20-mean-free-path-thick altostratus cloud between 3 and 4 km altitude or a 14-mean-free-path-thick stratus cloud at altitudes between 0.5 and 1.0 km altitude. Point isotropic 0.4278, 0.75, and 1.07 μm wavelength sources were positioned at altitudes of

0.1, 0.5, 3, and 10 km. The clouds were treated as scattering media and the ground surface was considered to be a Lambert reflector. The satellite altitude was taken to be 35800 km. The POLO-generated data were convoluted with a RADFLO-generated source term for a 2-KT event to investigate the effect of the cloud layer on the times at which first maximum power and one-tenth first maximum power occurs. When the source is positioned under a cloud layer, the retarded time of first maximum power tends to increase with look angle. The retarded time at which one-tenth of first maximum power occurs also tends to increase with look angle. When the source is above either cloud layer at 10-km altitude, the retarded time at which first maximum occurs tends to decrease with an increase in the look angle and the time at which one-tenth of first maximum power occurs remains nearly a constant for all look angles.

Attempts to use POLO to compute the time- and angle-dependent distributions of the light escaping from the top of a cloud located above a point isotropic source resulted in data with large statistical errors. These large statistical errors are believed to be caused by the use of a point-estimating function that has an R^{-2} dependence on the source-receiver distance R. The large statistical variation in the POLO data tend to become insignificant when the receivers are positioned at satellite altitude. An effort has been initialed to develop a version of POLO that uses a surface-receiver estimating function instead of a point-receiver estimating function to determine the radiation intensity at receiver location at the top of the cloud.

A study was initiated to investigate the possible application of discrete ordinates methods of radiation transport to study time-dependent radiation transport through clouds. The use of discrete ordinates methods requires that the phase function be expanded in terms of Legendre polynomials. A method for computing the coefficients

for the Legendre polynomial expansion from the use of Mie theory was developed but it was found that the number of coefficients required to represent the phase function is on the order of $2\alpha + 2$ where $\alpha = 2\pi r/\lambda$ is the aerosol size parameter. Clouds typically have aerosols up to 20 to 30 microns in radius. For 0.5 μm wavelength light, the size parameter could be as large as 375, thus requiring a Legendre polynomial of the order of 752.

ACKNOWLEDGMENTS

In addition to the authors, a number of other RRA staff members contributed to the work described herein. These staff members include R. B. Livesay, J. K. Warkentin, L. G. Mooney, W. G. Blättner, J. M. Newell, and J. H. Price.

A special acknowledgment is given to Major Robert Wiley, Captain George Radke, and Captain James Lange of the Air Force Technical Applications Center, who served as contract monitors during the period 1 July 1975 to 30 September 1976.

TABLE OF CONTENTS

LIST OF FIGURES

LIST OF FIGURES (Continued

LIST OF FIGURES (Continued)

LIST OF FIGURES (Continued)

LIST OF TABLES

LIST OF TABLES (Continued)

LIST OF TABLES (Continued)

I. INTRODUCTION

This report is the second volume of a two-volume Final Report prepared under Contract No. F08606-74-C-0011 for the period 1 July 1975 through 30 September 1976. The work reported on involved making modifications to the computer programs previously developed for use in studying the atmospheric transport of the thermal radiation produced by nuclear sources. The work also involved applying these computer procedures to a number of different thermal radiation transport problems.

The POLO Monte Carlo procedure (Ref. 1), which computes radiation transport for point sources in a spherical-shell atmosphere, was modified in order to utilize the gaseous absorption cross-section data compiled by McClatchey (Ref. 2) at AFGL. These new cross-section data allow the POLO procedure to treat absorption by a larger number of atmospheric gases and to treat gaseous absorption within finite-sized wavelength intervals in the infrared wavelengths instead of for discrete wavelengths. The POLO procedure was also modified so that it could compute and print out the intensity of the scattered radiation at point receivers as a function of a polar and an azimuthal angle as well as time. The modifications made to POLO for the purpose of incorporating the AFGL gaseous absorption cross-section data and printing out the polar and azimuthal angle distributions of the scattered intensities as a function of time are described in Section II.

The modified version of POLO was used to do a parametric study of the effects of atmospheric scattering on the transmission of the radiation emitted by point isotropic sources in the 2.7 μm band. The atmospheric transmission to a satellite-based receiver position was evaluated as a function of the satellite look angle for a satellite at 35,800 km altitude and point isotropic sources at altitudes of 0.1, 0.5, 2, 5, and 10 km in both tropical and midlatitude summer model atmospheres. The atmospheric models and the results obtained from the POLO calculations are discussed in Section III.

A study was conducted, using the POLO and POLY (Ref. 1) procedures, to determine the effect of source anisotropy on the time distribution of the thermal radiation signal that would be seen by a wideband silicon receiver positioned on a satellite at 20,187-km altitude. A description of the results obtained for two different anisotropic sources and for a point isotropic source is given in Section IV.

Section V describes a set of calculated atmospheric transport data that were generated with the POLO procedure for a 40-km meteorological range atmosphere. The receivers were at synchronous satellite altitude. The time-dependent air-scattering data generated with POLO were curve-fitted for use with the TMTAU procedure (Ref. 3). The curve-fit data are also discussed in Section V.

Section VI describes the calculational methods developed for convoluting time- and spatial-dependent source and atmospheric transmission data. Modifications that were made to the POLY and TMTAU procedures so that they could interpolate the POLO-generated atmospheric data or the curve-fit coefficients for the POLO data over wavelength are also described. The accuracy of the calculational methods used in the modified convolution procedures was checked through comparison with the results of an analytic solution. The results obtained are also discussed in Section VI.

The effects of clouds on the time-dependent transmission of the thermal radiation emitted by nuclear sources was studies with use of the POLO and POLY procedure. POLO calculations were performed for point isotropic sources at wavelengths of 0.4278, 0.75, and 1.07 μm, and source heights of 0.1, 0.5, 3, and 10 km. The detectors were positioned at 35,800-km altitude for look angles of 0, 45, 75, and 90 degrees. Two model atmospheres were used in the POLO calculations. The first model atmosphere used was a 10-km meteorological range Haze C atmosphere with a 14 mean-free-path thick stratus cloud positioned between 0.5- and 1.0-km altitude. The second atmosphere used was a 10-km meteorological range Haze C atmosphere with a 20 mean-free-path thick altostratus cloud posi-

tioned between 3- and 4-km altitude. The POLO-computed transmission date were convoluted in the POLY procedure with source data from RADFLO for a 2-KT event. The results of both the POLO calculations of the atmospheric transmittance and the POLY calculations of the thermal power at the detector for retarded times up to 140 μsec are described in Section VII.

The POLO procedure was used to compute the angular and time distributions of the scattered intensity at the top of a cloud. An analysis of those calculations showed that large statistical deviations occurred in the calculational data. A discussion of these results and possible reasons for the large statistical errors for detectors at cloud top is also given in Section VII.

There have been several occasions where calculated air transmission data for satellite altitudes other than that of 35800 km have been needed. There currently exists a large body of POLO-calculated atmospheric transport data for a satellite altitude of 35800 km. A study was performed utilizing the POLO procedures to determine the time-dependent scattered fluxes reaching satellites at altitudes of 20186.8, 93261.626, and 35800 km. Ratios of the calculated scattered fluxes at altitudes of 20186.8 and 93621.626 km to the calculated scattered flux at 35800-km altitude were found to agree within a few percent with the similar ratios computed for the direct fluxes. Because of this good agreement, it is suggested that the method described in Section VI be used to convert scattered fluxes and direct fluxes computed by use of POLO for an altitude of 35800 km to any other satellite altitude.

The difficulties in computing accurate transmission data for detectors positioned at cloud top with the POLO program resulted in a study on the possible application of discrete ordinates techniques to cloud transmission problems. The TDA code (Ref. 4), a one-dimensional discrete ordinates code was obtained from the Radiation Shielding Information Center. It soon became apparent that in order to be able to

use TDA, or any other time-dependent discrete-ordinates code, to study optical radiation transport it would be necessary to have a calculational method for expanding the aerosol phase function in terms of a Legendre polynomial of order n. A method was developed to accomplish this expansion from data computed with the MIE-2 procedure. The calculational method developed to compute the Legendre coefficients for Mie scattering is discussed in Section VIII.

II. MODIFICATIONS TO THE POLO PROCEDURE

During the previous year, several modifications were made to the POLO program to improve the application of the program to problems of interest to AFTAC. Currently, three versions of the POLO program are operational on the computer at AFTAC. The original version of POLO, designated TPOLOW, is still operational and is being used in time-dependent light-transport studies for wavelengths in the visible range. This version of the POLO program produces an output tape in the format required by the TMTAU and POLY programs.

In a version of POLO, designated as TPOLOG, a new method for treating gaseous absorption was incorporated into the POLO program. The gaseous absorption data compiled by McClatchey (Ref. 2) for CO_2, H_2O, O_3, N_2O, CO, CH_4, and O_2 are contained on a library tape which is analyzed by the TPOLOG program to select the cross-section data for the desired constituents and wavelength intervals. The data are available on tape with a resolution of $\Delta\nu$ = 20 cm^{-1} at 5 cm^{-1} spacing between 10 cm^{-1} and 13155 cm^{-1} (0.76-1000 μm). Therefore, TPOLOG treats gaseous absorption in the IR for a wavelength band rather than for a discrete wavelength. The gaseous absorption transmission model used in TPOLOG with the McClatchey data is described in Ref. 5.

The TPOLOG program was further modified to create a version of POLO designated as TPOLOL. TPOLOL allows for a detector with polar angle, azimuthal angle, and time resolution. The polar angle at the detector is measured, depending on the option selected, either from the earth radial through the receiver position or from the source-receiver axis. An effort was made to minimize the differences in the utilization of the TPOLOG and TPOLOL procedures. TPOLOL currently exists at AFTAC on disc pack TF2PAK under RRACODES in all sections as TPOLOL.

2.1 Comparison of TPOLOG Calculations with LOWTRAN3 Data

(U) TPOLOG calculations of the direct transmittance in the 2.65 μm to 3.0 μm wavelength range for a point source at a height of

0.5 km and a detector positioned at a satellite altitude of 35800 km were run for comparison with LOWTRAN3 (Ref. 6) calculations. The calculations were made for two model atmospheres. The atmosphere denoted as Model A had less water vapor content than did the atmosphere denoted as Model B. The LOWTRAN3 code was run with the same atmospheric models as were used in the TPOLOG calculations. A comparison of the direct-transmittance data obtained from both calculations for the two atmospheric models when the satellite is positioned directly overhead is shown in Fig. 1 for the range 2.8249 μm - 2.9940 μm (3,540 cm^{-1} and 3,340 cm^{-1}, respectively). In the figure, the direct-transmittance data obtained from LOWTRAN3 are connected with straight lines; whereas the TPOLOG-calculated direct-transmittance data are plotted using circles and triangles. The differences that occur for the individual data is believed to be due to the different method of treating absorption in TPOLOG and in LOWTRAN3. TPOLOG uses an interpolation between absorption cross sections as a function of temperature in order to give the correct cross section at the specific temperature of each atmospheric layer. The transmission formula in TPOLOG (Ref. 5) takes into account the pressure dependency. The absorption coefficients in LOWTRAN3 are input for 296°K temperature and 1 atm pressure and are then adjusted to the correct temperature and pressure of each atmospheric layer (the adjustment takes into account the change of the line widths with temperature, but not the change of the line strengths).

Unfortunately, the transmission functions incorporated in LOWTRAN3 do not allow the use of the program to calculate transmissions that are less than 0.001 for most of the species considered. LOWTRAN3 transmission data in the range 2.65 μm were all calculated to be 0.0 and therefore, cannot be compared with the TPOLOG data in the same wavelength range.

A comparison of the direct transmittances for the Model B atmosphere that were calculated by both programs is shown in Fig. 2 for satellite polar position angles, θ_o, of 0°, 30°, 60°, and 78°. The

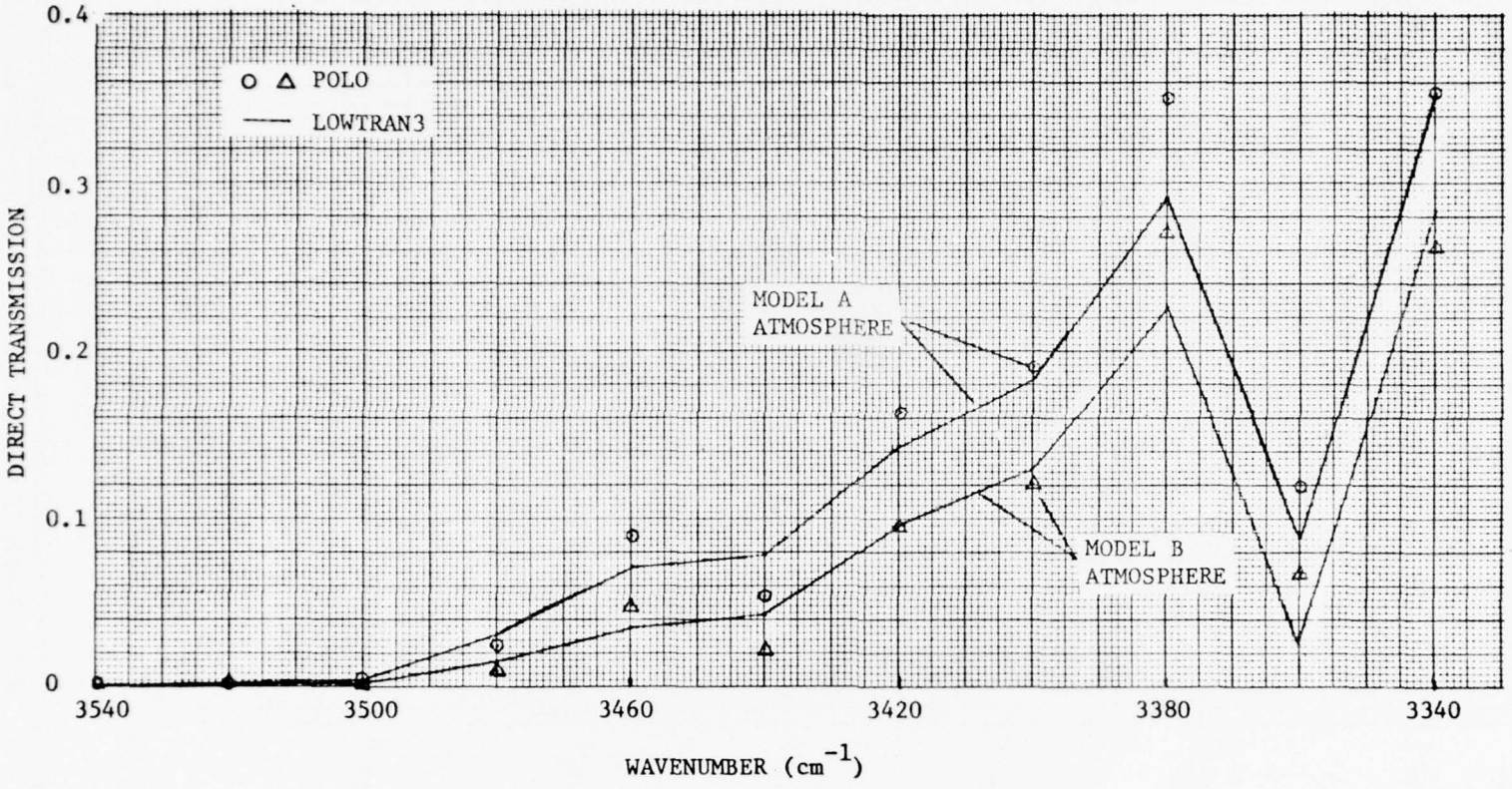

Fig. 1. Direct Transmittance vs Wavelength, $\theta_o = 0°$

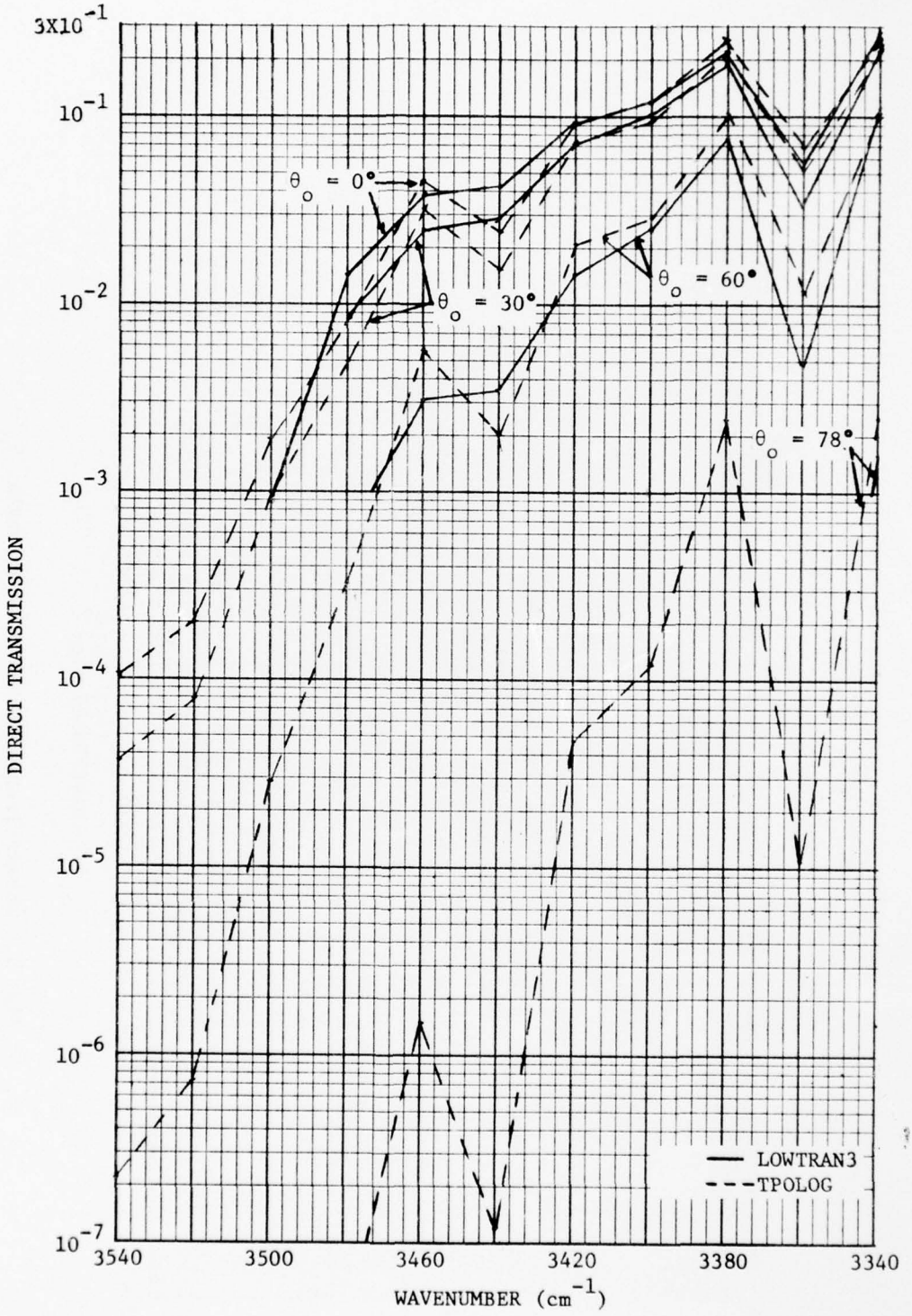

Fig. 2. Direct Transmission vs Wavenumber and Polar Position Angle; Model B Atmosphere, Height of Source = 0.5 km

comparison is good for transmittances greater than 0.001 and for all of the polar position angles, with the exception that the LOWTRAN3 data seem to be slightly lower than the TPOLOG data for θ_o = 60° and 78°. This is explained by the fact that LOWTRAN3 considers the bending of light by the atmospheric refraction; whereas the version of TPOLOG that was used to calculate the infrared data does not. The atmospheric refraction tends to bend the light rays to lower atmospheric layers, resulting in larger pathlengths and lower transmissions. Since the overall comparison between the LOWTRAN3 and TPOLOG data is good, it was, therefore, decided not to modify LOWTRAN3 to neglect the effect of the refractive index which would require major changes in LOWTRAN3.

The good comparison between transmission data computed with LOWTRAN3 and TPOLOG verifies the method used in TPOLOG to account for gaseous absorption. The method used in TPOLOG seems to have the advantage that transmission data can be obtained for values smaller than 0.001; however, no information is available on the accuracy of the computed data for very small transmissions.

III. TPOLOG CALCULATIONS IN THE IR FOR SATELLITE DETECTORS

TPOLOG multiple-scattering calculations in the IR for detector systems at satellite positions have been performed in the range 2.65 - 3.00 μm. This wavelength is of particular interest because of the H_2O and CO_2 absorption band in that region of the spectrum. Because of the high, but different, concentration of these species at low altitudes, H_2O absorption is dominant in the atmospheric layers close to the ground surface; CO_2 absorption is dominant above 5-kilometer altitudes and can still be observed at altitudes about 40 km (Ref. 7).

3.1 Model Atmospheres

Atmospheric models for a tropical and a mid-latitude summer atmosphere were chosen. The dependency of the atmospheric pressure on altitude for these models was taken out of the U. S. 1966 Supplement Atmospheres (Ref. 8). Data for temperature and dew point below the tropopause were supplied by the contract monitor. The temperature data obtained were smoothed and then extended to higher altitudes using the tropical and mid-latitude models of Ref. 8.

Although the TPOLOG program allows for gaseous absorption for a total of seven species, only the absorption by H_2O, CO_2, and N_2O have to be considered in the wavelength range of interest (Ref. 9). CO_2 and N_2O was assumed to be uniformly mixed in the entire atmosphere with mixing ratios of $3X10^{-4}$ and $5X10^{-7}$ (Ref. 10), respectively. The H_2O densities below 10-km altitude were calculated from the measured dew point and temperature, using the USAF SKEW T, log p Diagram supplied by the contract monitor, and tables given in Ref. 11. The data were then smoothed and combined with data given by Selby et al. (Ref. 9) for both the tropical and mid-latitude summer model.

The dependency of the aerosol concentration upon altitude was assumed to be that of the 1970 measurements taken by Elterman (Ref. 12).

Aerosol models for tropospheric and stratospheric particles were taken from Ref. 13 to describe the aerosol size distribution and the wavelength dependency of the aerosol scattering coefficient (see also Ref. 7). The ground-level meteorological ranges for both the tropical and mid-latitude atmospheres were taken to be 25 km.

3.2 Calculational Results

TPOLOG calculations for the 2.7-micron wavelength band were run for the tropical and mid-latitude atmospheric models. The gaseous absorption cross-section data compiled by McClatchey at AFCRL (Ref. 2) were used in the TPOLOG calculations. The satellite altitude was taken to be 35,800 km and detectors were positioned at polar position angles (polar angle between a radial through the source and a radial through the satellite's position) of 0, 30, 60, 78, and 82 degrees. The source altitudes considered were 0.1, 0.5, 2, 5, and 10 km.

The TPOLOG calculations were run for 23 wavelengths spaced between 2.6525 μm and 3.0030 μm. The scattering and continuum absorption cross sections were input for three wavelength intervals; the first and second intervals each contained seven wavelengths and the third interval contained nine wavelengths. For the 2.7-μm wavelength band, the atmospheric gases that contribute to the molecular absorption were water vapor, CO_2, and N_2O. The atmospheric optical thickness for each of the model atmospheres, excluding gaseous absorption, were as follows:

WAVELENGTH INTERVAL (μm)	OPTICAL THICKNESS EXCLUDING MOLECULAR ABSORPTION	
	MID-LATITUDE ATMOSPHERE	TROPICAL ATMOSPHERE
2.6525-2.7491	4.033676×10^{-2}	4.065740×10^{-2}
2.7491-2.8490	3.595484×10^{-2}	3.625945×10^{-2}
2.8490-3.0030	3.334809×10^{-2}	3.363596×10^{-2}

A significant fraction (45% to 65%, depending upon altitude) of the above optical thicknesses resulted from aerosol particle absorption.

The TPOLOG printed output gave the scattered and direct flux at each receiver position as a function of the ground albedo for each of the 23 source wavelengths. The ground surface was assumed to be a Lambert reflector. Calculations were run for source heights of 0.1, 0.5, 2, 5, and 10 km. The receivers were positioned at an altitude above the ground surface of 35,800 km and at polar position angles θ_o of 0°, 30°, 60°, 78°, and 82°.

The calculated direct and scattered fluxes were folded with a filter function and a source term that assumed a uniform emission with wavelength within the interval being considered. The results were then multiplied by the quantity $4\pi R^2$ where R is the source-receiver distance to obtain the direct and scattered transmittances to the satellite. The total source emission over the wavelength interval from 2.6525 μm to 3.0030 μm was assumed to be 1.0 photon. The results shown in this report are for a filter function that had a value of 1.0 for all wavelengths.

The results obtained from the TPOLOG calculations as a function of source height and satellite polar position angle for the direct transmission and for the scattered transmission when the ground albedo has values of 0.0 and 0.8 are tabulated in Tables I and II for the tropical and mid-latitude atmospheres, respectively. From the data shown in these tables, it is seen that the direct transmittance for the mid-latitude atmosphere is higher than that computed for the tropical atmosphere at source heights less than about 3 km. For source heights above 3 km, the direct transmittances for the mid-latitude atmosphere are less than those computed for the tropical atmosphere. Note also that for a satellite polar position angle of 82° the direct transmittance is negligible compared to the scattered transmittance when the source height is less than 2 km.

The ratio of the calculated scattered transmittance to the total transmittance is shown in Fig. 3 for the tropical atmosphere

TABLE I. TRANSMITTANCE FOR TROPICAL ATMOSPHERE VS SOURCE HEIGHT AND SATELLITE POLAR POSITION ANGLE

SOURCE HEIGHT (km)	POLAR POSITION ANGLE (deg)	DIRECT	SCATTERED α=0.0	SCATTERED α=0.8
0.1	0	.36274-01*	.82111-03	.53821-01
	30	.29245-01	.84865-03	.35703-01
	60	.10436-01	.53534-03	.62431-02
	78	.13459-03	.77877-04	.14280-03
	82	.10000-59	.22037-04	.40074-04
0.5	0	.47720-01	.86938-03	.38256-01
	30	.39288-01	.76768-03	.26154-01
	60	.15552-01	.55974-03	.51586-02
	78	.33379-03	.10195-03	.15525-03
	82	.81053-10	.27865-04	.40129-04
2.0	0	.12945+00	.12333-02	.19153-01
	30	.11472+00	.12861-02	.14066-01
	60	.65047-01	.12334-02	.39608-02
	78	.71075-02	.61538-03	.66637-03
	82	.62801-06	.17180-03	.18312-03
5.0	0	.35552+00	.14986-02	.17416-01
	30	.33513+00	.15849-02	.12941-01
	60	.25960+00	.26229-02	.51181-02
	78	.11138+00	.21619-02	.22291-02
	82	.77616-02	.72961-03	.75118-03
10.0	0	.58527+00	.12844-02	.15899-01
	30	.56239+00	.14384-02	.11910-01
	60	.47452+00	.21385-02	.44427-02
	78	.29720+00	.29174-02	.29664-02
	82	.11785+00	.19947-02	.20293-02

*Read .36274-01 as $.36274 \times 10^{-1}$

TABLE II. TRANSMITTANCE FOR MID-LATITUDE ATMOSPHERE VS SOURCE HEIGHT AND SATELLITE POLAR POSITION ANGLE

SOURCE HEIGHT (km)	POLAR POSITION ANGLE (deg)	DIRECT	SCATTERED α=0.0	SCATTERED α=0.8
0.1	0	.54960-01*	.13844-02	.82036-01
	30	.45673-01	.14248-02	.56400-01
	60	.18859-01	.92310-03	.11481-01
	78	.49567-03	.16821-03	.27061-03
	82	.10000-59	.34801-04	.50752-04
0.5	0	.64063-01	.13330-02	.69568-01
	30	.53884-01	.13129-02	.48714-01
	60	.23628-01	.96268-03	.10544-01
	78	.83301-03	.14580-03	.24890-03
	82	.18018-07	.31472-04	.51345-04
2.0	0	.11423+00	.11580-02	.36015-01
	30	.10041+00	.11248-02	.26145-01
	60	.54729-01	.10232-02	.68139-02
	78	.52365-02	.33354-03	.41487-03
	82	.19577-05	.83812-04	.97084-04
5.0	0	.26506+00	.95450-03	.28691-01
	30	.24652+00	.10885-02	.21402-01
	60	.17793+00	.12587-02	.62602-02
	78	.55871-01	.75916-03	.84328-03
	82	.20003-02	.26570-03	.28457-03
10.0	0	.59227+00	.11784-02	.27105-01
	30	.56936+00	.13243-02	.20270-01
	60	.48103+00	.16754-02	.63774-02
	78	.30074+00	.13907-02	.14680-02
	82	.78988-01	.58408-03	.60004-03

*Read .54960-01 as $.54960 \times 10^{-1}$

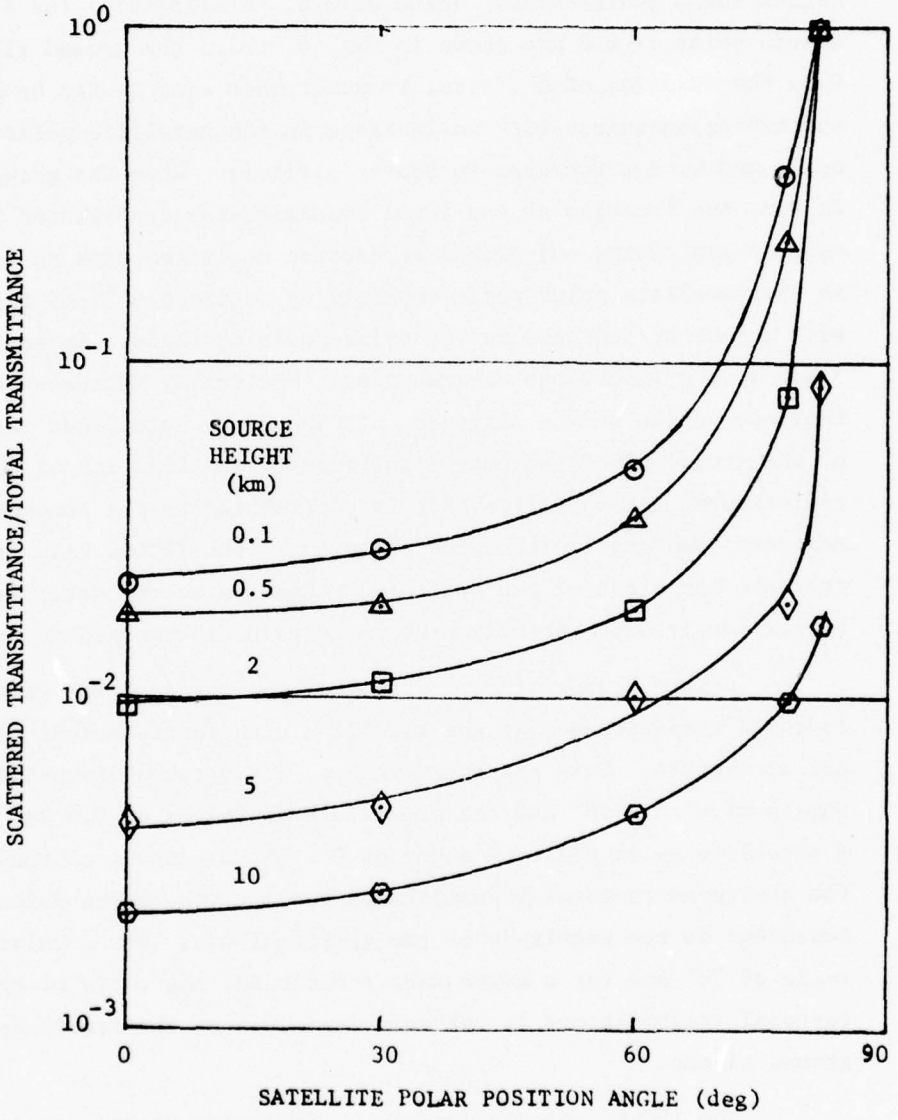

Fig. 3. Ratio of the Scattered-to-Total Transmittance in the Tropical Atmosphere vs Satellite Polar Position Angle for Source Height of 0.1, 0.5, 2, 5, and 10 km and a Ground Albedo of 0.0

as a function of the satellite polar position angle and the source height for a ground albedo value of 0.0. Similar data for a ground albedo value of 0.8 are shown in Fig. 4. When the ground albedo is 0.0, the fraction of the total transmittance contributed by atmospheric scattering increases with an increase in the satellite polar position angle and with a decrease in source altitude. When the ground albedo is 0.8, the fraction of the total transmittance contributed by atmospheric scattering and ground reflection decreases with an increase in the satellite polar position angle up to about 65° and then increases with a further increase in the polar position angle. As seen in Figs. 3 and 4, the importance of atmospheric scattering decreases with an increase in the source altitude. It should be noted that the magnitude of the ground albedo affects significantly the fraction of the total radiation at the satellite that is contributed by the atmospheric-scattered and ground-reflected radiation. The TPOLOG calculations show that the magnitude of the scattered radiation at the satellite increases approximately exponentially with an increase in the ground albedo.

Figure 5 shows the variation of the ratio of the scattered-to-total transmittance at the satellite with source height for the tropical atmosphere. Data are shown in Fig. 5 for satellite polar position angles of 0° and 78° and for ground albedo values of 0.0 and 0.8. For a satellite polar position angle of 0°, the magnitude of the ratio of the scattered-to-total transmittance for a given source height is highly dependent on the magnitude of the ground albedo. For a polar position angle of 78° and for a given source altitude, the ratio of the scattered-to-total transmittance is not very dependent on the magnitude of the ground albedo.

The TPOLOG calculations show, for point sources emitting in the 2.7 μm wavelength band, that the air-scattered and ground-reflected radiation can be an important component of the data measured by infrared sensors on satellites, and neglecting that component in an analysis of the measured data can lead to significant error in estimating the magnitude of the source that produced the measured data.

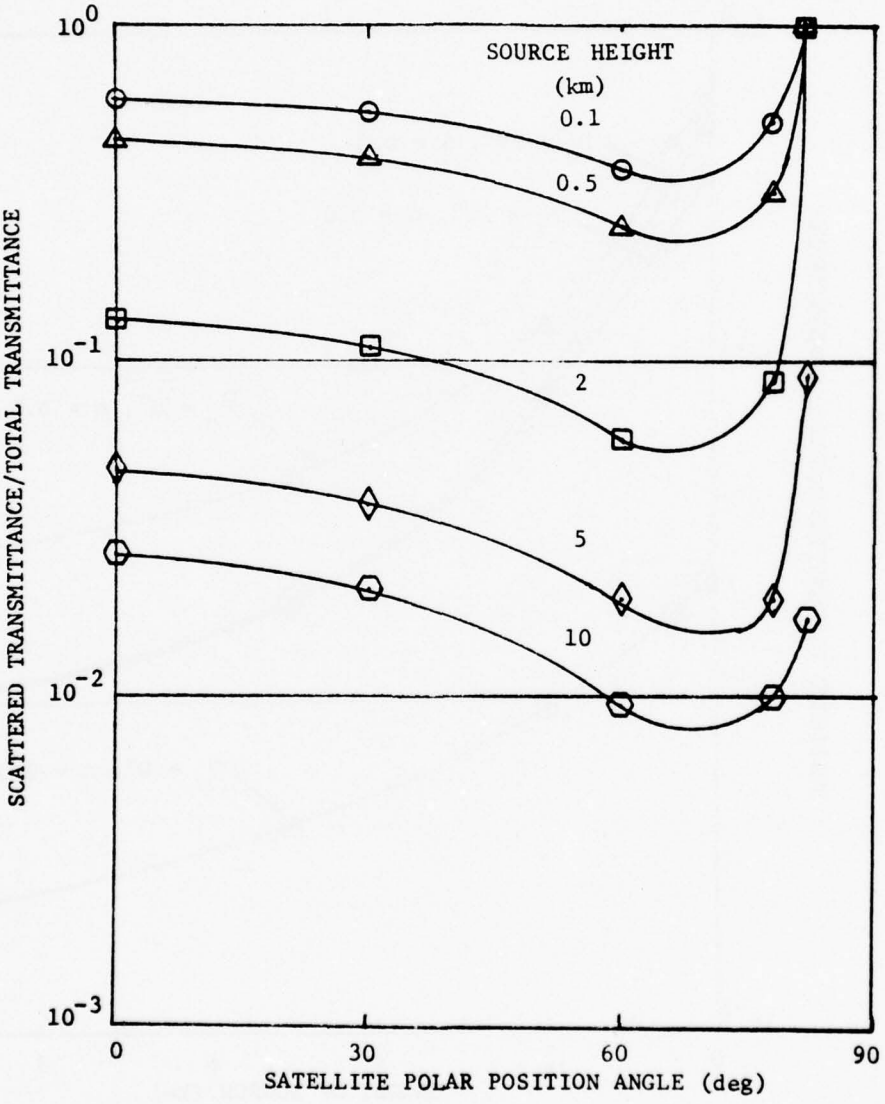

Fig. 4. Ratio of the Scattered-to-Total Transmittance in the Tropical Atmosphere vs Satellite Polar Position Angle for Source Heights of 0.1, 0.5, 2, 5, and 10 km and a Ground Albedo of 0.8

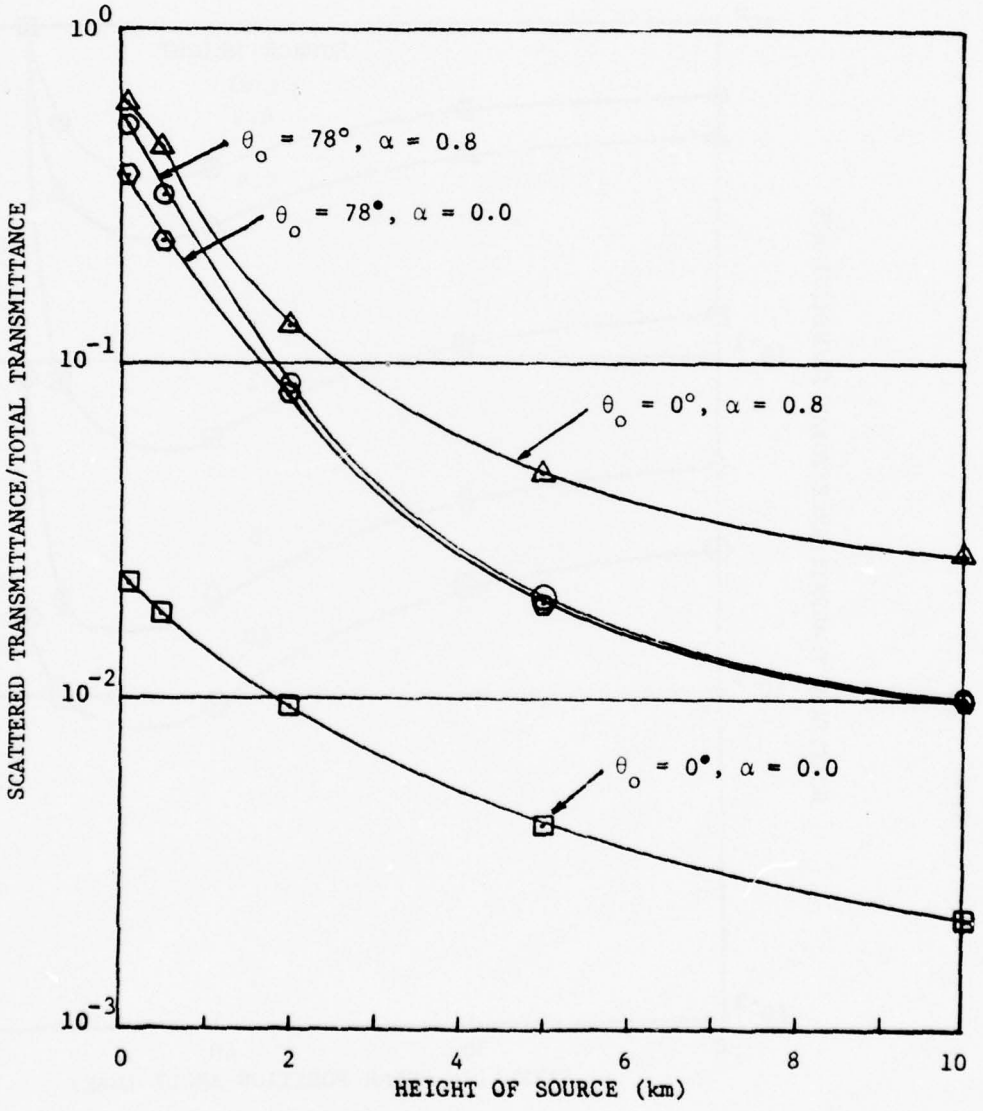

Fig. 5. Ratio of the Scattered-to-Total Transmittance in the Tropical Atmosphere vs Height of Source for Satellite Polar Position Angles of 0° and 78° and Ground Albedo Values of 0.0 and 0.8

IV. POLO CALCULATIONS FOR ANISOTROPIC SOURCES

A study was conducted to determine the effect of source anisotropy on the time distribution of the optical signal received by a wideband silicon receiver located on a satellite positioned 20,187 kilometers above the earth's surface. Point anisotropic sources were considered which emit different fractions of the total radiance uniformly in the forward and backward hemispheres. The forward and backward hermispheres are separated by a vertical plane containing the source point that is perpendicular to the plane containing the receiver locations. The forward hemisphere is the hemisphere on the receiver side of the plane. The source-receiver geometry for the calculations is shown in Fig. 6. Source altitudes of 500 meters, 3 kilometers, and 10 kilometers were considered in model atmospheres having meteorological ranges of 3, 10, and 25 kilometers. Receivers were located at look angles, θ_L, of 0, 30, 45, 60, 70, 75, 80, and 90 degrees for the sources at 500 meters altitude and at 0, 30, 60, 70, 80, and 90 degrees for the sources at 3 and 10 kilometers altitude.

Atmospheric transmission calculations for each source-receiver combination in each of the three model atmospheres were performed with the POLO program for source wavelengths of 0.4278, 0.75, and 1.07 microns. The direct fluxes that were obtained for the three different 0.75-micron wavelength sources located at 500-meters altitude in the 25-kilometer meteorological range atmosphere are compared in the table below. The anisotropic-1 source emits 2/3 of its radiation in the forward hemisphere and 1/3 in the backward hemisphere. The anisotropic-2 source emits 2/3 of its radiation in the backward hemisphere and 1/3 in the forward hemisphere.

The direct flux at the satellite for each look angle and source model when the source wavelength is 0.75 μm is:

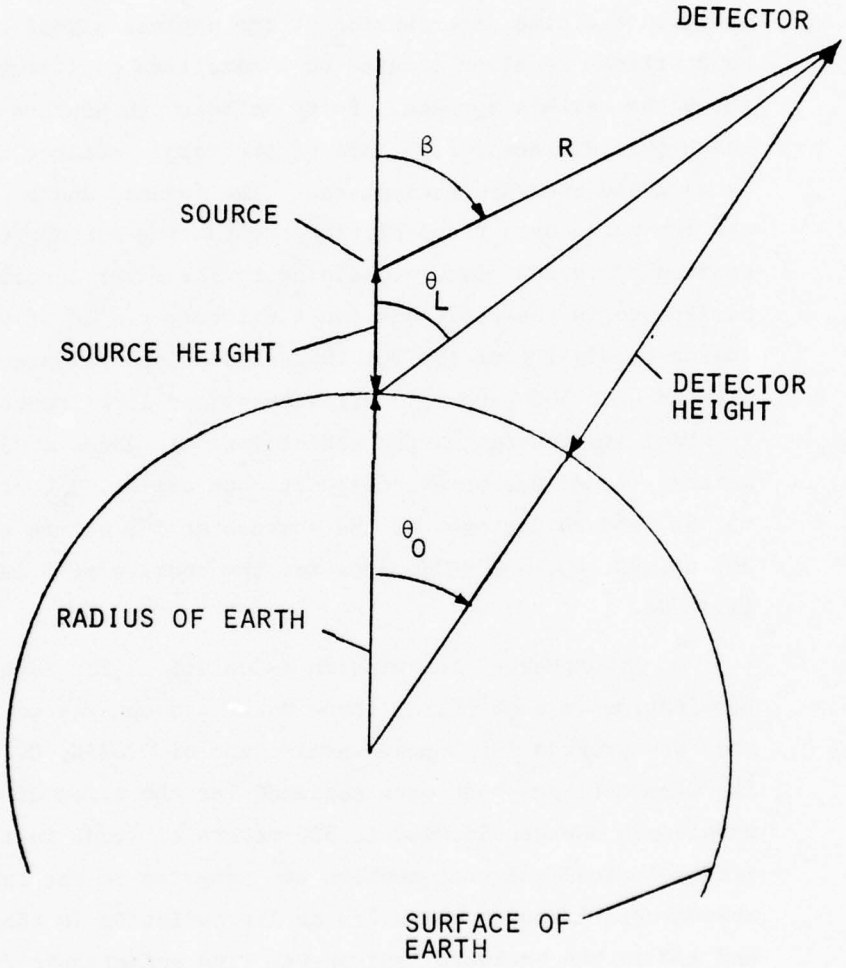

Fig. 6. Source-Receiver Geometry

LOOK ANGLE (deg)	DIRECT FLUX (photons km^{-2}/source photon)		
	ISOTROPIC SOURCE	ANISOTROPIC-1	ANISOTROPIC-2
0	.16346-9	.16346-9	.16346-9
30	.14801-9	.19735-9	.98673-10
60	.10504-9	.14005-9	.70027-10
90	.18777-14	.24236-14	.12118-14

These data are for a source height of 0.5 km in the 25-km meteorological range atmosphere. For the two anisotropic source models studies, the direct flux at $\theta_L = 0°$ is identical to that for an isotropic source.

A plot of the variation of the total flux at the detector with a look angle for a 0.75-μ wavelength source is given in Fig. 7 for a ground albedo of 0.0 and in Fig. 8 for a ground albedo of 0.8. The fluxes in Figs. 7 and 8 are for a source altitude of 0.5 km and a 25-km meteorological range atmosphere. It appears that the possibility of determining whether a source is anisotropic or not with the use of measured data from at least two satellites is the greatest for look angles between 40° and 70° and when the surface albedo is small. The two satellites would, of course, have to be on opposite sides of the source.

The atmospheric transmission computed with POLO for the three wavelengths were used in the POLY procedure to predict the atmospheric transmission for 14 wavelength intervals covering the range from 0.4 to 1.10 microns. The atmospheric transmissions for each of the 14 wavelength intervals were convoluted in POLY with a time-dependent source term generated with the RADFLO program for a 2-KT event. Then these data were weighted in POLY with a response function for a wide-band silicon detector (Fig. 9) and integrated over wavelength. The wavelength intervals and the average response within the intervals are listed in Table III. The RADFLO source term weighted with the response function and integrated over wavelength is plotted versus time out to $24X10^{-5}$ seconds in Fig. 10. Figure 10 shows the response that should be observed if atmospheric attenuation and scattering did not perturb the optical

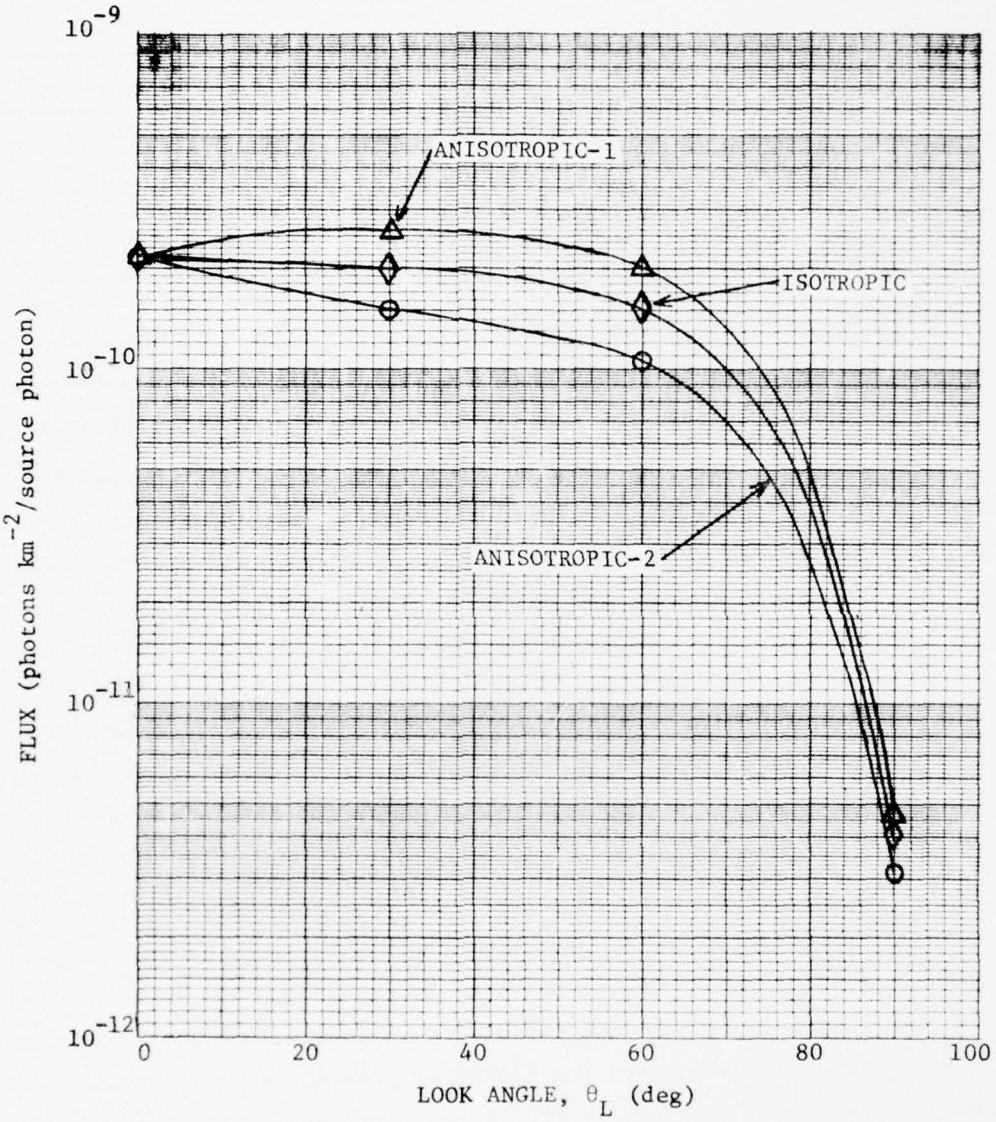

Fig. 7. Variation of the Total Flux at Satellite with Look Angle: Ground Albedo = 0.0

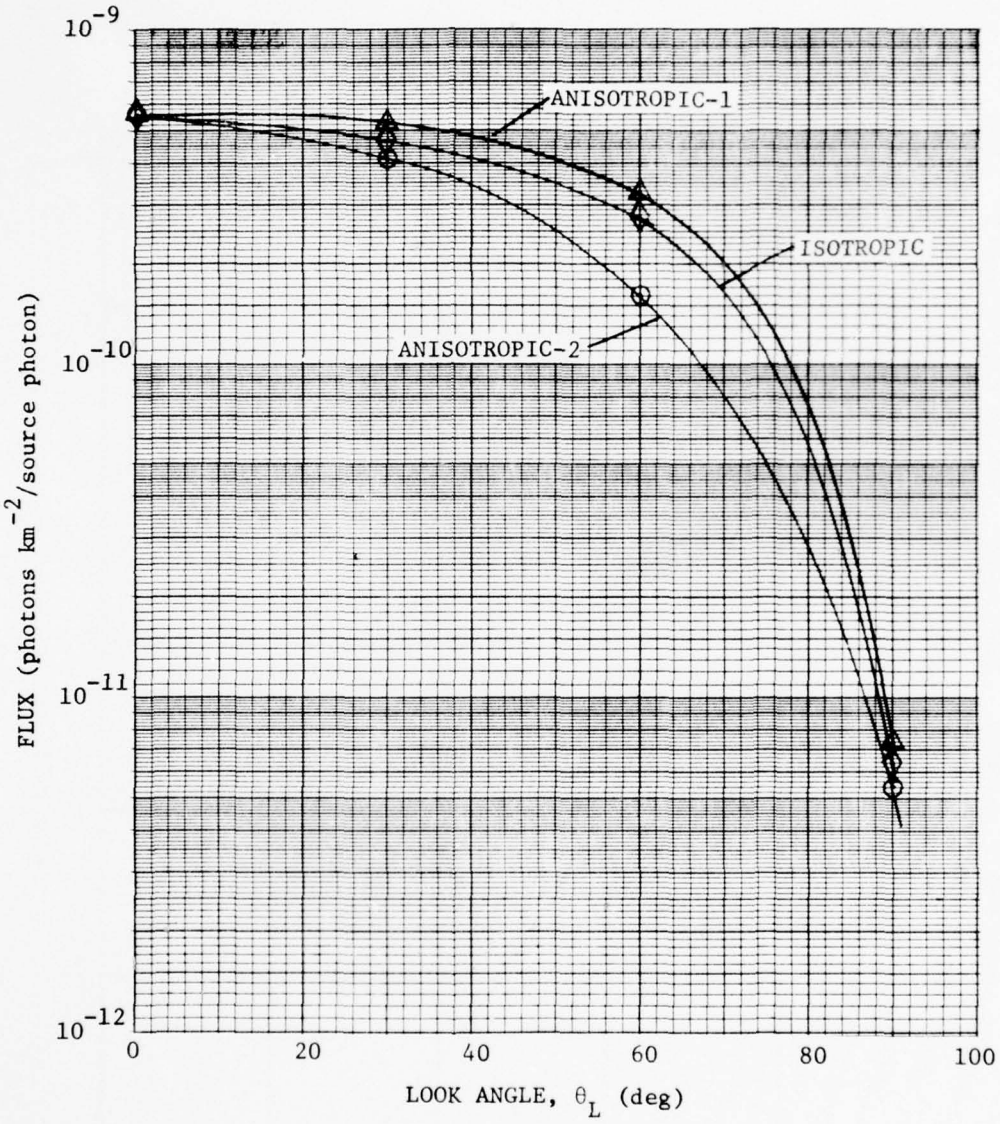

Fig. 8. Variation of the Total Flux at Satellite with Look Angle: Ground Albedo = 0.8

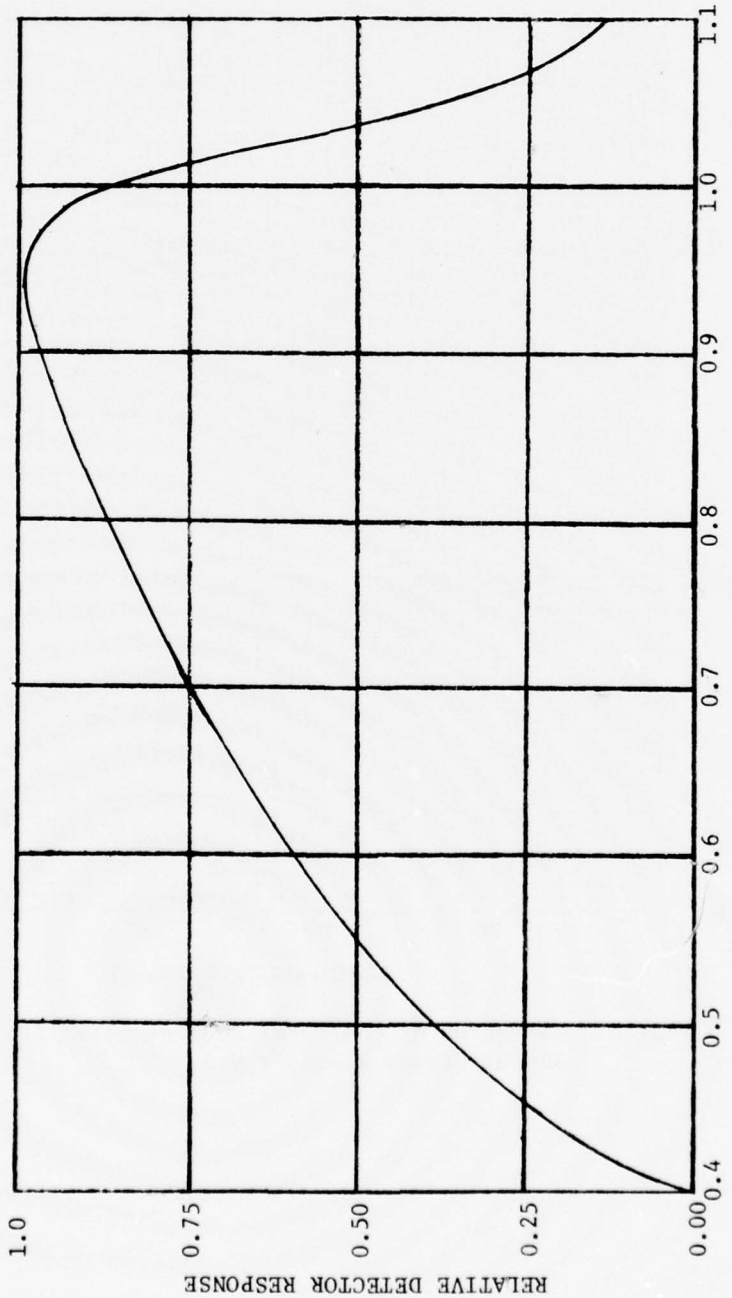

Fig. 9. Detector Response Function

TABLE III. WIDE-BAND SILICON RESPONSE FUNCTION VERSUS WAVELENGTH

WAVELENGTH INTERVAL (micron)	AVERAGE RESPONSE
0.4000-0.4500	0.1312
0.4500-0.4850	0.3000
0.4850-0.5253	0.4000
0.5253-0.5700	0.4937
0.5700-0.6266	0.5875
0.6266-0.6812	0.6779
0.6812-0.7358	0.7548
0.7358-0.8029	0.8354
0.8029-0.8700	0.9125
0.8700-0.9309	0.9725
0.9309-0.9918	0.9800
0.9918-1.0200	0.8375
1.0200-1.0600	0.4820
1.0600-1.1000	0.1980

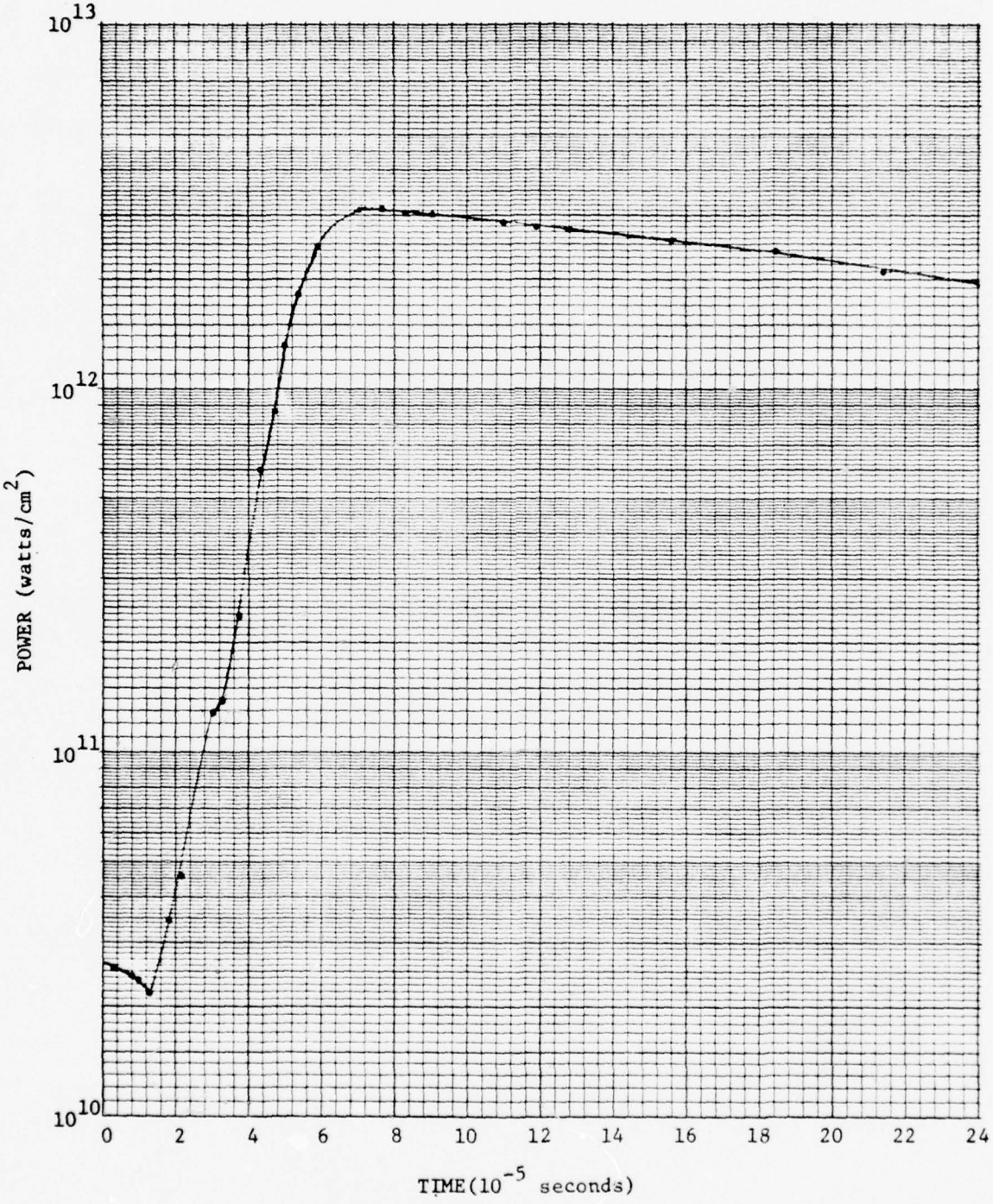

Fig. 10. Power vs Time Distribution for RADFLO Source Term Weighted by Detector Response Function and Integrated over Wavelength

signal. Note that first maximum occurs at approximately $7.08X10^{-5}$ seconds. The optical signal seen at a receiver position includes not only the direct but also the scattered radiation and since the scattered radiation is delayed in time, the time distribution of the optical signal at the receiver position may be quite different from the time distribution of the radiation emitted from the source. Since the source angular distribution affects the ratio of the scattered to direct radiation observed at a receiver position, it may also affect the time distribution of the optical signal at the receiver position. That is, receivers at the same look angle and radial distances relative to the source but at different azimuthal positions will show a different response if the source is anisotropic.

Figures 11 and 12 show the calculated time response for receivers located at 30- and 90-degree look angles from each of three sources considered. The upper curves are for a source emitting two-thirds of its radiation in the forward hemisphere and one-third in the backward hemisphere (FORWARD), the center curves are for an isotropic source (ISOTROPIC), and the lower curves are for a source emitting one-third of its radiation in the forward hemisphere and two-thirds in the backward hemisphere (BACKWARD). Note that not only does the anisotropy of the source affect the magnitude of the optical signal received at the detector position, but the time at which first maximum is reached also appears to be shifted to later times as the source becomes peaked in the backward direction. The shift in the time of first maximum raises a question concerning the time scale that should be used in comparing optical signals from detectors located at different receiver positions.

The time intervals used in the POLY program to record the time-dependent optical signal are in the order of 10 to 20 microseconds in width for time periods near the time of first maximum. Therefore, it is difficult to determine within 10 to 20 microseconds when first maximum actually occurs. An examination of the optical signals generated with the POLY program indicates that scattering may shift the time of first

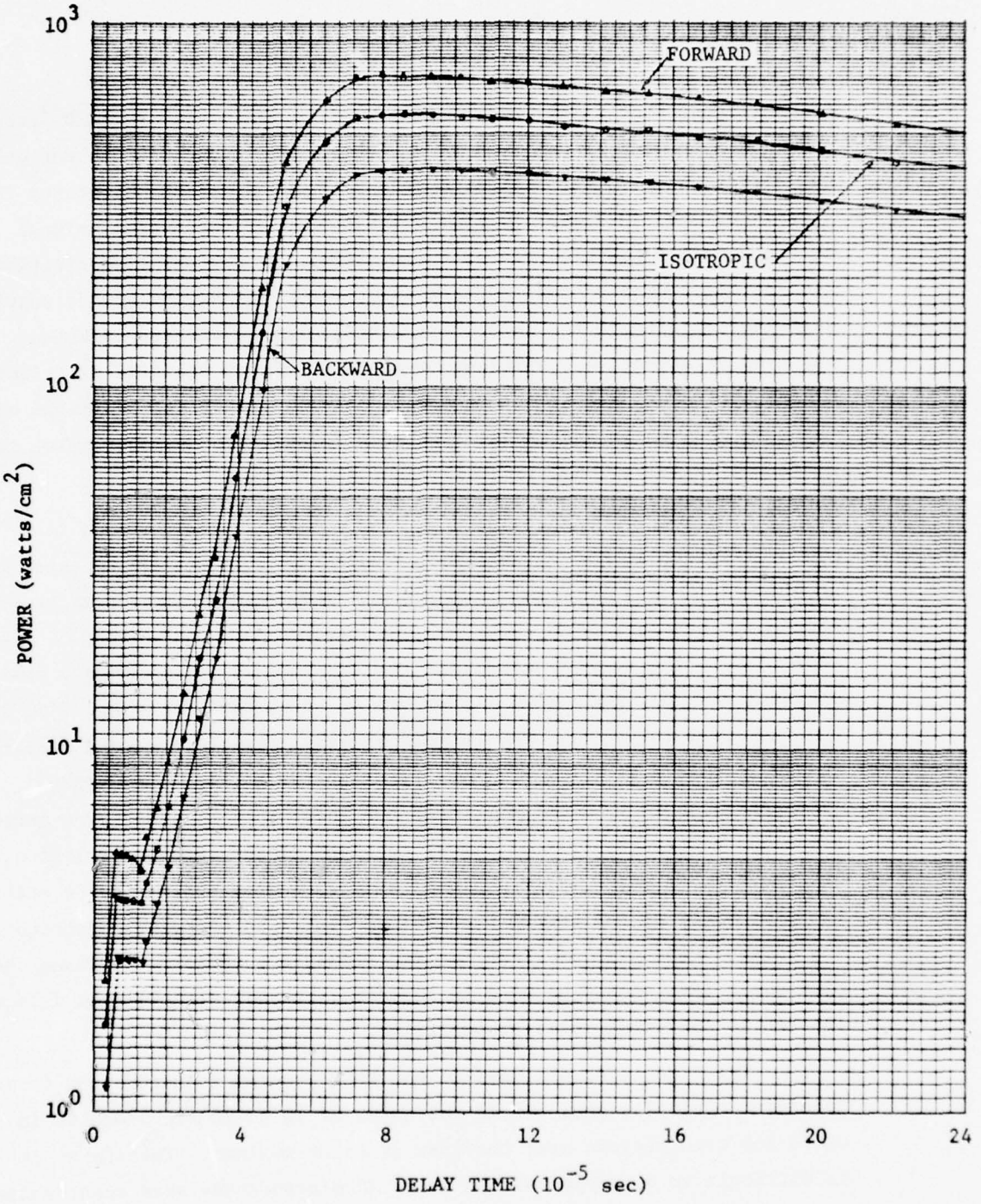

Fig. 11. POLY Calculations of the Time-Dependent Power Signal for a Look Angle of 30°: Ground Albedo = 0.0, 25 km Meteorological Range Atmosphere

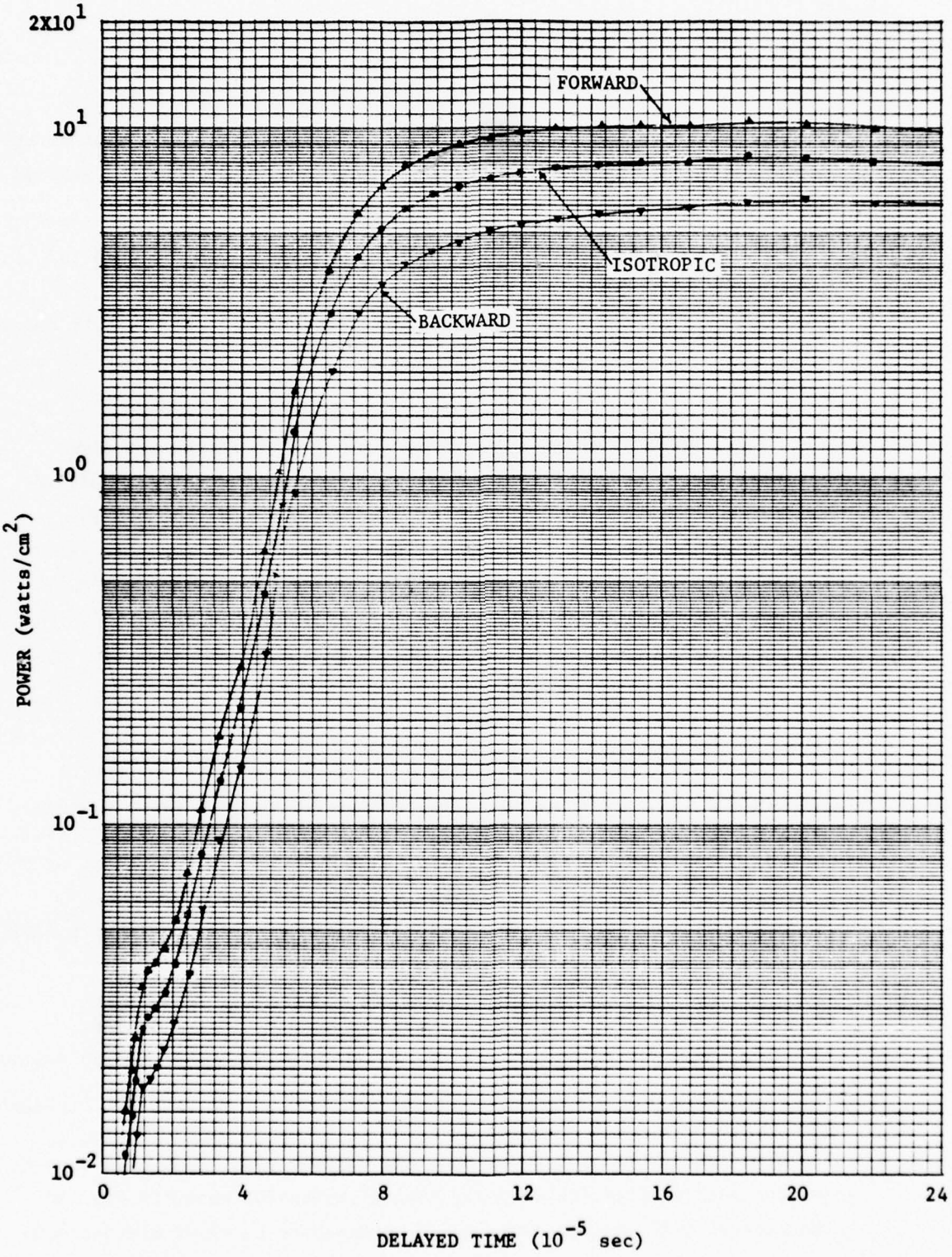

Fig. 12. POLY Calculations of the Time-Dependent Power Signal for a Look Angle of 90°: Ground Albedo = 0.0, 25 km Meteorological Range Atmosphere

maximum by several 10's of microseconds. This is especially true if the ground-reflected signal reaches the receiver position after the peak in the direct radiation.

In order to determine the time scale that should be used in comparing optical signals from different receivers, the time of 1/2 maximum power and 1/10 maximum power were determined from the POLY data. These times are shown in Tables IV and IX for ground albedos of 0.0 and 0.1.

The time at which the average power occurs in the ith time interval varies with the time interval. Since it was not possible to obtain the time at which the average power occurred in each of the time intervals directly from the POLY calculations, it was felt that it was better to assume for the purposes of this study that the average power in the ith time interval occurred at a time

$$\bar{t}_i = t_{i-1} + (t_i - t_{i-1}) \ln 2$$

for times before first maximum instead of at a time given by the midpoint of the time interval. The time of 1/2 maximum power is then given by logarithmic interpolation:

$$T_{1/2max} = \bar{t}_{j-1} + (\bar{t}_j - \bar{t}_{j-1}) \left[\ln \left(P_{1/2max} / P(\bar{t}_{j-1}) \right) / \ln \left(P(\bar{t}_j) / P(\bar{t}_{j-1}) \right) \right]$$

where $\bar{t}_{j-1}$ and $\bar{t}_j$ are the times of the two powers $P(\bar{t}_{j-1})$ and $P(\bar{t}_j)$ bounding the power $P_{1/2max}$ = 1/2 maximum power. The time of 1/10 maximum power, $T_{1/10max}$, is computed by replacing the power at 1/2 max, $P_{1/2max}$, in the above equation with the power at 1/10 maximum power $P_{1/10max}$. The times of 1/2 maximum power and 1/10 maximum power have been determined for the unattenuated source power time distribution shown in Fig. 10. The time of 1/10 maximum power was determined to be 39.09 microseconds

TABLE IV. POWER AT FIRST MAXIMUM, TIMES OF ONE-HALF AND ONE-TENTH FIRST MAXIMUM: 25 KM METEOROLOGICAL RANGE ATMOSPHERE, HEIGHT OF SOURCE = 0.5 KM, GROUND ALBEDOS = 0.0 AND 0.1

	GROUND ALBEDO # 0.0			GROUND ALBEDO # 0.1		
SOURCE TYPE	FIRST* MAX	TIME OF** 1/2 MAX	TIME OF** 1/10 MAX	FIRST* MAX	TIME OF** 1/2 MAX	TIME OF** 1/10 MAX
		LOOK ANGLE # 0 DEGREES				
FORWARD	759.0	55.11	40.57	865.0	55.69	41.09
ISOTROPIC	608.8	55.28	40.70	715.0	55.96	41.34
BACKWARD	459.0	55.58	40.96	565.0	56.38	41.73
		LOOK ANGLE # 30 DEGREES				
FORWARD	728.2	55.27	40.73	814.3	55.72	41.15
ISOTROPIC	563.9	55.43	40.86	647.5	55.99	41.38
BACKWARD	399.5	55.72	41.09	480.6	56.44	41.77
		LOOK ANGLE # 60 DEGREES				
FORWARD	539.3	55.69	41.23	577.7	55.91	41.45
ISOTROPIC	412.8	55.81	41.32	449.1	56.10	41.60
BACKWARD	286.2	56.03	41.50	320.6	56.45	41.89
		LOOK ANGLE # 70 DEGREES				
FORWARD	427.2	55.95	41.58	448.1	56.11	41.72
ISOTROPIC	326.6	56.07	41.66	346.0	56.26	41.85
BACKWARD	225.9	56.27	41.83	243.9	56.54	42.08
		LOOK ANGLE # 80 DEGREES				
FORWARD	238.7	56.47	42.32	245.6	56.56	42.41
ISOTROPIC	181.9	56.55	42.42	188.2	56.72	42.51
BACKWARD	125.1	56.82	42.54	131.2	57.26	42.72
		LOOK ANGLE # 90 DEGREES				
FORWARD	10.31	72.35	52.31	10.84	72.87	52.59
ISOTROPIC	5.229	73.39	52.77	8.725	74.01	53.11
BACKWARD	6.192	76.27	53.67	6.660	77.56	54.10

* (watts/cm^2)

** (μsec)

TABLE V. POWER AT FIRST MAXIMUM, TIMES OF ONE-HALF AND ONE-TENTH FIRST MAXIMUM: 25 KM METEOROLOGICAL RANGE ATMOSPHERE, HEIGHT OF SOURCE = 3.0 KM, GROUND ALBEDOS = 0.0 AND 0.1

	GROUND ALBEDO # 0.0			GROUND ALBEDO # 0.1		
SOURCE TYPE	FIRST* MAX	TIME OF** 1/2 MAX	TIME OF** 1/10 MAX	FIRST* MAX	TIME OF** 1/2 MAX	TIME OF** 1/10 MAX
		LOOK ANGLE # 0 DEGREES				
FORWARD	795.5	54.94	40.35	855.0	55.68	40.85
ISOTROPIC	623.2	55.12	40.48	689.7	56.17	41.20
BACKWARD	451.1	55.46	40.73	528.6	57.67	41.88
		LOOK ANGLE # 30 DEGREES				
FORWARD	740.4	55.15	40.56	790.5	55.81	41.01
ISOTROPIC	570.1	55.32	40.68	622.2	56.20	41.30
BACKWARD	400.6	55.65	40.94	460.1	57.57	41.93
		LOOK ANGLE # 60 DEGREES				
FORWARD	590.6	55.67	41.04	612.8	55.99	41.27
ISOTROPIC	451.8	55.80	41.14	474.5	56.25	41.46
BACKWARD	314.3	56.10	41.37	338.3	56.97	41.86
		LOOK ANGLE # 70 DEGREES				
FORWARD	503.9	55.91	41.34	516.7	56.11	41.49
ISOTROPIC	384.5	56.03	41.43	397.1	56.29	41.63
BACKWARD	265.9	56.28	41.63	279.4	56.82	41.95
		LOOK ANGLE # 80 DEGREES				
FORWARD	344.3	56.28	42.00	349.0	56.37	42.07
ISOTROPIC	261.9	56.37	42.07	266.2	56.49	42.16
BACKWARD	179.7	56.56	42.22	184.2	56.90	42.37
		LOOK ANGLE # 90 DEGREES				
FORWARD	39.81	60.03	44.62	400.5	60.12	44.66
ISOTROPIC	31.02	60.10	44.66	302.5	60.21	44.71
BACKWARD	20.32	60.31	44.76	206.2	60.54	44.86

* (watts/cm^2)

** (μsec)

TABLE VI. POWER AT FIRST MAXIMUM, TIMES OF ONE-HALF AND ONE-TENTH FIRST MAXIMUM: 25 KM METEOROLOGICAL RANGE ATMOSPHERE, HEIGHT OF SOURCE = 10.0 KM, GROUND ALBEDOS = 0.0 AND 0.1

	GROUND ALBEDO # 0.0			GROUND ALBEDO # 0.1		
SOURCE TYPE	FIRST* MAX	TIME OF** 1/2 MAX	TIME OF** 1/10 MAX	FIRST* MAX	TIME OF** 1/2 MAX	TIME OF** 1/10 MAX
		LOOK ANGLE # 0 DEGREES				
FORWARD	802.4	54.57	40.03	802.6	54.57	40.03
ISOTROPIC	613.6	54.65	40.09	613.7	54.65	40.09
BACKWARD	425.0	54.81	40.22	425.2	54.82	40.22
		LOOK ANGLE # 30 DEGREES				
FORWARD	746.7	54.64	40.10	747.0	54.64	40.10
ISOTROPIC	566.5	54.71	40.15	566.7	54.71	40.15
BACKWARD	387.1	54.86	40.26	387.4	54.87	40.27
		LOOK ANGLE # 60 DEGREES				
FORWARD	610.7	54.93	40.33	613.0	54.97	40.36
ISOTROPIC	462.7	55.01	40.39	469.4	55.17	40.50
BACKWARD	316.2	55.21	40.53	328.1	55.62	40.81
		LOOK ANGLE # 70 DEGREES				
FORWARD	554.5	55.24	40.58	558.9	55.33	40.64
ISOTROPIC	420.6	55.33	40.65	424.4	55.43	40.72
BACKWARD	287.2	55.52	40.79	293.2	55.75	40.95
		LOOK ANGLE # 80 DEGREES				
FORWARD	449.9	55.61	40.98	451.2	55.64	41.00
ISOTROPIC	340.3	55.67	41.03	341.4	55.70	41.05
BACKWARD	231.0	55.80	41.14	232.1	55.85	41.17
		LOOK ANGLE # 90 DEGREES				
FORWARD	107.0	56.50	42.59	107.0	56.50	42.59
ISOTROPIC	80.52	56.53	42.61	80.55	56.53	42.61
BACKWARD	54.05	56.58	42.64	54.07	56.58	42.65

* (watts/cm^2)

** (μsec)

TABLE VII. POWER AT FIRST MAXIMUM, TIMES OF ONE-HALF AND ONE-TENTH FIRST MAXIMUM: 3 KM METEOROLOGICAL RANGE ATMOSPHERE, HEIGHT OF SOURCE = 0.5 KM, GROUND ALBEDOS = 0.0 AND 0.1

	GROUND ALBEDO # 0.0			GROUND ALBEDO # 0.1		
SOURCE TYPE	FIRST* MAX	TIME OF** 1/2 MAX	TIME OF** 1/10 MAX	FIRST* MAX	TIME OF** 1/2 MAX	TIME OF** 1/10 MAX
		LOOK ANGLE # 0 DEGREES				
FORWARD	757.5	55.92	41.39	851.9	56.41	41.84
ISOTROPIC	673.1	56.10	41.55	766.6	56.62	42.04
BACKWARD	588.6	56.32	41.76	681.5	57.16	42.30
		LOOK ANGLE # 30 DEGREES				
FORWARD	791.8	55.96	41.49	878.6	56.34	41.86
ISOTROPIC	633.1	56.21	41.70	711.5	56.64	42.12
BACKWARD	474.4	56.63	42.07	546.0	57.70	42.58
		LOOK ANGLE # 60 DEGREES				
FORWARD	538.5	56.12	41.90	565.8	56.30	42.11
ISOTROPIC	422.4	56.35	42.13	446.9	56.57	42.33
BACKWARD	307.2	56.99	42.49	329.6	57.60	42.76
		LOOK ANGLE # 70 DEGREES				
FORWARD	377.5	56.22	41.92	392.2	56.38	42.06
ISOTROPIC	297.3	56.51	42.14	310.3	56.75	42.31
BACKWARD	218.1	57.52	42.59	230.0	58.02	42.81
		LOOK ANGLE # 80 DEGREES				
FORWARD	112.2	58.73	44.14	117.1	60.09	44.31
ISOTROPIC	90.02	60.62	44.53	94.62	61.07	44.74
BACKWARD	68.66	62.35	45.31	72.87	62.89	45.58
		LOOK ANGLE # 90 DEGREES				
FORWARD	5.433	79.81	58.31	5.942	79.92	58.68
ISOTROPIC	4.809	82.77	59.78	5.259	82.96	60.12
BACKWARD	4.210	87.29	62.09	4.605	87.53	62.39

* (watts/cm^2)

** (μsec)

TABLE VIII. POWER AT FIRST MAXIMUM, TIMES OF ONE-HALF AND ONE-TENTH FIRST MAXIMUM: 3 KM METEOROLOGICAL RANGE ATMOSPHERE, HEIGHT OF SOURCE = 3.0 KM, GROUND ALBEDOS = 0.0 AND 0.1

	GROUND ALBEDO # 0.0			GROUND ALBEDO # 0.1		
SOURCE TYPE	FIRST* MAX	TIME OF** 1/2 MAX	TIME OF** 1/10 MAX	FIRST* MAX	TIME OF** 1/2 MAX	TIME OF** 1/10 MAX
		LOOK ANGLE # 0 DEGREES				
FORWARD	830.6	55.48	40.73	882.4	56.11	41.17
ISOTROPIC	673.3	55.91	41.05	730.2	56.90	41.63
BACKWARD	520.9	56.88	41.66	582.3	59.35	42.47
		LOOK ANGLE # 30 DEGREES				
FORWARD	796.8	55.97	41.46	841.0	56.51	41.52
ISOTROPIC	640.0	56.53	41.55	690.0	58.08	42.09
BACKWARD	493.9	59.05	42.39	545.4	61.10	43.18
		LOOK ANGLE # 60 DEGREES				
FORWARD	648.5	56.48	41.68	664.5	56.76	41.84
ISOTROPIC	506.7	55.98	41.93	52482	57.67	42.16
BACKWARD	370.4	58.56	42.50	389.9	59.55	42.85
		LOOK ANGLE # 70 DEGREES				
FORWARD	552.0	56.50	41.84	560.4	56.64	41.93
ISOTROPIC	436.7	57.31	42.17	445.4	57.69	42.30
BACKWARD	328.1	59.48	42.95	337.5	59.99	43.14
		LOOK ANGLE # 80 DEGREES				
FORWARD	368.1	56.42	42.17	370.1	56.47	42.20
ISOTROPIC	291.6	56.56	42.27	284.0	56.63	42.33
BACKWARD	196.6	57.17	42.53	199.3	57.43	42.62
		LOOK ANGLE # 90 DEGREES				
FORWARD	15.03	66.54	48.66	15.20	66.69	48.74
ISOTROPIC	11.96	67.68	49.12	12.16	68.03	49.25
BACKWARD	8.98	70.18	50.08	9.174	70.61	50.25

* (watts/cm^2)

** (μsec)

TABLE IX. POWER AT FIRST MAXIMUM, TIMES OF ONE-HALF AND ONE-TENTH FIRST MAXIMUM: 3 KM METEOROLOGICAL RANGE ATMOSPHERE, HEIGHT OF SOURCE = 10.0 KM, GROUND ALBEDOS = 0.0 AND 0.1

	GROUND ALBEDO # 0.0			GROUND ALBEDO # 0.1		
SOURCE TYPE	FIRST* MAX	TIME OF** 1/2 MAX	TIME OF** 1/10 MAX	FIRST* MAX	TIME OF** 1/2 MAX	TIME OF** 1/10 MAX
		LOOK ANGLE # 0 DEGREES				
FORWARD	794.5	54.56	40.03	794.6	54.56	40.18
ISOTROPIC	606.1	54.63	40.08	619.2	54.87	40.24
BACKWARD	429.8	55.08	40.40	474.6	56.19	41.16
		LOOK ANGLE # 30 DEGREES				
FORWARD	733.9	54.38	39.91	785.4	55.15	40.43
ISOTROPIC	578.6	54.90	40.26	633.1	55.91	40.95
BACKWARD	436.5	56.18	41.15	486.1	58.42	41.99
		LOOK ANGLE # 60 DEGREES				
FORWARD	633.3	55.26	40.57	643.7	55.49	40.70
ISOTROPIC	484.9	55.50	40.71	495.1	55.73	40.87
BACKWARD	338.9	55.96	41.03	349.3	56.29	41.26
		LOOK ANGLE # 70 DEGREES				
FORWARD	593.2	56.10	41.18	598.5	56.20	41.25
ISOTROPIC	452.3	56.27	41.30	458.1	56.39	41.39
BACKWARD	314.1	56.65	41.58	319.6	57.08	41.71
		LOOK ANGLE # 80 DEGREES				
FORWARD	472.8	55.99	41.23	474.1	56.02	41.25
ISOTROPIC	357.8	56.06	41.28	358.8	56.09	41.30
BACKWARD	242.9	56.20	41.38	243.9	56.24	41.41
		LOOK ANGLE # 90 DEGREES				
FORWARD	108.4	56.35	42.38	408.4	56.35	42.38
ISOTROPIC	81.53	56.36	42.39	81.54	56.37	42.39
BACKWARD	54.69	56.41	42.43	54.69	56.41	42.43

* (watts/cm^2)

** (μsec)

and the time for 1/2 maximum power was determined to be 51.72 microseconds. It can be seen in Tables IV and IX that for those cases where the direct component of the radiation is dominant, i.e., small look angles and high source altitudes, the time of 1/2 maximum power is approximately 55 microseconds and the time of 1/10 maximum power is approximately 40 microseconds. The times to 1/2 maximum power and to 1/10 maximum power tend to increase in those cases where scattering predominates.

The source angular distribution has a small effect on the times of 1/2 maximum and 1/10 maximum power. For small look angles, the peaking of the source in the backward direction shifts the time of 1/2 first maximum by approximately 0.85 microseconds and the time of 1/10 first maximum by approximately 0.52 microseconds. For the 90-degree look angle, the average shift in the time of 1/2 first maximum is 2.66 microseconds and the average shift in the time of 1/10 first maximum is 1.13 microseconds; however, for those cases where the source is at 500 meters altitude, the shift in time of 1/2 first maximum is as much as 7.48 microseconds and the shift in the time of 1/10 first maximum is as much as 3.78 microseconds.

V. POLO CALCULATIONS FOR A 40-KM METEOROLOGICAL RANGE ATMOSPHERE

POLO calculations have been previously reported (Ref. 14) for receivers at synchronous satellite positions and sources within model atmospheres having ground meteorological ranges of 3, 10, and 25 km. During the reporting period additional POLO computations have been made for a model atmosphere with a 40-km meteorological range at ground level. The POLO calculations were performed for source altitudes of 0.1, 0.5, 3, and 10 km, for source wavelengths of 0.4278, 0.5, 0.6, 0.75, and 1.07 μm, and for receiver look angles of 0, 30, 45, 60, 70, 75, 80, and 90 degrees. Ten ground albedo values ranging from 0.0 to 0.9 were used. The POLO-calculated scattered fluxes were computed for delayed times between 10^{-8} and 10^{-2} secs. The source was taken in POLO to be a point-isotropic instantaneous emitter. A description of the atmospheric model and of the information made available in this new data set, as well as a discussion of the usefulness of the data, are contained in this section.

5.1 Choice of Wavelengths

Wavelengths had to be chosen such that an integration over wavelength for a realistic source distribution and receiver response in the TMTAU procedure would give accurate data without use of excessive computer time. Using data computed by use of the RADFLO computer program for a low-yield device and assuming a detector response as given in Fig. 9, the product of the RADFLO data and the receiver response function was calculated as a function of wavelength for different emission times. The resulting data are plotted in Fig. 13. It can be seen from Fig. 13 that the relative effectiveness of the radiation reaching the detector system varies greatly with both wavelength and time. For early time intervals, most of the radiation being detected is in the range between 0.4 and 0.8 μm with the maximum in the signal

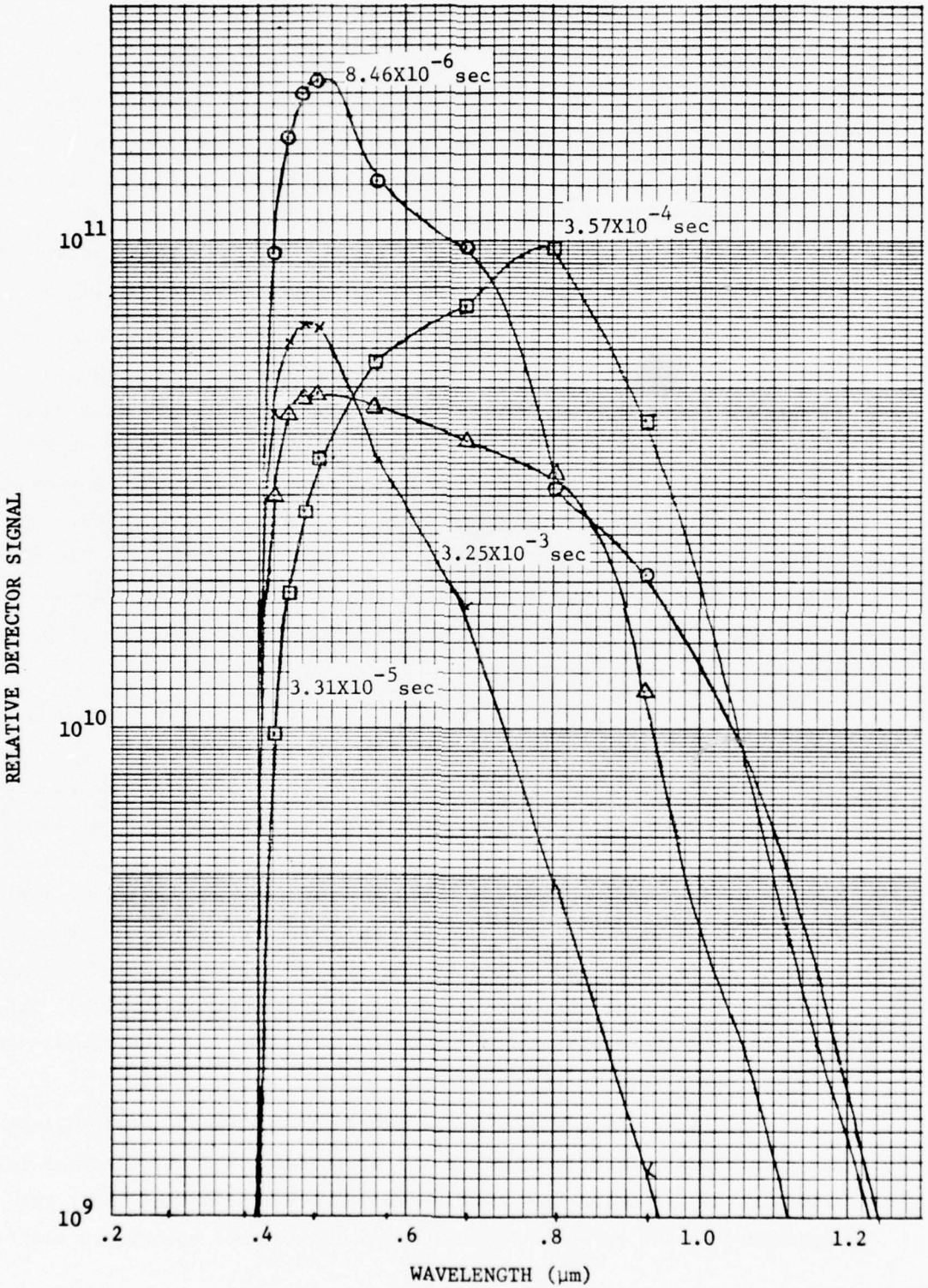

Fig. 13. Relative Detector Signal for Several Times of Emission versus Wavelength

occurring for wavelengths in the 0.44 μm to 0.49 μm interval. For later times, the wavelength at which the maximum signal occurs will shift to longer wavelengths. For larger yield devices, it is expected that the wavelength at which the maximum signal occurs for a given time will shift to longer wavelengths since the smog absorption at small wavelengths is expected to increase with increasing yield.

It is expected that the POLO-calculated transmission data would vary smoothly with wavelength. The decrease in the scattering and extinction cross sections result in scattered transmission data that reduce in magnitude with increasing wavelength, whereas the direct transmission tends to increase in magnitude with increasing wavelength. The magnitude of the total transmission data changes more rapidly at shorter wavelengths than it does for the longer wavelengths. Therefore, it was decided that the POLO problems for the 40-km meteorological range atmosphere should be run for wavelengths of 0.4278, 0.5, 0.6, 0.75, and 1.07 μm.

5.2 Model Atmosphere

The U. S. Standard Atmosphere, 1962 (Ref. 15) was used to calculate the molecular scattering coefficient as a function of altitude. The Elterman 1968 (Ref. 16) model was chosen to describe the aerosol content of the atmosphere above 5-km altitude. The value of the aerosol coefficient at sea level for 0.55 μm was chosen to give a meteorological range of 40 km. The dependency of the aerosol scattering coefficient between 0.0 and 5-km altitude was assumed to vary exponentially. The dependency of the ozone absorption coefficient upon wavelength and altitude was taken from Ref. 9.

Deirmendjian's Haze C model (Ref. 17) was assumed to describe the aerosol size distribution for all altitudes. MIE calculations for this size distribution have been performed previously (Ref. 13); the dependency of the aerosol scattering and the aerosol absorption coeffi-

cients for 0.5, 0.6, and 0.75 μm were, therefore, taken from Ref. 13. The data for 0.4278 μm and 1.07 μm were calculated from Ref. 13 under the assumption that the coefficients vary exponentially with wavelengths between 0.4 μm and 1.55 μm.

The shape of the curve giving the wavelength dependence of the aerosol scattering coefficient at sea level for the 40-km meteorological range atmosphere was found to be slightly different from that used previously (Ref. 14) for the 3-, 10-, and 25-km meteorological range atmospheres. This difference results from the fact that for the 40-km meteorological range atmosphere the variation of the aerosol scattering coefficient with wavelength was based on the MIE-2 calculations for the Haze C aerosol size distribution, whereas for the 3-, 10-, and 25-km meteorological range atmospheres the wavelength dependence of the aerosol cross section was taken from the data reported by Elterman for a "clear standard atmosphere" (Ref. 16).

The angular scattering data for the 40-km model and for 0.5, 0.6, and 0.7 μm were taken from new MIE calculations (Ref. 13). For 0.4278 and 1.07 μm, the phase functions that were used for the problems in Ref. 14 were used for the calculations for the 40-km model also.

Water vapor absorption for 1.07 μm was assumed to be negligible in the calculations for the 40-km model.

5.3 POLO Problem Parameters

There were 180 problems run with the TPOLOW version of POLO. Four source heights (0.1, 0.5, 3.0, and 10.0 kilometers), five source wavelengths (.4278, .5, .6, .75, and 1.07 microns) and eight look angles (0, 30, 45, 60, 70, 75, 80, and 90 degrees) constituted a set of 160 problems which were run for two time ranges. One hundred sixty POLO problems were run for the first time range while only 20 problems were run for the second time range. Each POLO problem computed the direct intensity and time-dependent scattered intensities for ten values of the ground albedos (0.0 to 0.9 in increments of 0.1).

The two time ranges, each containing 50 intervals, were chosen such that an overlap of 30 time intervals occurred. The early-time range was from 0 to 10^{-4} second with an upper bound for the first time interval of one shake. All problems run in this time range were run for one look angle, 5,000 histories, a maximum of 20 collisions, and five ground reflections.

A minimum weight cutoff of $5X10^{-6}$ was used to terminate histories for those photons whose weight was reduced below the cutoff value where the photon weight is defined as the fraction of the source photon that remains after undergoing absorption and scattering interactions. Biasing was used with the source angular distribution to force more of the source photons to leave the point source along directions toward the receiver position and to force collisions to occur within an ellipsoid with foci at the source and receiver positions so that the photons would arrive at the receiver within a retarded time of $5X10^{-5}$ sec. Biasing of source directions and of collision locations was used in POLO to provide the best statistical results for the early-time portion of the time-dependent scattering calculations.

The second time range was from 0 to 10^{-2} second with the upper bound of the first interval at 10^{-6} second. All problems run in this time range were run for all eight look angles, 1,500 histories, a maximum of 20 collisions and five ground reflections, a minimum weight of $5X10^{-5}$, and no biasing. Comparison of data from the two time ranges demonstrated good agreement throughout the overlap region. The average ratio of the early-time group to the late-time group in the last overlap time interval which contained information (i.e., $4.5X10^{-5} < t \leq 5X10^{-5}$) was .996 for all problems with a 0-degree look angle and .821 for all problems with a 90-degree look angle. Results for these two look angles are the best and worst (respectively) statistically. A combined set of 70 time intervals was developed by using data from the early-time group for the first 43 time intervals (0 to $5X10^{-5}$ second) and the last 27 time intervals of the late-time group ($5X10^{-5}$ to $1X10^{-2}$ second).

An eight-digit problem number was associated with each of the 180 problems. Problem numbers were of the form MMLLLNJJ where MM was the meteorological range in kilometers (always 40), LLL was the wavelength in hundredths of a micron, N indicated the source height (N = 0, 1, 2, 3 corresponding to 0.1, 0.5, 3.0, and 10.0 kilometer altitudes) and JJ was the look angle in degrees (except for JJ = 99 which indicated all eight look angles were contained in one problem). Problem numbers of data formed from combining on time were the same as the early-time problems.

The direct flux and scattered flux integrated over time for albedos of 0.0, 0.1, 0.2, 0.4, and 0.8 are tabulated in Tables X, XI, XII, and XIII as a function of look angle and source wavelength for source heights of 0.1, 0.5, 3.0, and 10 km, respectively.

5.4 Variations with Meteorological Range

Comparison of the POLO calculations for a 40-kilometer meteorological range with the data previously generated for the 3-, 10-, and 25-kilometer meteorological ranges shows for source wavelengths of 0.4278 and 0.75 μm that smooth semilogarithmic curves can easily be fitted to the data as a function of meteorological range. The data for the four different meteorological ranges can be used to generate other meteorological ranges without additional POLO calculations. Plots of this data are given in Figs. 14 and 15. Similar plots for the 1.07-micron data are given in Fig. 16.

In previous POLO calculations for meteorological ranges of 3, 10, and 25 km, the data for 1.07 μm were represented by an average over the wavelength interval from 1.025 μm to 1.175 μm. This wavelength range contains the H_2O ϕ-band around 1.13 μm. From absorption data given in Ref. 18, it was estimated for a look angle of 0° that the ϕ-band will reduce the averaged intensity within the 1.025 to 1.175 μm wavelength interval by approximately a factor of 2 over that which would have occurred if H_2O absorption were neglected, which is in good agreement with the data shown in Fig. 16. For larger look angles, only

TABLE X. DIRECT AND SCATTERED FLUXES AT A RECEIVER LOCATED AT 35800 KM ALTITUDE FROM A SOURCE LOCATED AT .1 KM IN A 40-KM METEOROLOGICAL RANGE ATMOSPHERE

(photons km^{-2}/source photon)

PROBLEM NUMBER	WAVELENGTH (MICRON)	LOOK ANGLE (DEG)	DIRECT	SCATTERED				
				ALBEDO=.0	ALBEDO=.1	ALBEDO=.2	ALBEDO=.4	ALBEDO=.9
40043000	.4278	0.	3.726E-11	2.940E-11	4.316E-11	5.754E-11	8.829E-11	1.792E-10
40043030	.4278	30.	3.297E-11	2.939E-11	4.042E-11	5.195E-11	7.664E-11	1.498E-10
40043045	.4278	45.	2.745E-11	2.731E-11	3.534E-11	4.537E-11	6.172E-11	1.151E-10
40043060	.4278	60.	1.910E-11	2.444E-11	2.929E-11	3.441E-11	4.550E-11	7.910E-11
40043070	.4278	70.	1.142E-11	2.048E-11	2.321E-11	2.606E-11	3.217E-11	5.031E-11
40043075	.4278	75.	6.985E-12	1.633E-11	1.805E-11	1.985E-11	2.372E-11	3.528E-11
40043080	.4278	80.	2.735E-12	1.302E-11	1.402E-11	1.507E-11	1.735E-11	2.433E-11
40043090	.4278	90.	1.018E-21	7.934E-13	8.830E-13	9.785E-13	1.187E-12	1.827E-12
40050000	.5000	0.	4.313E-11	2.225E-11	3.644E-11	5.108E-11	8.177E-11	1.679E-10
40050030	.5000	30.	3.904E-11	2.261E-11	3.328E-11	4.429E-11	6.740E-11	1.326E-10
40050045	.5000	45.	3.376E-11	2.191E-11	3.011E-11	3.856E-11	5.627E-11	1.060E-10
40050060	.5000	60.	2.557E-11	1.986E-11	2.464E-11	2.956E-11	3.987E-11	6.868E-11
40050070	.5000	70.	1.747E-11	1.692E-11	1.969E-11	2.254E-11	2.850E-11	4.514E-11
40050075	.5000	75.	1.221E-11	1.380E-11	1.567E-11	1.758E-11	2.160E-11	3.287E-11
40050080	.5000	80.	6.209E-12	9.861E-12	1.084E-11	1.184E-11	1.394E-11	1.984E-11
40050090	.5000	90.	4.757E-19	8.381E-13	9.073E-13	9.787E-13	1.128E-12	1.549E-12
40060000	.6000	0.	4.644E-11	1.689E-11	2.961E-11	4.260E-11	6.949E-11	1.425E-10
40060030	.6000	30.	4.252E-11	1.682E-11	2.736E-11	3.812E-11	6.035E-11	1.205E-10
40060045	.6000	45.	3.748E-11	1.652E-11	2.456E-11	3.278E-11	4.971E-11	9.536E-11
40060060	.6000	60.	2.964E-11	1.629E-11	2.101E-11	2.583E-11	3.577E-11	6.257E-11
40060070	.6000	70.	2.168E-11	1.385E-11	1.648E-11	1.916E-11	2.469E-11	3.963E-11
40060075	.6000	75.	1.625E-11	1.202E-11	1.376E-11	1.554E-11	1.921E-11	2.916E-11
40060080	.6000	80.	9.498E-12	8.362E-12	9.236E-12	1.013E-11	1.197E-11	1.699E-11
40060090	.6000	90.	3.036E-17	6.178E-13	6.542E-13	6.915E-13	7.689E-13	9.808E-13

TABLE X. (Continued)

(photons km^{-2}/source photon)

PROBLEM NUMBER	WAVELENGTH (MICRON)	LOOK ANGLE (DEG)	DIRECT	SCATTERED				
				ALBEDO=.0	ALBEDO=.1	ALBEDO=.2	ALBEDO=.4	ALBEDO=.9
40075000	.7500	0.	5.210E-11	1.310E-11	2.633E-11	3.974E-11	6.710E-11	1.388E-10
40075030	.7500	30.	4.855E-11	1.319E-11	2.424E-11	3.546E-11	5.899E-11	1.188E-10
40075045	.7500	45.	4.408E-11	1.404E-11	2.212E-11	3.031E-11	4.707E-11	9.121E-11
40075060	.7500	60.	3.726E-11	1.418E-11	1.935E-11	2.459E-11	3.530E-11	6.344E-11
40075070	.7500	70.	3.022E-11	1.355E-11	1.666E-11	1.981E-11	2.666E-11	4.319E-11
40075075	.7500	75.	2.507E-11	1.260E-11	1.461E-11	1.664E-11	2.080E-11	3.170E-11
40075080	.7500	80.	1.781E-11	1.044E-11	1.161E-11	1.279E-11	1.521E-11	2.156E-11
40075090	.7500	90.	1.996E-15	1.335E-12	1.399E-12	1.465E-12	1.599E-12	1.958E-12
40107000	1.0700	0.	5.566E-11	8.459E-12	2.158E-11	3.480E-11	6.155E-11	1.302E-10
40107030	1.0700	30.	5.240E-11	8.895E-12	1.958E-11	3.036E-11	5.217E-11	1.082E-10
40107045	1.0700	45.	4.839E-11	9.721E-12	1.772E-11	2.578E-11	4.207E-11	8.390E-11
40107060	1.0700	60.	4.251E-11	1.045E-11	1.576E-11	2.110E-11	3.191E-11	5.970E-11
40107070	1.0700	70.	3.660E-11	1.054E-11	1.374E-11	1.696E-11	2.349E-11	4.027E-11
40107075	1.0700	75.	3.225E-11	1.010E-11	1.234E-11	1.459E-11	1.916E-11	3.093E-11
40107080	1.0700	80.	2.577E-11	9.177E-12	1.048E-11	1.180E-11	1.448E-11	2.142E-11
40107090	1.0700	90.	5.867E-14	1.883E-12	1.939E-12	1.996E-12	2.111E-12	2.410E-12

TABLE XI. DIRECT AND SCATTERED FLUXES AT A RECEIVER LOCATED AT 35800 KM ALTITUDE FROM A SOURCE LOCATED AT .5 KM IN A 40-KM METEOROLOGICAL RANGE ATMOSPHERE

(photons km^{-2}/source photon)

PROBLEM NUMBER	WAVELENGTH (MICRON)	LOOK ANGLE (DEG)	DIRECT	SCATTERED				
				ALBEDO=.0	ALBEDO=.1	ALBEDO=.2	ALBEDO=.4	ALBEDO=.9
40043100	.4278	0.	3.922E-11	2.940E-11	4.276E-11	5.668E-11	8.637E-11	1.736E-10
40043130	.4278	30.	3.498E-11	2.874E-11	3.937E-11	5.047E-11	7.417E-11	1.440E-10
40043145	.4278	45.	2.951E-11	2.836E-11	3.622E-11	4.443E-11	6.197E-11	1.137E-10
40043160	.4278	60.	2.115E-11	2.682E-11	3.106E-11	3.551E-11	4.508E-11	7.375E-11
40043170	.4278	70.	1.325E-11	2.179E-11	2.430E-11	2.692E-11	3.251E-11	4.901E-11
40043175	.4278	75.	8.499E-12	1.699E-11	1.863E-11	2.034E-11	2.400E-11	3.479E-11
40043180	.4278	80.	3.653E-12	1.140E-11	1.229E-11	1.322E-11	1.524E-11	2.132E-11
40043190	.4278	90.	3.192E-20	9.355E-13	1.030E-12	1.130E-12	1.344E-12	1.980E-12
40050100	.5000	0.	4.492E-11	2.257E-11	3.583E-11	4.953E-11	7.835E-11	1.598E-10
40050130	.5000	30.	4.091E-11	2.331E-11	3.369E-11	4.442E-11	6.694E-11	1.304E-10
40050145	.5000	45.	3.575E-11	2.264E-11	3.027E-11	3.815E-11	5.468E-11	1.012E-10
40050160	.5000	60.	2.773E-11	2.068E-11	2.522E-11	2.990E-11	3.975E-11	6.754E-11
40050170	.5000	70.	1.966E-11	1.836E-11	2.095E-11	2.363E-11	2.926E-11	4.507E-11
40050175	.5000	75.	1.427E-11	1.483E-11	1.653E-11	1.829E-11	2.200E-11	3.245E-11
40050180	.5000	80.	7.818E-12	1.048E-11	1.138E-11	1.231E-11	1.426E-11	1.982E-11
40050190	.5000	90.	8.558E-18	8.753E-13	9.329E-13	9.932E-13	1.123E-12	1.509E-12
40060100	.6000	0.	4.796E-11	1.655E-11	2.897E-11	4.165E-11	6.781E-11	1.385E-10
40060130	.6000	30.	4.413E-11	1.749E-11	2.740E-11	3.753E-11	5.844E-11	1.150E-10
40060145	.6000	45.	3.922E-11	1.732E-11	2.482E-11	3.246E-11	4.821E-11	9.053E-11
40060160	.6000	60.	3.161E-11	1.661E-11	2.109E-11	2.566E-11	3.510E-11	6.060E-11
40060170	.6000	70.	2.382E-11	1.469E-11	1.719E-11	1.975E-11	2.503E-11	3.930E-11
40060175	.6000	75.	1.838E-11	1.270E-11	1.430E-11	1.594E-11	1.933E-11	2.858E-11
40060180	.6000	80.	1.140E-11	9.647E-12	1.051E-11	1.139E-11	1.322E-11	1.820E-11
40060190	.6000	90.	3.267E-16	6.339E-13	6.686E-13	7.044E-13	7.790E-13	9.863E-13

TABLE XI. (Continued)

(photons km^{-2}/source photon)

PROBLEM NUMBER	WAVELENGTH (MICRON)	LOOK ANGLE (DEG)	DIRECT	SCATTERED				
				ALBEDO=.0	ALBEDO=.1	ALBEDO=.2	ALBEDO=.4	ALBEDO=.9
40075100	.7500	0.	5.339E-11	1.237E-11	2.531E-11	3.843E-11	6.518E-11	1.353E-10
40075130	.7500	30.	4.994E-11	1.356E-11	2.350E-11	3.356E-11	5.409E-11	1.078E-10
40075145	.7500	45.	4.564E-11	1.437E-11	2.232E-11	3.037E-11	4.677E-11	8.964E-11
40075160	.7500	60.	3.913E-11	1.461E-11	1.949E-11	2.443E-11	3.450E-11	6.081E-11
40075170	.7500	70.	3.245E-11	1.420E-11	1.717E-11	2.019E-11	2.634E-11	4.244E-11
40075175	.7500	75.	2.755E-11	1.289E-11	1.493E-11	1.699E-11	2.118E-11	3.213E-11
40075180	.7500	80.	2.047E-11	1.138E-11	1.253E-11	1.370E-11	1.609E-11	2.232E-11
40075190	.7500	90.	1.289E-14	1.746E-12	1.812E-12	1.880E-12	2.017E-12	2.378E-12
40107100	1.0700	0.	5.660E-11	7.936E-12	2.002E-11	3.221E-11	5.686E-11	1.202E-10
40107130	1.0700	30.	5.343E-11	8.567E-12	1.899E-11	2.939E-11	5.040E-11	1.043E-10
40107145	1.0700	45.	4.956E-11	9.595E-12	1.744E-11	2.535E-11	4.135E-11	8.246E-11
40107160	1.0700	60.	4.396E-11	1.007E-11	1.516E-11	2.029E-11	3.064E-11	5.726E-11
40107170	1.0700	70.	3.844E-11	1.048E-11	1.357E-11	1.668E-11	2.297E-11	3.915E-11
40107175	1.0700	75.	3.441E-11	1.054E-11	1.271E-11	1.490E-11	1.931E-11	3.064E-11
40107180	1.0700	80.	2.836E-11	9.604E-12	1.089E-11	1.218E-11	1.480E-11	2.151E-11
40107190	1.0700	90.	2.172E-13	1.909E-12	1.976E-12	2.049E-12	2.197E-12	2.580E-12

TABLE XII. DIRECT AND SCATTERED FLUXES AT A RECEIVER LOCATED AT 35800 KM ALTITUDE FROM A SOURCE LOCATED AT 3.0 KM IN A 40-KM METEOROLOGICAL RANGE ATMOSPHERE

(photon km^{-2}/source photon)

PROBLEM NUMBER	WAVELENGTH (MICRON)	LOOK ANGLE (DEG)	DIRECT	SCATTERED				
				ALBEDO=.0	ALBEDO=.1	ALBEDO=.2	ALBEDO=.4	ALBEDO=.9
40043200	.4278	0.	4.703E-11	2.924E-11	4.072E-11	5.269E-11	7.820E-11	1.530E-10
40043230	.4278	30.	4.314E-11	2.895E-11	3.817E-11	4.777E-11	6.824E-11	1.282E-10
40043245	.4278	45.	3.815E-11	2.916E-11	3.563E-11	4.240E-11	5.685E-11	9.944E-11
40043260	.4278	60.	3.039E-11	2.734E-11	3.107E-11	3.499E-11	4.344E-11	6.886E-11
40043270	.4278	70.	2.247E-11	2.369E-11	2.601E-11	2.843E-11	3.362E-11	4.892E-11
40043275	.4278	75.	1.702E-11	2.017E-11	2.159E-11	2.308E-11	2.631E-11	3.602E-11
40043280	.4278	80.	1.015E-11	1.449E-11	1.527E-11	1.608E-11	1.783E-11	2.310E-11
40043290	.4278	90.	1.417E-15	1.322E-12	1.406E-12	1.494E-12	1.686E-12	2.267E-12
40050200	.5000	0.	5.147E-11	2.091E-11	3.246E-11	4.438E-11	6.937E-11	1.398E-10
40050230	.5000	30.	4.788E-11	2.184E-11	3.100E-11	4.045E-11	6.032E-11	1.165E-10
40050245	.5000	45.	4.333E-11	2.306E-11	2.985E-11	3.684E-11	5.152E-11	9.288E-11
40050260	.5000	60.	3.638E-11	2.125E-11	2.522E-11	2.933E-11	3.795E-11	6.232E-11
40050270	.5000	70.	2.920E-11	1.885E-11	2.113E-11	2.347E-11	2.841E-11	4.238E-11
40050275	.5000	75.	2.401E-11	1.717E-11	1.867E-11	2.022E-11	2.347E-11	3.274E-11
40050280	.5000	80.	1.683E-11	1.370E-11	1.452E-11	1.537E-11	1.716E-11	2.226E-11
40050290	.5000	90.	4.780E-14	1.367E-12	1.428E-12	1.491E-12	1.625E-12	2.011E-12
40060200	.6000	0.	5.316E-11	1.411E-11	2.478E-11	3.569E-11	5.825E-11	1.193E-10
40060230	.6000	30.	4.969E-11	1.497E-11	2.360E-11	3.242E-11	5.065E-11	9.983E-11
40060245	.6000	45.	4.536E-11	1.572E-11	2.234E-11	2.909E-11	4.303E-11	8.055E-11
40060260	.6000	60.	3.881E-11	1.687E-11	2.072E-11	2.467E-11	3.284E-11	5.494E-11
40060270	.6000	70.	3.211E-11	1.564E-11	1.788E-11	2.016E-11	2.489E-11	3.766E-11
40060275	.6000	75.	2.724E-11	1.415E-11	1.558E-11	1.703E-11	2.003E-11	2.817E-11
40060280	.6000	80.	2.034E-11	1.173E-11	1.249E-11	1.326E-11	1.486E-11	1.921E-11
40060290	.6000	90.	3.190E-13	1.112E-12	1.147E-12	1.183E-12	1.258E-12	1.463E-12

TABLE XII. (Continued)

(photons km^{-2}/source photon)

PROBLEM NUMBER	WAVELENGTH (MICRON)	LOOK ANGLE (DEG)	DIRECT	SCATTERED				
				ALBEDO=.0	ALBEDO=.1	ALBEDO=.2	ALBEDO=.4	ALBEDO=.9
40075200	.7500	0.	5.756E-11	9.240E-12	2.097E-11	3.285E-11	5.705E-11	1.204E-10
40075230	.7500	30.	5.447E-11	1.014E-11	1.926E-11	2.850E-11	4.737E-11	9.686E-11
40075245	.7500	45.	5.075E-11	1.097E-11	1.807E-11	2.527E-11	3.995E-11	7.840E-11
40075260	.7500	60.	4.546E-11	1.198E-11	1.633E-11	2.073E-11	2.970E-11	5.319E-11
40075270	.7500	70.	4.038E-11	1.254E-11	1.512E-11	1.772E-11	2.304E-11	3.696E-11
40075275	.7500	75.	3.673E-11	1.221E-11	1.390E-11	1.562E-11	1.911E-11	2.826E-11
40075280	.7500	80.	3.132E-11	1.153E-11	1.250E-11	1.349E-11	1.550E-11	2.076E-11
40075290	.7500	90.	2.602E-12	2.678E-12	2.739E-12	2.802E-12	2.931E-12	3.281E-12
40107200	1.0700	0.	5.952E-11	5.648E-12	1.695E-11	2.834E-11	5.136E-11	1.105E-10
40107230	1.0700	30.	5.661E-11	6.186E-12	1.583E-11	2.554E-11	4.517E-11	9.548E-11
40107245	1.0700	45.	5.320E-11	7.089E-12	1.418E-11	2.133E-11	3.576E-11	7.271E-11
40107260	1.0700	60.	4.859E-11	8.403E-12	1.303E-11	1.768E-11	2.709E-11	5.117E-11
40107270	1.0700	70.	4.448E-11	9.645E-12	1.247E-11	1.531E-11	2.105E-11	3.576E-11
40107275	1.0700	75.	4.170E-11	9.414E-12	1.130E-11	1.319E-11	1.702E-11	2.682E-11
40107280	1.0700	80.	3.769E-11	9.579E-12	1.073E-11	1.188E-11	1.421E-11	2.019E-11
40107290	1.0700	90.	8.542E-12	3.206E-12	3.271E-12	3.336E-12	3.469E-12	3.807E-12

TABLE XIII. DIRECT AND SCATTERED FLUXES AT A RECEIVER LOCATED AT 35800 KM ALTITUDE FROM A SOURCE LOCATED AT 10.0 KM IN A 40-KM METEOROLOGICAL RANGE ATMOSPHERE

(photons km^{-2}/source photon)

PROBLEM NUMBER	WAVELENGTH (MICRON)	LOOK ANGLE (DEG)	DIRECT	SCATTERED				
				ALBEDO=.0	ALBEDO=.1	ALBEDO=.2	ALBEDO=.4	ALBEDO=.9
40043300	.4278	0.	5.548E-11	3.012E-11	3.866E-11	4.761E-11	6.679E-11	1.238E-10
40043330	.4278	30.	5.220E-11	2.845E-11	3.528E-11	4.344E-11	5.778E-11	1.034E-10
40043345	.4278	45.	4.816E-11	2.635E-11	3.360E-11	3.908E-11	5.077E-11	8.526E-11
40043360	.4278	60.	4.221E-11	2.849E-11	3.172E-11	3.509E-11	4.226E-11	6.319E-11
40043370	.4278	70.	3.623E-11	2.460E-11	2.635E-11	2.816E-11	3.206E-11	4.368E-11
40043375	.4278	75.	3.184E-11	2.245E-11	2.385E-11	2.529E-11	2.835E-11	3.714E-11
40043380	.4278	80.	2.536E-11	1.884E-11	1.949E-11	2.017E-11	2.161E-11	2.583E-11
40043390	.4278	90.	6.565E-13	2.493E-12	2.563E-12	2.635E-12	2.786E-12	3.211E-12
40050300	.5000	0.	5.714E-11	1.907E-11	2.823E-11	3.765E-11	5.733E-11	1.121E-10
40050330	.5000	30.	5.400E-11	1.966E-11	2.690E-11	3.436E-11	4.998E-11	9.377E-11
40050345	.5000	45.	5.021E-11	2.106E-11	2.654E-11	3.213E-11	4.400E-11	7.704E-11
40050360	.5000	60.	4.477E-11	2.029E-11	2.556E-11	2.693E-11	3.398E-11	5.366E-11
40050370	.5000	70.	3.948E-11	1.869E-11	2.057E-11	2.251E-11	2.696E-11	3.788E-11
40050375	.5000	75.	3.565E-11	1.727E-11	1.854E-11	1.984E-11	2.258E-11	3.022E-11
40050380	.5000	80.	2.995E-11	1.479E-11	1.551E-11	1.625E-11	1.779E-11	2.210E-11
40050390	.5000	90.	2.461E-12	2.347E-12	2.406E-12	2.466E-12	2.593E-12	2.950E-12
40060300	.6000	0.	5.687E-11	1.163E-11	2.079E-11	3.015E-11	4.951E-11	1.019E-10
40060330	.6000	30.	5.371E-11	1.224E-11	1.972E-11	2.736E-11	4.316E-11	8.591E-11
40060345	.6000	45.	4.987E-11	1.318E-11	1.878E-11	2.450E-11	3.633E-11	6.829E-11
40060360	.6000	60.	4.435E-11	1.334E-11	1.677E-11	2.027E-11	2.750E-11	4.702E-11
40060370	.6000	70.	3.896E-11	1.299E-11	1.503E-11	1.711E-11	2.142E-11	3.408E-11
40060375	.6000	75.	3.507E-11	1.215E-11	1.345E-11	1.478E-11	1.753E-11	2.495E-11
40060380	.6000	80.	2.932E-11	1.029E-11	1.101E-11	1.175E-11	1.326E-11	1.735E-11
40060390	.6000	90.	3.645E-12	1.752E-12	1.794E-12	1.837E-12	1.925E-12	2.166E-12

TABLE XIII. (Continued)

(photons km^{-2}/source photon)

PROBLEM NUMBER	WAVELENGTH (MICRON)	LOOK ANGLE (DEG)	DIRECT	SCATTERED				
				ALBEDO=.0	ALBEDO=.1	ALBEDO=.2	ALBEDO=.4	ALBEDO=.9
40075300	.7500	0.	5.996E-11	7.280E-12	1.770E-11	2.826E-11	4.979E-11	1.062E-10
40075330	.7500	30.	5.709E-11	7.750E-12	1.634E-11	2.509E-11	4.275E-11	8.911E-11
40075345	.7500	45.	5.375E-11	8.650E-12	1.523E-11	2.190E-11	3.547E-11	7.096E-11
40075360	.7500	60.	4.928E-11	9.578E-12	1.362E-11	1.771E-11	2.605E-11	4.788E-11
40075370	.7500	70.	4.540E-11	1.039E-11	1.292E-11	1.547E-11	2.067E-11	3.423E-11
40075375	.7500	75.	4.283E-11	1.068E-11	1.238E-11	1.411E-11	1.762E-11	2.677E-11
40075380	.7500	80.	3.918E-11	1.058E-11	1.155E-11	1.254E-11	1.455E-11	1.977E-11
40075390	.7500	90.	1.362E-11	3.491E-12	3.558E-12	3.625E-12	3.762E-12	4.116E-12
40107300	1.0700	0.	6.093E-11	4.074E-12	1.475E-11	2.551E-11	4.727E-11	1.031E-10
40107330	1.0700	30.	5.816E-11	4.420E-12	1.322E-11	2.209E-11	4.003E-11	8.608E-11
40107345	1.0700	45.	5.497E-11	5.191E-12	1.196E-11	1.879E-11	3.259E-11	6.801E-11
40107360	1.0700	60.	5.088E-11	6.477E-12	1.074E-11	1.504E-11	2.373E-11	4.600E-11
40107370	1.0700	70.	4.755E-11	6.493E-12	9.229E-12	1.199E-11	1.756E-11	3.184E-11
40107375	1.0700	75.	4.552E-11	7.644E-12	9.630E-12	1.163E-11	1.567E-11	2.604E-11
40107380	1.0700	80.	4.282E-11	8.110E-12	9.272E-12	1.044E-11	1.281E-11	1.891E-11
40107390	1.0700	90.	2.303E-11	4.105E-12	4.191E-12	4.278E-12	4.453E-12	4.900E-12

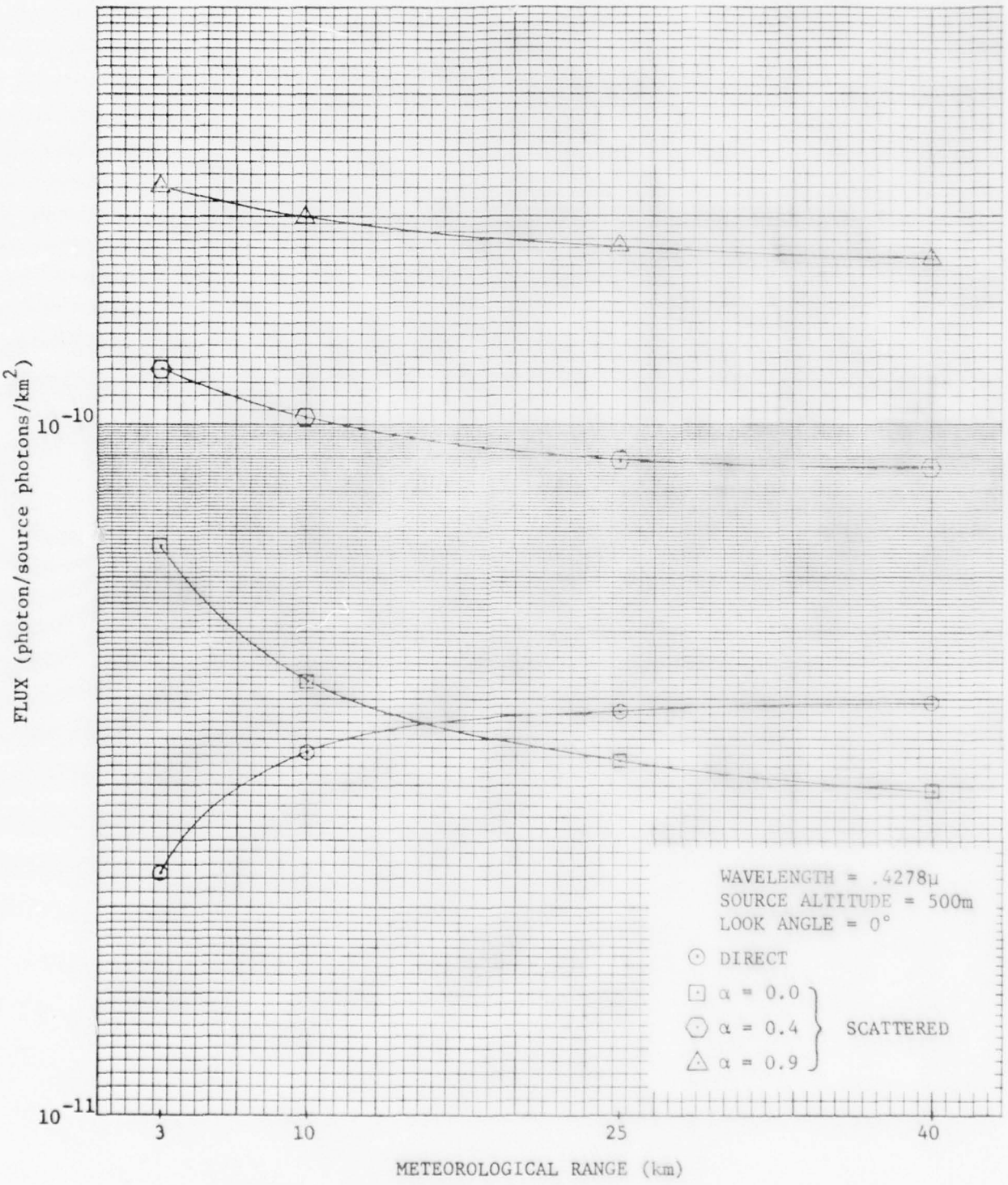

Fig. 14. Variation of POLO Calculations for 0.4278-micron Wavelength Light with Meteorological Range

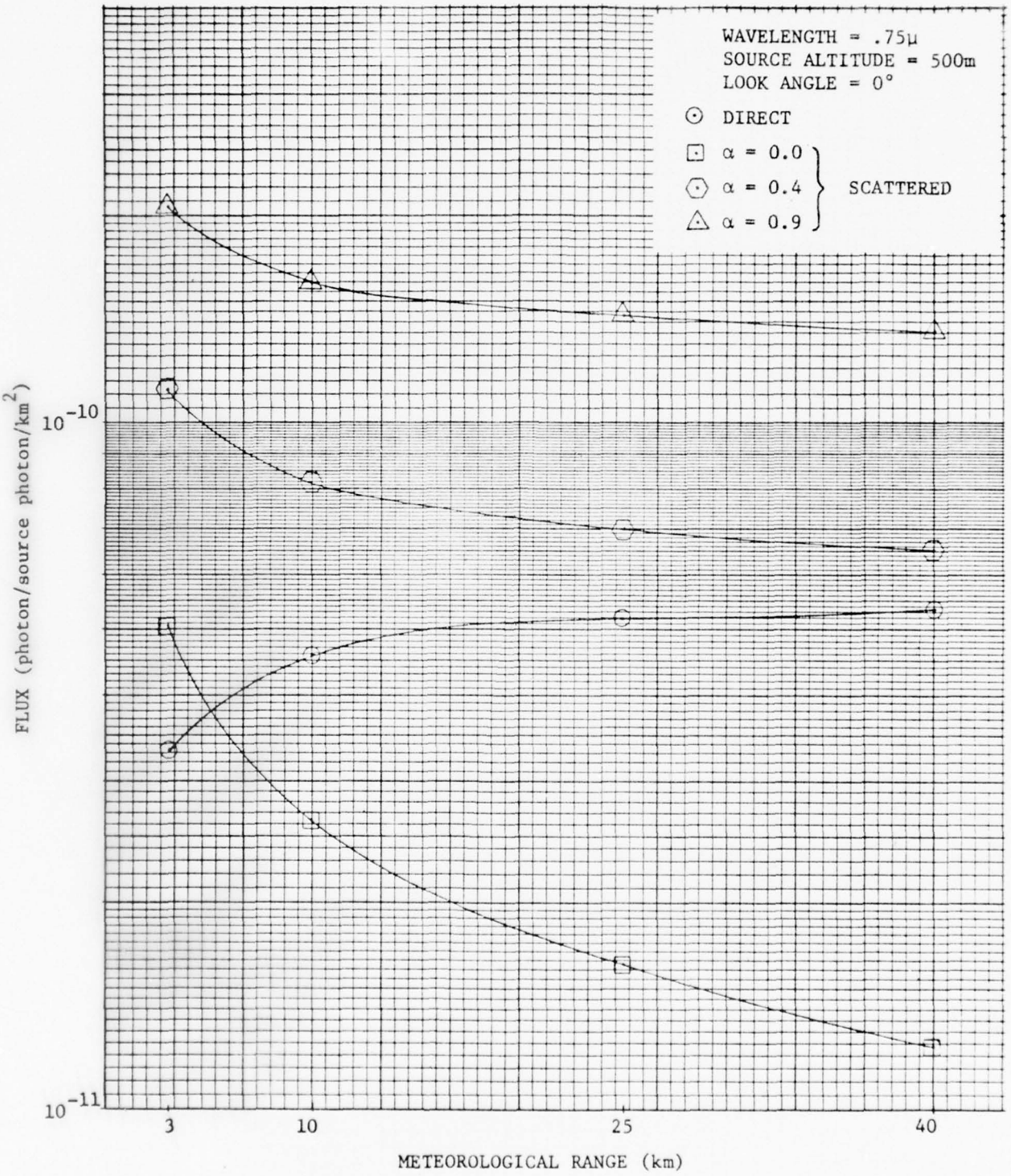

Fig. 15. Variation of POLO Calculations for 0.75-micron Wavelength Light with Meteorological Range

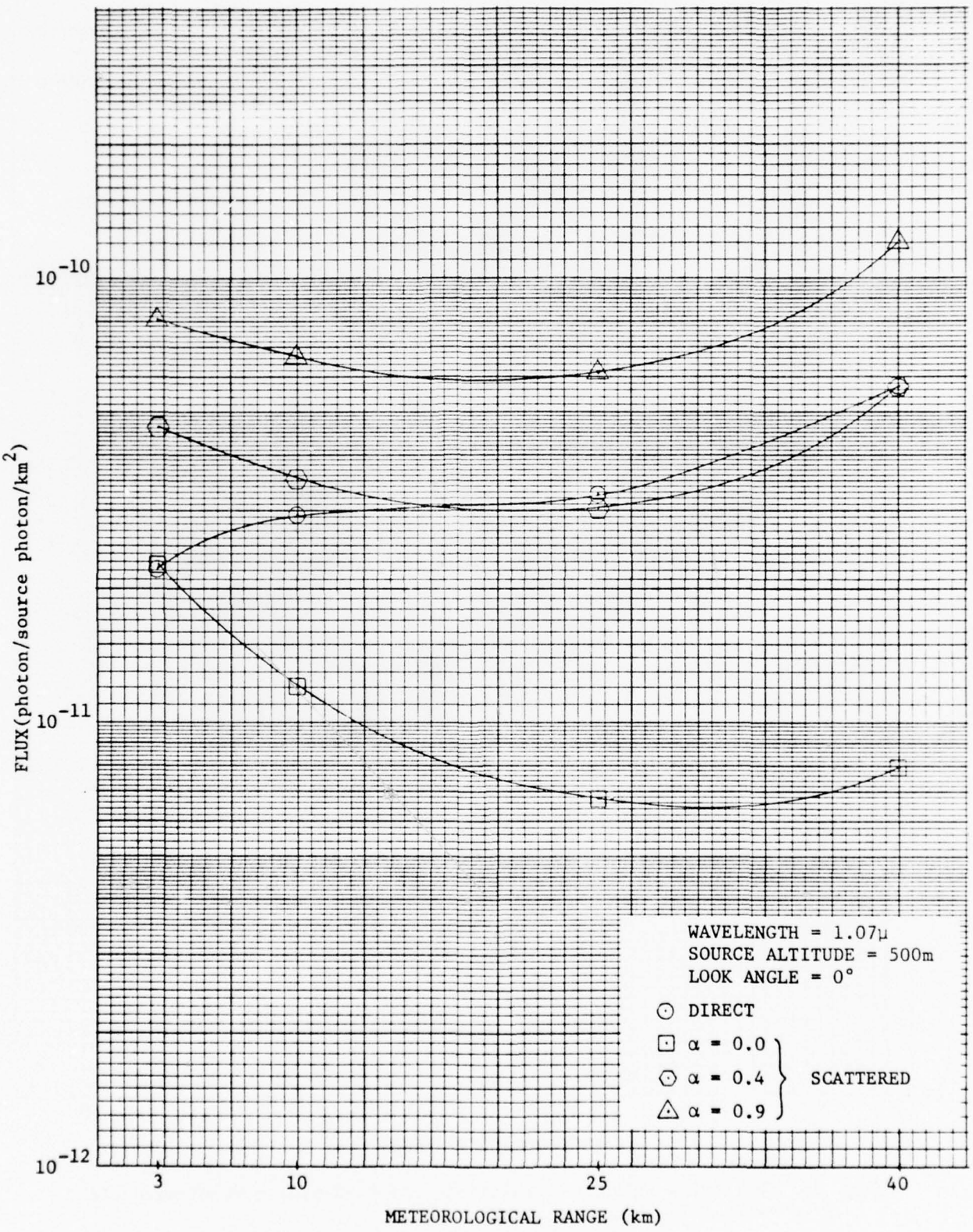

Fig. 16. Variation of POLO Calculations for 1.07-micron Wavelength Light with Meteorological Range

small additional effects of the H_2O band are expected and there should be no appreciable further reduction in intensity.

The data shown in Ref. 18 reveal further that there is no sizeable absorption by H_2O (or any other absorbing species) in the range 1.00 - 1.07 μm. Even though the previous POLO calculations were accomplished for three subintervals ranging from 1.025 μm - 1.075 μm, 1.075 μ - 1.125 μm, and 1.125 μm - 1.175 μm, no printout was obtained for the data within these small subintervals and, therefore, no direct comparison with the new data, which neglected water vapor absorption, can be obtained.

5.5 Curve-Fit Coefficients for Input to TMTAU

To use the POLO data for a 40-km meteorological range atmosphere in the TMTAU code requires that the data be expressed mathematically as a series of exponential terms. Two codes, CFIT and DFIT, were developed to curve fit the POLO data in this manner. The fitted data is output in a format suitable for input to TMTAU. CFIT and DFIT were developed from the TPOFIT code which was used previously to fit the POLO data for atmospheres with ground-level meteorological ranges of 3, 10, and 25 km.

The POLO data are given as, $I_S(t)$, the scattered flux at the receiver within differential time bins. The curve-fit codes first calculates the cumulative scattered flux, $I(\tau)$, as a function of retarded time, τ, by

$$I(\tau) = \int_0^{\tau} I_S(t)dt \quad .$$

A typical set of these curves is shown in Fig. 17. The family of curves shown there is for a source altitude of 0.5 km, a wavelength of 0.6 microns, and an albedo of $\alpha = 0.9$. These curves were plotted from 70 data points for times ranging from 10^{-8} to 10^{-2} seconds. The receiver angle parameter denotes the polar position angle between the

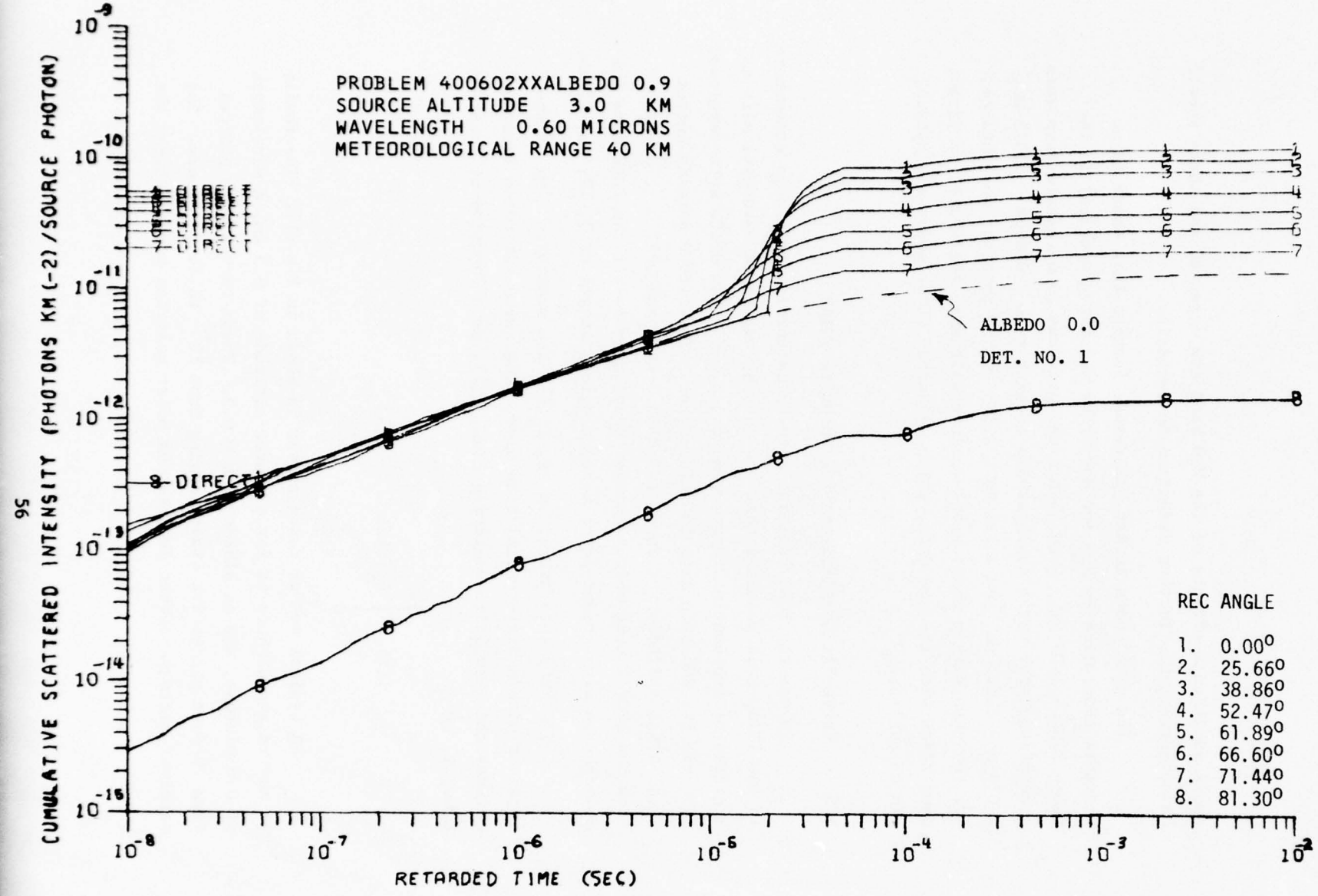

Fig. 17. Example Plot of the Cumulative Intensity vs Retarded Time for λ = 0.6 micron, Source Height = 3 km

radials through the source and detector positions. A drastic change in slope for the curves plotted in Fig. 17 can be noted at the point of inflection, τ_o, for the curves for receiver polar position angles one through seven. It is at this time that the reflected intensity from the ground starts arriving at the detector. The dashed line in Fig. 17 shows $I(\tau)$ for receiver polar position angle number one ($\theta_o = 0°$) and for a ground albedo of 0. In fitting the POLO data, a maximum of six terms were used for the zero albedo case. A maximum of three terms were used to fit the reflected contributions past time τ_o. Thus, the data are expressed as:

$$I(\tau) = K_1 - \sum_{i=1}^{i\leq 6} a_i e^{-b_i \tau} + K_2 - \sum_{j=1}^{j\leq 3} a_j e^{-b_j(\tau-\tau_o)} \qquad (1)$$

where:

K_1 = maximum $I(\tau)$ for zero albedo case,

K_2 = maximum $I(\tau)$, including reflection, minus K_1,

τ_o = earliest arrival time of reflected photons.

It is the function of the curve-fit codes to evaluate the a_i, a_j, b_i, and b_j constants for each curve. The method used to obtain these constants has been described in Ref. 3 as a "partitioned least squares" method.

Data output from the curve-fitting codes consists of two files, print and punch. The print file is usually assigned to the line printer. A sample print file output is shown in Table XIV and listing of a sample set of the punch file data is shown in Table XV.

The sample listing in Table XIV shows only the first 35 of the 70 time points which were used. Pairs of curve-fit coefficients are shown at the top of the page. Whenever a pair are both zero, this means that less than the maximum allowable number of terms (6 for zero albedo,

TABLE XIV. SAMPLE LISTING OF THE PRINT FILE FROM THE CFIT CODE

ALBEDO	PART	K	A1	B1	A2	B2	A3	B3
.8	1	9.24027E-12	1.82166E-12	-3.19544E 03	5.43251E-12	-2.22634E 04	1.73472E-12	-5.86479E 05
			2.43991E-13	-2.94124E 07	.00000E 00	.00000E 00	.00000E 00	.00000E 00
	2	9.81229E-11	2.69651E-11	-4.95341E 03	6.89566E-11	-9.69626E 04	.00000E 00	.00000E 00

TIME	POLO DATA	FITTED DATA	DEVIATION	PERCENT ERROR	DIFF DATA	DERIVATIVE
1.500E-08	1.1132339E-13	1.113232BE-13	-1.0842022E-19	-9.7392054E-05	5.7501347E-06	5.7515472E-06
2.000E-08	1.4356328E-13	1.3845782E-13	-5.1054538E-15	-3.5562391E 00	6.4479773E-06	5.1172447E-06
3.000E-08	1.8322258E-13	1.8427360E-13	1.0510256E-15	5.7363284E-01	3.9659299E-06	4.0958930E-06
4.000E-08	2.2123709E-13	2.2123536E-13	-1.7347235E-18	-7.8410143E-04	3.8014523E-06	3.3333245E-06
5.000E-08	2.5055170E-13	2.5158174E-13	1.0300463E-15	4.1111112E-01	2.9314588E-06	2.7636106E-06
6.000E-08	2.6873724E-13	2.7698416E-13	8.2469296E-15	3.0687704E 00	1.8185556E-06	2.3376142E-06
7.000E-08	2.9811836E-13	2.9868902E-13	5.7066981E-16	1.9142389E-01	2.9381263E-06	2.0187254E-06
8.500E-08	3.2888709E-13	3.2627633E-13	-2.6107588E-15	-7.9381573E-01	2.0512471E-06	1.6834792E-06
1.000E-07	3.6266405E-13	3.4977316E-13	-1.2890893E-14	-3.5544987E 00	2.2517870E-06	1.4648340E-06
1.500E-07	4.7049094E-13	4.1329180E-13	-5.7199146E-14	-1.2157327E 01	2.1565402E-06	1.1451293E-06
2.000E-07	5.4755853E-13	4.6779507E-13	-7.9763453E-14	-1.4567106E 01	1.5413516E-06	1.0510084E-06
2.500E-07	6.0394571E-13	5.1920881E-13	-8.4736905E-14	-1.4030545E 01	1.1277425E-06	1.0093181E-06
3.000E-07	6.7876591E-13	5.6892425E-13	-1.0984166E-13	-1.6182541E 01	1.4964025E-06	9.8025157E-07
3.500E-07	7.2641356E-13	6.1728921E-13	-1.0912435E-13	-1.5022343E 01	9.5295331E-07	9.5464566E-07
4.000E-07	7.6905827E-13	6.6441123E-13	-1.0464703E-13	-1.3607162E 01	8.5289537E-07	9.3038062E-07
5.000E-07	8.6507966E-13	7.5511819E-13	-1.0996146E-13	-1.2711137E 01	9.6021267E-07	8.8422638E-07
6.000E-07	9.2051713E-13	8.4134436E-13	-7.9172779E-14	-8.6008959E 00	5.5437465E-07	8.4073349E-07
7.000E-07	9.8718082E-13	9.2334560E-13	-6.3835222E-14	-6.4664125E 00	6.6663711E-07	7.9970636E-07
8.500E-07	1.0625641E-12	1.0389476E-12	-2.3616525E-14	-2.2225971E 00	5.0255511E-07	7.4247680E-07
1.000E-06	1.1463018E-12	1.1463287E-12	2.6888214E-17	2.3456479E-03	5.5825342E-07	6.9003539E-07
1.500E-06	1.3970014E-12	1.4533002E-12	5.6298716E-14	4.0299673E 00	5.0139909E-07	5.4487731E-07
2.000E-06	1.5899277E-12	1.6972838E-12	1.0735596E-13	6.7522526E 00	3.8585267E-07	4.3629137E-07
2.500E-06	1.7203027E-12	1.8941246E-12	1.7382189E-13	1.0104143E 01	2.6074963E-07	3.5498601E-07
3.000E-06	1.8929355E-12	2.0556508E-12	1.6271533E-13	8.5959253E 00	3.4526596E-07	2.9403151E-07
4.000E-06	2.1424737E-12	2.3057918E-12	1.6331814E-13	7.6228733E 00	2.4953812E-07	2.1381226E-07
5.000E-06	2.3756214E-12	2.4946564E-12	1.1903499E-13	5.0106878E 00	2.3314760E-07	1.6812959E-07
6.000E-06	2.5970641E-12	2.6483893E-12	5.1325263E-14	1.9762793E 00	2.2144275E-07	1.4168154E-07
7.000E-06	2.7359651E-12	2.7815545E-12	4.5589400E-14	1.6662998E 00	1.3890099E-07	1.2595626E-07
8.000E-06	2.8697227E-12	2.9022765E-12	3.2553821E-14	1.1343880E 00	1.3375751E-07	1.1621802E-07
9.000E-06	2.9936132E-12	3.0150969E-12	2.1483683E-14	7.1765035E-01	1.2389052E-07	1.0983183E-07
1.000E-05	3.1274766E-12	3.1225630E-12	-4.9136042E-15	-1.5711081E-01	1.3386335E-07	1.0533165E-07
1.250E-05	3.4687869E-12	3.3757953E-12	-9.2991587E-14	-2.6808090E 00	1.3652408E-07	9.7825250E-08
1.500E-05	3.7075317E-12	3.6132547E-12	-9.4277017E-14	-2.5428505E 00	9.5497910E-08	9.2311154E-08
1.750E-05	3.9340657E-12	3.8378762E-12	-9.6189549E-14	-2.4450407E 00	9.0614037E-08	8.7459966E-08
2.000E-05	4.1667676E-12	4.0508343E-12	-1.1593330E-13	-2.7823315E 00	9.3080530E-08	8.2953875E-08

TABLE XV. PUNCH FILE OUTPUT FROM CURVE-FITTING POLO DATA

```
PROB050100REC 1DIRI=4.4921E-11 MIN D/S=  .281TCRIT=1.5000E-08
2.2572E-115.0259E-126.3999E 038.6928E-124.1215E 046.5697E-123.7126E 05050100 1 1
1.9654E-127.9558E 06 .0000E 00 .0000E 00 .0000E 00 .0000E 00
 .0000E 00 .0000E 00 .0000E 00 .0000E 00 .0000E 00 .0000E 00 .0000E 008.0000E-03
2.2572E-115.0259E-126.3999E 038.6928E-124.1215E 046.5697E-123.7126E 05050100 1 3
1.9654E-127.9558E 06 .0000E 00 .0000E 00 .0000E 00 .0000E 00
2.6954E-114.8664E-125.7283E 032.3733E-126.3190E 04 .0000E 00 .0000E 002.0000E-05
2.2572E-115.0259E-126.3999E 038.6928E-124.1215E 046.5697E-123.7126E 05050100 1 6
1.9654E-127.9558E 06 .0000E 00 .0000E 00 .0000E 00 .0000E 00
7.0947E-111.4677E-115.5662E 036.5286E-126.4091E 04 .0000E 00 .0000E 002.0000E-05
2.2572E-115.0259E-126.3999E 038.6928E-124.1215E 046.5697E-123.7126E 05050100 1 9
1.9654E-127.9558E 06 .0000E 00 .0000E 00 .0000E 00 .0000E 00
1.1977E-102.8053E-115.4157E 031.1430E-116.2744E 04 .0000E 00 .0000E 002.0000E-05
PROB050130REC 2DIRI=4.0915E-11 MIN D/S=  .314TCRIT=1.5000E-08
2.3307E-113.9131E-123.4113E 031.1389E-114.2832E 045.7832E-124.1089E 05050130 2 1
1.6501E-124.6111E 06 .0000E 00 .0000E 00 .0000E 00 .0000E 00
 .0000E 00 .0000E 00 .0000E 00 .0000E 00 .0000E 00 .0000E 00 .0000E 008.0000E-03
1.6501E-124.6111E 06 .0000E 00 .0000E 00 .0000E 00 .0000E 00
2.1112E-113.8709E-125.0447E 032.3198E-126.2258E 04 .0000E 00 .0000E 001.5000E-05
2.3307E-113.9131E-123.4113E 031.1389E-114.2832E 045.7832E-124.1089E 05050130 2 6
1.6501E-124.6111E 06 .0000E 00 .0000E 00 .0000E 00 .0000E 00
5.5465E-111.1633E-114.9024E 037.8644E-126.9559E 04 .0000E 00 .0000E 001.5000E-05
2.3307E-113.9131E-123.4113E 031.1389E-114.2832E 045.7832E-124.1089E 05050130 2 9
1.6501E-124.6111E 06 .0000E 00 .0000E 00 .0000E 00 .0000E 00
9.3485E-112.2201E-114.7872E 031.3397E-116.8123E 04 .0000E 00 .0000E 001.5000E-05
PROB050145REC 3DIRI=3.5754E-11 MIN D/S=  .353TCRIT=1.5000E-08
2.2639E-114.2617E-124.1327E 031.0494E-114.7300E 045.4400E-123.9599E 05050145 3 1
1.9848E-125.2783E 06 .0000E 00 .0000E 00 .0000E 00 .0000E 00
 .0000E 00 .0000E 00 .0000E 00 .0000E 00 .0000E 00 .0000E 00 .0000E 008.0000E-03
2.2639E-114.2617E-124.1327E 031.0494E-114.7300E 045.4400E-123.9599E 05050145 3 3
1.9848E-125.2783E 06 .0000E 00 .0000E 00 .0000E 00 .0000E 00
1.5511E-113.0068E-124.7859E 032.6084E-127.3848E 04 .0000E 00 .0000E 001.2500E-05
2.2639E-114.2617E-124.1327E 031.0494E-114.7300E 045.4400E-123.9599E 05050145 3 6
1.9848E-125.2783E 06 .0000E 00 .0000E 00 .0000E 00 .0000E 00
4.0722E-118.9672E-124.7115E 036.8894E-127.2138E 04 .0000E 00 .0000E 001.2500E-05
2.2639E-114.2617E-124.1327E 031.0494E-114.7300E 045.4400E-123.9599E 05050145 3 9
1.9848E-125.2783E 06 .0000E 00 .0000E 00 .0000E 00 .0000E 00
6.8591E-111.7000E-114.6357E 031.1609E-117.0619E 04 .0000E 00 .0000E 001.2500E-05
PROB050160REC 4DIRI=2.7730E-11 MIN D/S=  .411TCRIT=1.5000E-08
2.0678E-114.2011E-123.2749E 039.0001E-124.4932E 045.2766E-123.6954E 05050160 4 1
1.9019E-125.0768E 06 .0000E 00 .0000E 00 .0000E 00 .0000E 00
 .0000E 00 .0000E 00 .0000E 00 .0000E 00 .0000E 00 .0000E 00 .0000E 008.0000E-03
2.0678E-114.2011E-123.2749E 039.0001E-124.4932E 045.2766E-123.6954E 05050160 4 3
1.9019E-125.0768E 06 .0000E 00 .0000E 00 .0000E 00 .0000E 00
9.2229E-121.9670E-123.8858E 031.6595E-126.1885E 04 .0000E 00 .0000E 001.0000E-05
2.0678E-114.2011E-123.2749E 039.0001E-124.4932E 045.2766E-123.6954E 05050160 4 6
1.9019E-125.0768E 06 .0000E 00 .0000E 00 .0000E 00 .0000E 00
2.4249E-115.7998E-123.9159E 035.1127E-127.0636E 04 .0000E 00 .0000E 001.0000E-05
2.0678E-114.2011E-123.2749E 039.0001E-124.4932E 045.2766E-123.6954E 05050160 4 9
1.9019E-125.0768E 06 .0000E 00 .0000E 00 .0000E 00 .0000E 00
4.0903E-111.0899E-113.9308E 038.5128E-126.9181E 04 .0000E 00 .0000E 001.0000E-05
```

TABLE XV. (Continued)

```
PROB050170REC 5DIRI=1.9663E-11 MIN D/S=  .436TCRIT=1.5000E-08
1.8358E-113.5491E-123.1391E 039.3303E-125.5455E 044.2470E-127.6339E 05050170 5 1
9.6032E-138.2788E 06 .0000E 00 .0000E 00 .0000E 00 .0000E 00
 .0000E 00 .0000E 00 .0000E 00 .0000E 00 .0000E 00 .0000E 00 .0000E 008.0000E-03
1.8358E-113.5491E-123.1391E 039.3303E-125.5455E 044.2470E-127.6339E 05050170 5 3
9.6032E-138.2788E 06 .0000E 00 .0000E 00 .0000E 00 .0000E 00
5.2754E-121.3428E-123.8677E 031.4720E-127.0498E 04 .0000E 00 .0000E 007.0000E-06
1.8358E-113.5491E-123.1391E 039.3303E-125.5455E 044.2470E-127.6339E 05050170 5 6
9.6032E-138.2788E 06 .0000E 00 .0000E 00 .0000E 00 .0000E 00
1.3850E-113.8816E-123.8799E 033.8266E-126.9561E 04 .0000E 00 .0000E 007.0000E-06
1.8358E-113.5491E-123.1391E 039.3303E-125.5455E 044.2470E-127.6339E 05050170 5 9
9.6032E-138.2788E 06 .0000E 00 .0000E 00 .0000E 00 .0000E 00
2.3329E-117.1679E-123.8819E 036.3527E-126.8804E 04 .0000E 00 .0000E 007.0000E-06
PROB050175REC 6DIRI=1.4271E-11 MIN D/S=  .440TCRIT=1.5000E-08
1.4827E-113.2515E-123.0974E 036.5050E-124.5665E 043.0914E-124.0913E 05050175 6 1
1.7188E-123.5467E 06 .0000E 00 .0000E 00 .0000E 00 .0000E 00
 .0000E 00 .0000E 00 .0000E 00 .0000E 00 .0000E 00 .0000E 00 .0000E 008.0000E-03
1.4827E-113.2515E-123.0974E 036.5050E-124.5665E 043.0914E-124.0913E 05050175 6 3
1.7188E-123.5467E 06 .0000E 00 .0000E 00 .0000E 00 .0000E 00
9.4663E-121.0165E-123.8838E 031.3116E-126.7850E 04 .0000E 00 .0000E 004.0000E-06
1.4827E-113.2515E-123.0974E 036.5050E-124.5665E 043.0914E-124.0913E 05050175 6 6
1.7188E-123.5467E 06 .0000E 00 .0000E 00 .0000E 00 .0000E 00
9.1163E-122.9117E-123.8867E 033.4144E-126.7201E 04 .0000E 00 .0000E 004.0000E-06
1.4827E-113.2515E-123.0974E 036.5050E-124.5665E 043.0914E-124.0913E 05050175 6 9
1.7188E-123.5467E 06 .0000E 00 .0000E 00 .0000E 00 .0000E 00
1.5381E-115.3334E-123.8806E 035.6463E-126.6550E 04 .0000E 00 .0000E 004.0000E-06
PROB050180REC 7DIRI=7.8177E-12 MIN D/S=  .394TCRIT=1.5000E-08
1.0481E-112.9217E-123.7316E 034.0945E-124.4525E 041.5526E-122.3745E 05050180 7 1
1.6064E-121.9096E 06 .0000E 00 .0000E 00 .0000E 00 .0000E 00
 .0000E 00 .0000E 00 .0000E 00 .0000E 00 .0000E 00 .0000E 00 .0000E 008.0000E-03
1.0481E-112.9217E-123.7316E 034.0945E-124.4525E 041.5526E-122.3745E 05050180 7 3
1.6064E-121.9096E 06 .0000E 00 .0000E 00 .0000E 00 .0000E 00
1.8261E-127.2418E-133.8531E 038.2408E-136.4920E 04 .0000E 00 .0000E 002.5000E-06
1.0481E-112.9217E-123.7316E 034.0945E-124.4525E 041.5526E-122.3745E 05050180 7 6
1.6064E-121.9096E 06 .0000E 00 .0000E 00 .0000E 00 .0000E 00
4.8115E-122.0325E-123.8547E 032.0922E-126.4352E 04 .0000E 00 .0000E 002.5000E-06
1.0481E-112.9217E-123.7316E 034.0945E-124.4525E 041.5526E-122.3745E 05050180 7 9
1.6064E-121.9096E 06 .0000E 00 .0000E 00 .0000E 00 .0000E 00
8.1414E-123.6643E-123.8509E 033.3862E-126.3829E 04 .0000E 00 .0000E 002.5000E-06
PROB050190REC 8DIRI=8.5583E-18 MIN D/S=  .000TCRIT=2.5000E-06
8.7532E-136.2088E-135.5831E 032.6294E-133.4404E 04 .0000E 00 .0000E 00050190 8 1
 .0000E 00 .0000E 00 .0000E 00 .0000E 00 .0000E 00 .0000E 00
 .0000E 00 .0000E 00 .0000E 00 .0000E 00 .0000E 00 .0000E 00 .0000E 008.0000E-03
8.7532E-136.2088E-135.5831E 032.6294E-133.4404E 04 .0000E 00 .0000E 00050190 8 3
 .0000E 00 .0000E 00 .0000E 00 .0000E 00 .0000E 00 .0000E 00
1.1784E-131.2407E-137.5080E 03 .0000E 00 .0000E 00 .0000E 00 .0000E 001.0000E-06
8.7532E-136.2088E-135.5831E 032.6294E-133.4404E 04 .0000E 00 .0000E 00050190 8 6
 .0000E 00 .0000E 00 .0000E 00 .0000E 00 .0000E 00 .0000E 00
3.1699E-133.3272E-137.0604E 03 .0000E 00 .0000E 00 .0000E 00 .0000E 001.0000E-06
8.7532E-136.2088E-135.5831E 032.6294E-133.4404E 04 .0000E 00 .0000E 00050190 8 9
 .0000E 00 .0000E 00 .0000E 00 .0000E 00 .0000E 00 .0000E 00
5.4856E-135.7399E-136.6059E 03 .0000E 00 .0000E 00 .0000E 00 .0000E 001.0000E-06
```

9 for other albedo cases) were used to fit the curves. The number of terms to be used is a user input option to the curve-fitting codes.

The column headed POLO DATA in Table XIV is the cumulative sum of the POLO data; the column FITTED DATA is the cumulative sum calculated by the code using the curve-fit coefficients. The STANDARD DEVIATION AND PERCENT ERROR are calculated in the standard manner and refer to the difference in the POLO DATA and the FITTED DATA in the output from the CFIT code. If the output is from the DFIT code, then they refer to the difference between DIFF DATA and DERIVATIVE. The DIFF DATA is calculated numerically from the POLO DATA as $\Delta I/\Delta t$, whereas DERIVATIVE data is the analytic derivative, dI/dt, of the curve which is produced by inserting the curve-fit coefficients in the above equation. Both codes make several tries at generating an adequate set of curve-fit coefficients. Each code selects the best set of these coefficients based on the standard deviation calculated over all time points.

The problem parameters used to define the POLO problems for which curve-fitted data were generated are shown in Table XVI. The curve-fit parameters were all generated using the CFIT code. An eight-digit problem number is associated with each of the 160 problems. Problem numbers are of the form MM LLL N XX where:

MM is the meteorological range in kilometers,
LLL is the wavelength in hundredths of microns,
N is associated with the source height (N = 0,1,2,3 corresponds to 0.1, 0.5, 3.0, and 10.0 km),
XX is the look angle in degrees.

The POLO problems for the 40-km meteorological range atmosphere were all run for detectors positioned at synchronous satellite altitude. In Table XVI the XX number always varies over each eight-problem set as 0, 30, 45, 60, 70, 75, 80, and 90. For each problem curve-fit data were obtained for ground albedo values of 0.0, 0.2, 0.5, and 0.8.

The punch file output shown in Table XV is a sample listing of a selected part of the data which now exists on punched cards. The

TABLE XVI. SEQUENCE OF CURVE-FITTED POLO DATA FROM CFIT PUNCH FILE

40-KM METEOROLOGICAL RANGE

SEQUENCE NUMBER	PROBLEM NUMBER	SOURCE ALT(km)	WAVELENGTH OF SOURCE(μm)
1-8	400430XX	0.1	0.43
9-16	400500XX	0.1	0.50
17-24	400600XX	0.1	0.60
25-32	400750XX	0.1	0.75
33-40	401070XX	0.1	1.07
41-48	400431XX	0.5	0.43
49-56	400501XX	0.5	0.50
57-64	400601XX	0.5	0.60
65-72	400751XX	0.5	0.75
73-80	401071XX	0.5	1.07
81-88	400432XX	3.0	0.43
89-96	400502XX	3.0	0.50
97-104	400602XX	3.0	0.60
105-112	400752XX	3.0	0.75
113-120	401072XX	3.0	1.07
121-128	400433XX	10.0	0.43
129-136	400503XX	10.0	0.50
137-144	400603XX	10.0	0.60
145-152	400753XX	10.0	0.75
153-160	401073XX	10.0	1.07

format of these data is compatible with the input requirements of the TMTAU program. Note that in the problem number, the number 40 has been dropped as a prefix. The angle set which is the last two digits refers to the look angle rather than receiver angle.

Curve-fit coefficients of the POLO results for the 40-kilometer visibility atmosphere were generated for four different values of the ground albedo, 0.0, 0.2, 0.5, and 0.8, and these data now exist on tape at AFTAC. Since the TMTAU procedure assumes that curve-fit data for ten values of the ground albedo are on tape, the remaining data (data for ground albedo values other than 0.0, 0.2, 0.5, and 0.8) were given values of zero and stored on the tape in the appropriate places. Therefore, the existing version of TMTAU can be used with the 40-km meteorological range data if the ground albedo requested is one of the four mentioned above. The data resides on tape number 001706 (a standard label, TAPE9, external label FORTYKM-RBL, tape) in three forms.

Label 1 (DSN=FORTY) contains card images of the data for only four values of the ground albedo. Label 2 (DSN=FORTY10) contains card images of the data spaced for all ten albedos. That is, there are three blank cards inserted for the data for each missing value of the ground albedo. Both label 1 and label 2 have DCB=(RECFM=FB,LRECL=80,BLKSIZE=3200).

Figure 18 shows the data for problem 40043300 as it resides under label 1. Label 3 (DSN-FORTYB) contains the curve-fit data in binary format which is the required format of the TMTAU and TMTRF01 procedures. Label 3 has DCB=(RECFM=VS,LRECL=92,BLKSIZE=3200). Problem numbers for the data are those discussed above with the exception that the card image data shows the problem number modulo 40000000.

Figure 19 shows a list of the header cards from the 160 problems which reside on tape 1706 with the addition of a sequencing number. On cards, the P in PROB is in column one.

```
PROB043300REC 1DIRI=5.5482E-11 MIN D/S=  .448TCRIT=1.5000E-08
3.0125E-111.4796E-114.9939E 031.2350E-118.4449E 032.5177E-125.5746E 05043300 1 1
2.9007E-133.1733E 07 .0000E 00 .0000E 00 .0000E 00 .0000E 00
 .0000E 00 .0000E 00 .0000E 00 .0000E 00 .0000E 00 .0000E 00 .0000E 008.0000E-03
3.0125E-111.4796E-114.9939E 031.2350E-118.4449E 032.5177E-125.5746E 05043300 1 3
2.9007E-133.1733E 07 .0000E 00 .0000E 00 .0000E 00 .0000E 00
1.7480E-111.9994E-111.3437E 04 .0000E 00 .0000E 00 .0000E 00 .0000E 005.0000E-05
3.0125E-111.4796E-114.9939E 031.2350E-118.4449E 032.5177E-125.5746E 05043300 1 6
2.9007E-133.1733E 07 .0000E 00 .0000E 00 .0000E 00 .0000E 00
4.6972E-115.3228E-111.2505E 04 .0000E 00 .0000E 00 .0000E 00 .0000E 005.0000E-05
3.0125E-111.4796E-114.9939E 031.2350E-118.4449E 032.5177E-125.5746E 05043300 1 9
2.9007E-133.1733E 07 .0000E 00 .0000E 00 .0000E 00 .0000E 00
8.1123E-119.1095E-111.1595E 04 .0000E 00 .0000E 00 .0000E 00 .0000E 005.0000E-05
```

Fig. 18. Curve-Fit Coefficients for POLO Problem 40043300

```
 1  PROB043300REC 1DIRI=5.5482E-11 MIN D/S=   .448TCRIT=1.5000E-08
 2  PROB043330REC 2DIRI=5.2199E-11 MIN D/S=   .505TCRIT=1.5000E-08
 3  PROB043345REC 3DIRI=4.8161E-11 MIN D/S=   .565TCRIT=1.5000E-08
 4  PROB043360REC 4DIRI=4.2209E-11 MIN D/S=   .668TCRIT=1.5000E-08
 5  PROB043370REC 5DIRI=3.6232E-11 MIN D/S=   .829TCRIT=1.5000E-08
 6  PROB043375REC 6DIRI=3.1844E-11 MIN D/S=   .957TCRIT=1.5000E-08
 7  PROB043380REC 7DIRI=2.5356E-11 MIN D/S=   .982TCRIT=1.5000E-08
 8  PROB043390REC 8DIRI=6.5649E-13 MIN D/S=   .204TCRIT=1.5000E-08
 9  PROB050300REC 1DIRI=5.7141E-11 MIN D/S=   .510TCRIT=1.5000E-08
10  PROB050330REC 2DIRI=5.4004E-11 MIN D/S=   .576TCRIT=1.5000E-08
11  PROB050345REC 3DIRI=5.0208E-11 MIN D/S=   .652TCRIT=1.5000E-08
12  PROB050360REC 4DIRI=4.4766E-11 MIN D/S=   .834TCRIT=1.5000E-08
13  PROB050370REC 5DIRI=3.9476E-11 MIN D/S= 1.042TCRIT=1.5000E-08
14  PROB050375REC 6DIRI=3.5650E-11 MIN D/S= 1.180TCRIT=1.5000E-08
15  PROB050380REC 7DIRI=2.9950E-11 MIN D/S= 1.355TCRIT=1.5000E-08
16  PROB050390REC 8DIRI=2.4613E-12 MIN D/S=   .834TCRIT=1.5000E-08
17  PROB060300REC 1DIRI=5.6869E-11 MIN D/S=   .558TCRIT=1.5000E-08
18  PROB060330REC 2DIRI=5.3709E-11 MIN D/S=   .625TCRIT=1.5000E-08
19  PROB060345REC 3DIRI=4.9874E-11 MIN D/S=   .730TCRIT=1.5000E-08
20  PROB060360REC 4DIRI=4.4352E-11 MIN D/S=   .943TCRIT=1.5000E-08
21  PROB060370REC 5DIRI=3.8963E-11 MIN D/S= 1.178TCRIT=1.5000E-08
22  PROB060375REC 6DIRI=3.5069E-11 MIN D/S= 1.406TCRIT=1.5000E-08
23  PROB060380REC 7DIRI=2.9323E-11 MIN D/S= 1.690TCRIT=1.5000E-08
24  PROB060390REC 8DIRI=3.6454E-12 MIN D/S= 1.683TCRIT=1.5000E-08
25  PROB075300REC 1DIRI=5.9963E-11 MIN D/S=   .564TCRIT=1.5000E-08
26  PROB075330REC 2DIRI=5.7095E-11 MIN D/S=   .641TCRIT=1.5000E-08
27  PROB075345REC 3DIRI=5.3747E-11 MIN D/S=   .757TCRIT=1.5000E-08
28  PROB075360REC 4DIRI=4.9282E-11 MIN D/S= 1.029TCRIT=1.5000E-08
29  PROB075370REC 5DIRI=4.5401E-11 MIN D/S= 1.326TCRIT=1.5000E-08
30  PROB075375REC 6DIRI=4.2832E-11 MIN D/S= 1.600TCRIT=1.5000E-08
31  PROB075380REC 7DIRI=3.9178E-11 MIN D/S= 1.982TCRIT=1.5000E-08
32  PROB075390REC 8DIRI=1.3617E-11 MIN D/S= 3.308TCRIT=1.5000E-08
33  PROB107300REC 1DIRI=6.0928E-11 MIN D/S=   .591TCRIT=1.5000E-08
34  PROB107330REC 2DIRI=5.8157E-11 MIN D/S=   .676TCRIT=1.5000E-08
35  PROB107345REC 3DIRI=5.4974E-11 MIN D/S=   .808TCRIT=1.5000E-08
36  PROB107360REC 4DIRI=5.0877E-11 MIN D/S= 1.106TCRIT=1.5000E-08
37  PROB107370REC 5DIRI=4.7553E-11 MIN D/S= 1.494TCRIT=1.5000E-08
38  PROB107375REC 6DIRI=4.5516E-11 MIN D/S= 1.748TCRIT=1.5000E-08
39  PROB107380REC 7DIRI=4.2816E-11 MIN D/S= 2.264TCRIT=1.5000E-08
40  PROB107390REC 8DIRI=2.3025E-11 MIN D/S= 4.699TCRIT=1.5000E-08
```

Fig. 19. Header Cards for Curve-Fit Data on Tape 1706

```
41  PROB043100REC 1DIRI=3.9216E-11 MIN D/S=  .226TCRIT=1.5000E-08
42  PROB043130REC 2DIRI=3.4978E-11 MIN D/S=  .243TCRIT=1.5000E-08
43  PROB043145REC 3DIRI=2.9511E-11 MIN D/S=  .259TCRIT=1.5000E-08
44  PROB043160REC 4DIRI=2.1149E-11 MIN D/S=  .287TCRIT=1.5000E-08
45  PROB043170REC 5DIRI=1.3254E-11 MIN D/S=  .270TCRIT=1.5000E-08
46  PROB043175REC 6DIRI=8.4988E-12 MIN D/S=  .244TCRIT=1.5000E-08
47  PROB043180REC 7DIRI=3.6527E-12 MIN D/S=  .171TCRIT=1.5000E-08
48  PROB043190REC 8DIRI=3.1924E-20 MIN D/S=  .000TCRIT=2.5000E-06
49  PROB050100REC 1DIRI=4.4921E-11 MIN D/S=  .281TCRIT=1.5000E-08
50  PROB050130REC 2DIRI=4.0915E-11 MIN D/S=  .314TCRIT=1.5000E-08
51  PROB050145REC 3DIRI=3.5754E-11 MIN D/S=  .353TCRIT=1.5000E-08
52  PROB050160REC 4DIRI=2.7730E-11 MIN D/S=  .411TCRIT=1.5000E-08
53  PROB050170REC 5DIRI=1.9663E-11 MIN D/S=  .436TCRIT=1.5000E-08
54  PROB050175REC 6DIRI=1.4271E-11 MIN D/S=  .440TCRIT=1.5000E-08
55  PROB050180REC 7DIRI=7.8177E-12 MIN D/S=  .394TCRIT=1.5000E-08
56  PROB050190REC 8DIRI=8.5583E-18 MIN D/S=  .000TCRIT=2.5000E-06
57  PROB060100REC 1DIRI=4.7961E-11 MIN D/S=  .346TCRIT=1.5000E-08
58  PROB060130REC 2DIRI=4.4129E-11 MIN D/S=  .384TCRIT=1.5000E-08
59  PROB060145REC 3DIRI=3.9223E-11 MIN D/S=  .433TCRIT=1.5000E-08
60  PROB060160REC 4DIRI=3.1611E-11 MIN D/S=  .522TCRIT=1.5000E-08
61  PROB060170REC 5DIRI=2.3816E-11 MIN D/S=  .606TCRIT=1.5000E-08
62  PROB060175REC 6DIRI=1.8385E-11 MIN D/S=  .643TCRIT=1.5000E-08
63  PROB060180REC 7DIRI=1.1400E-11 MIN D/S=  .626TCRIT=1.5000E-08
64  PROB060190REC 8DIRI=3.2669E-16 MIN D/S=  .000TCRIT=5.0000E-07
65  PROB075100REC 1DIRI=5.3391E-11 MIN D/S=  .395TCRIT=1.5000E-08
66  PROB075130REC 2DIRI=4.9944E-11 MIN D/S=  .463TCRIT=1.5000E-08
67  PROB075145REC 3DIRI=4.5636E-11 MIN D/S=  .509TCRIT=1.5000E-08
68  PROB075160REC 4DIRI=3.9129E-11 MIN D/S=  .643TCRIT=1.5000E-08
69  PROB075170REC 5DIRI=3.2451E-11 MIN D/S=  .765TCRIT=1.5000E-08
70  PROB075175REC 6DIRI=2.7547E-11 MIN D/S=  .857TCRIT=1.5000E-08
71  PROB075180REC 7DIRI=2.0474E-11 MIN D/S=  .917TCRIT=1.5000E-08
72  PROB075190REC 8DIRI=1.2894E-14 MIN D/S=  .005TCRIT=5.0000E-07
73  PROB107100REC 1DIRI=5.6601E-11 MIN D/S=  .471TCRIT=1.5000E-08
74  PROB107130REC 2DIRI=5.3425E-11 MIN D/S=  .512TCRIT=1.5000E-08
75  PROB107145REC 3DIRI=4.9559E-11 MIN D/S=  .601TCRIT=1.5000E-08
76  PROB107160REC 4DIRI=4.3959E-11 MIN D/S=  .768TCRIT=1.5000E-08
77  PROB107170REC 5DIRI=3.8440E-11 MIN D/S=  .982TCRIT=1.5000E-08
78  PROB107175REC 6DIRI=3.4408E-11 MIN D/S= 1.123TCRIT=1.5000E-08
79  PROB107180REC 7DIRI=2.8362E-11 MIN D/S= 1.319TCRIT=1.5000E-08
80  PROB107190REC 8DIRI=2.1719E-13 MIN D/S=  .084TCRIT=1.5000E-08
```

Fig. 19. (Continued)

```
 81  PROB043200REC 1DIRI=4.7033E-11 MIN D/S=   .307TCRIT=1.5000E-06
 82  PROB043230REC 2DIRI=4.3141E-11 MIN D/S=   .337TCRIT=1.5000E-08
 83  PROB043245REC 3DIRI=3.8148E-11 MIN D/S=   .384TCRIT=1.5000E-08
 84  PROB043260REC 4DIRI=3.0387E-11 MIN D/S=   .441TCRIT=1.5000E-08
 85  PROB043270REC 5DIRI=2.2471E-11 MIN D/S=   .459TCRIT=1.5000E-06
 86  PROB043275REC 6DIRI=1.7018E-11 MIN D/S=   .472TCRIT=1.5000E-08
 87  PROB043280REC 7DIRI=1.0149E-11 MIN D/S=   .439TCRIT=1.5000E-08
 88  PROB043290REC 8DIRI=1.4167E-15 MIN D/S=   .001TCRIT=5.0000E-07
 89  PROB050200REC 1DIRI=5.1471E-11 MIN D/S=   .368TCRIT=1.5000E-08
 90  PROB050230REC 2DIRI=4.7875E-11 MIN D/S=   .411TCRIT=1.5000E-08
 91  PROB050245REC 3DIRI=4.3333E-11 MIN D/S=   .467TCRIT=1.5000E-08
 92  PROB050260REC 4DIRI=3.6377E-11 MIN D/S=   .584TCRIT=1.5000E-08
 93  PROB050270REC 5DIRI=2.9202E-11 MIN D/S=   .689TCRIT=1.5000E-08
 94  PROB050275REC 6DIRI=2.4014E-11 MIN D/S=   .734TCRIT=1.5000E-08
 95  PROB050280REC 7DIRI=1.6830E-11 MIN D/S=   .756TCRIT=1.5000E-08
 96  PROB050290REC 8DIRI=4.7797E-14 MIN D/S=   .024TCRIT=5.0000E-07
 97  PROB060200REC 1DIRI=5.3160E-11 MIN D/S=   .446TCRIT=1.5000E-08
 98  PROB060230REC 2DIRI=4.9694E-11 MIN D/S=   .497TCRIT=1.5000E-08
 99  PROB060245REC 3DIRI=4.5359E-11 MIN D/S=   .563TCRIT=1.5000E-08
100  PROB060260REC 4DIRI=3.8809E-11 MIN D/S=   .706TCRIT=1.5000E-08
101  PROB060270REC 5DIRI=3.2111E-11 MIN D/S=   .853TCRIT=1.5000E-08
102  PROB060275REC 6DIRI=2.7240E-11 MIN D/S=   .967TCRIT=1.5000E-08
103  PROB060280REC 7DIRI=2.0343E-11 MIN D/S= 1.059TCRIT=1.5000E-08
104  PROB060290REC 8DIRI=3.1899E-13 MIN D/S=   .218TCRIT=1.5000E-08
105  PROB075200REC 1DIRI=5.7561E-11 MIN D/S=   .478TCRIT=1.5000E-08
106  PROB075230REC 2DIRI=5.4470E-11 MIN D/S=   .562TCRIT=1.5000E-08
107  PROB075245REC 3DIRI=5.0747E-11 MIN D/S=   .647TCRIT=1.5000E-08
108  PROB075260REC 4DIRI=4.5457E-11 MIN D/S=   .855TCRIT=1.5000E-08
109  PROB075270REC 5DIRI=4.0378E-11 MIN D/S= 1.092TCRIT=1.5000E-08
110  PROB075275REC 6DIRI=3.6734E-11 MIN D/S= 1.300TCRIT=5.0000E-07
111  PROB075280REC 7DIRI=3.1321E-11 MIN D/S= 1.508TCRIT=5.0000E-07
112  PROB075290REC 8DIRI=2.6020E-12 MIN D/S=   .793TCRIT=1.5000E-08
113  PROB107200REC 1DIRI=5.9517E-11 MIN D/S=   .539TCRIT=1.5000E-08
114  PROB107230REC 2DIRI=5.6613E-11 MIN D/S=   .593TCRIT=1.5000E-08
115  PROB107245REC 3DIRI=5.3200E-11 MIN D/S=   .732TCRIT=1.5000E-08
116  PROB107260REC 4DIRI=4.8587E-11 MIN D/S=   .949TCRIT=1.5000E-08
117  PROB107270REC 5DIRI=4.4481E-11 MIN D/S= 1.244TCRIT=1.5000E-08
118  PROB107275REC 6DIRI=4.1703E-11 MIN D/S= 1.555TCRIT=5.0000E-07
119  PROB107280REC 7DIRI=3.7689E-11 MIN D/S= 1.867TCRIT=5.0000E-07
120  PROB107290REC 8DIRI=8.5423E-12 MIN D/S= 2.244TCRIT=1.5000E-08
```

Fig. 19. (Continued)

```
121  PROB043300REC 1DIRI=5.5482E-11 MIN D/S=  .448TCRIT=1.5000E-08
122  PROB043330REC 2DIRI=5.2199E-11 MIN D/S=  .505TCRIT=1.5000E-08
123  PROB043345REC 3DIRI=4.8161E-11 MIN D/S=  .565TCRIT=1.5000E-08
124  PROB043360REC 4DIRI=4.2209E-11 MIN D/S=  .668TCRIT=1.5000E-08
125  PROB043370REC 5DIRI=3.6232E-11 MIN D/S=  .829TCRIT=1.5000E-08
126  PROB043375REC 6DIRI=3.1844E-11 MIN D/S=  .857TCRIT=1.5000E-08
127  PROB043380REC 7DIRI=2.5356E-11 MIN D/S=  .982TCRIT=1.5000E-08
128  PROB043390REC 8DIRI=6.5649E-13 MIN D/S=  .204TCRIT=1.5000E-08
129  PROB050300REC 1DIRI=5.7141E-11 MIN D/S=  .510TCRIT=1.5000E-08
130  PROB050330REC 2DIRI=5.4004E-11 MIN D/S=  .576TCRIT=1.5000E-08
131  PROB050345REC 3DIRI=5.0208E-11 MIN D/S=  .652TCRIT=1.5000E-08
132  PROB050360REC 4DIRI=4.4766E-11 MIN D/S=  .834TCRIT=1.5000E-08
133  PROB050370REC 5DIRI=3.9476E-11 MIN D/S= 1.042TCRIT=1.5000E-08
134  PROB050375REC 6DIRI=3.5650E-11 MIN D/S= 1.180TCRIT=1.5000E-08
135  PROB050380REC 7DIRI=2.9950E-11 MIN D/S= 1.355TCRIT=1.5000E-08
136  PROB050390REC 8DIRI=2.4613E-12 MIN D/S=  .834TCRIT=1.5000E-08
137  PROB060300REC 1DIRI=5.6869E-11 MIN D/S=  .558TCRIT=1.5000E-08
138  PROB060330REC 2DIRI=5.3709E-11 MIN D/S=  .625TCRIT=1.5000E-08
139  PROB060345REC 3DIRI=4.9874E-11 MIN D/S=  .730TCRIT=1.5000E-08
140  PROB060360REC 4DIRI=4.4352E-11 MIN D/S=  .943TCRIT=1.5000E-08
141  PROB060370REC 5DIRI=3.8963E-11 MIN D/S= 1.178TCRIT=1.5000E-08
142  PROB060375REC 6DIRI=3.5069E-11 MIN D/S= 1.406TCRIT=1.5000E-08
143  PROB060380REC 7DIRI=2.9323E-11 MIN D/S= 1.690TCRIT=1.5000E-08
144  PROB060390REC 8DIRI=3.6454E-12 MIN D/S= 1.683TCRIT=1.5000E-08
145  PROB075300REC 1DIRI=5.9963E-11 MIN D/S=  .564TCRIT=1.5000E-08
146  PROB075330REC 2DIRI=5.7095E-11 MIN D/S=  .641TCRIT=1.5000E-08
147  PROB075345REC 3DIRI=5.3747E-11 MIN D/S=  .757TCRIT=1.5000E-08
148  PROB075360REC 4DIRI=4.9282E-11 MIN D/S= 1.029TCRIT=1.5000E-08
149  PROB075370REC 5DIRI=4.5401E-11 MIN D/S= 1.326TCRIT=1.5000E-08
150  PROB075375REC 6DIRI=4.2832E-11 MIN D/S= 1.600TCRIT=1.5000E-08
151  PROB075380REC 7DIRI=3.9178E-11 MIN D/S= 1.982TCRIT=1.5000E-08
152  PROB075390REC 8DIRI=1.3617E-11 MIN D/S= 3.308TCRIT=1.5000E-08
153  PROB107300REC 1DIRI=6.0928E-11 MIN D/S=  .591TCRIT=1.5000E-08
154  PROB107330REC 2DIRI=5.8157E-11 MIN D/S=  .676TCRIT=1.5000E-08
155  PROB107345REC 3DIRI=5.4974E-11 MIN D/S=  .808TCRIT=1.5000E-08
156  PROB107360REC 4DIRI=5.0877E-11 MIN D/S= 1.106TCRIT=1.5000E-08
157  PROB107370REC 5DIRI=4.7553E-11 MIN D/S= 1.494TCRIT=1.5000E-08
158  PROB107375REC 6DIRI=4.5516E-11 MIN D/S= 1.748TCRIT=1.5000E-08
159  PROB107380REC 7DIRI=4.2816E-11 MIN D/S= 2.264TCRIT=1.5000E-08
160  PROB107390REC 8DIRI=2.3025E-11 MIN D/S= 4.699TCRIT=1.5000E-08
```

Fig. 19. (Continued)

VI. METHODS FOR FOLDING TIME- AND SPECTRAL-DEPENDENT SOURCE AND ATMOSPHERIC TRANSMISSION DATA

The two programs, TMTAU (Ref. 3) and POLY (Ref. 1), were previously developed for use in folding a time- and wavelength-dependent source term with atmospheric transmission data generated with the POLO program. These programs have both been improved during the past year. Both programs were originally developed to determine the time-dependent response of a wide-band receiver to the radiation transmitted through the atmosphere after being emitted from a time- and wavelength-dependent source. The total radiation $I(\tau)$, as a function of time τ at a receiver from a source $S(\lambda,t)$ that has transmission $I(\lambda,t)$, and a detector response $R(\lambda)$, where λ is the wavelength and t the time, is calculated with the double integral

$$I(\tau) = \int_{\lambda_1}^{\lambda_2} R(\lambda)d\lambda \int_{0}^{\tau} S(\lambda,t)I(\lambda,\tau-t)dt$$

The major difference in the TMTAU and POLY programs is that the POLY program utilizes the source and transmission data expressed in tabulated form, whereas the TMTAU program requires that the transmission function be expressed as analytical function of a particular type.

In previous versions of the TMTAU program, the transmission data were limited to that for three wavelengths and the time-dependent source data for the same three wavelengths were computed by TMTAU from blackbody scaling laws developed by T. White (Ref. 3). Subsequently, the TMTAU program was modified to allow the use of other source data such as that generated with the RADFLO program. Later, another version of TMTAU was developed which removed the limitation that the source and transmission functions be defined for only three wavelengths. This new version of TMTAU, designated (TMTRF01), does require, however, that the source and transmission functions be defined for the exact same wavelength values.

Examination of the wavelength dependence of the source data generated with the RADFLO program, which is currently being used in the TMTAU and POLY programs, lead to the conclusion that the source data should be defined at more than three wavelengths. The variation with wavelength of the atmospheric transmission data generated with the POLO program is much smoother than the source variation with wavelength. Therefore, a computer program designated POLICE was written to generate the curve-fit coefficients required by TMTRF01 which predict time-dependent transmission data for wavelengths other than those obtained with the POLO program. A description of the POLICE program is given in the following section of this report.

The POLY program approximates the convolution integral through applications of various forms of numerical integration to the raw POLO-calculated atmospheric transmission data and a tabulation of the product of the source term and the detector response function. The main advantage of the POLY program is that it eliminates the need to curve-fit the atmospheric transmission data. In the POLY program, the times and wavelengths used in the definition of the source term do not have to correspond in number or value to those used in the definition of the transmission data. Internal to the POLY program, an interpolation of the transmission data over wavelength is performed to define the transmission versus time for the wavelength values used in the definition of the source terms. A third set of times is used to specify the particular time values for which the time-dependent power at the detector is to be determined.

6.1 Code for Generating Curve-Fit Coefficients for Wavelengths not Considered in POLO Calculations

The POLICE code was developed to generate curve-fit coefficients for input to TMTRF01 which will predict time-dependent scattering data for wavelengths other than those run with the POLO program. The POLICE code aliminates the necessity of excessive numbers of POLO runs to gain

a sufficiently fine wavelength structure for the data used in TMTRF01. The code is variably dimensioned and is written in FORTRAN for use on an IBM system.

The direct flux for the wavelengths not treated by POLO is calculated optionally in POLICE by interpolation over wavelength of the direct fluxes computed with POLO or by use of the subroutine DBEAM. This is the same subroutine that is currently used in POLO to calculate the direct flux at a receiver position.

Curve-fit coefficients for the scattered fluxes at wavelengths not considered in the original POLO calculations are optionally calculated in two ways. Coefficients used to define the "standard" wavelengths (0.4278 μ, 0.75 μ, and 1.07 μ) are interpolated by constructing an interpolating polynomial of degree n-1 to the natural logarithms of the coefficients, where n is the number of standard wavelengths, and then evaluating the expression at the desired wavelengths. The interpolating polynomial is constructed using the divided difference method (Ref. 19). Time-dependent scattered flux data for the standard wavelengths are then generated from the coefficients for a time base which is user-controlled. Scattered flux data for the standard wavelengths are then interpolated over wavelength for each time in the same fashion as were the coefficients and the results temporarily stored. For each new wavelength, a comparison is then made between the data generated from the interpolated coefficients and the data interpolated from the standard data evaluated on the time base. If the comparison is acceptable, the interpolated coefficients are eventually output; if unacceptable, the data which were interpolated from the standard data evaluated on the time base will be retained for curve fitting.

An option in POLICE will allow the user to calculate the scattered flux at wavelengths other than λ = 0.4278 μ, 0.75 μ, and 1.07 μ by interpolating on a "build-up" term which is derived from

$$I_S(t,\lambda) = I_D(\lambda)\ B(t,\lambda)$$

for λ = 0.4278 μ, 0.75 μ, and 1.07 μ, where t is time, λ is wavelength, I_S is the scattered flux, I_D is direct flux and B is the build-up term. The scattered fluxes as a function of time are generated by POLICE for other wavelengths in this manner. The results are then compared with the scattered flux data generated from the interpolated curve-fit coefficients. If the comparison is acceptable, then the interpolated curve-fit coefficients are output. If the comparison is not acceptable, the scattered fluxes generated with the build-up factors are retained for curve fitting.

Three separate criteria for accepting interpolated curve-fit coefficients are input to POLICE: 1) the minimum ratio, 2) the maximum ratio, and 3) the mean ratio of the data when considered collectively over the time base. Should any criteria not be met, the data as interpolated from the standard data evaluated on the time base will be retained for curve fitting with the use of the CFIT or DFIT procedures.

6.2 Checkout of the TMTAU, TMTRF01 and POLYN Procedures

An exacting checkout of the TMTAU, TMTRF01 and POLYN procedures has been performed to insure proper operation of the procedures and to establish the precision of the results obtained from the three computer procedures. POLYN is an improved version of the POLY procedure. TMTRF01 and POLYN have been established at AFTAC on the disk pack TF2PAK under RRACODES. The checkout of the convolution codes was performed by comparing program results with analytic solution results. The comparisons showed good agreement, even with a nonrealistic source term.

A fictitious source $s(\lambda,t)$ was defined as

$$s(\lambda,t) = a_0 \lambda^2 e^{-a_1 t}$$

where $a_0 = 3$ and $a_1 = 10^4$. A fictitious transmission term $I(\lambda,x)$ was defined as

$$I(\lambda,x) = \alpha_0 \lambda^{-\alpha_1 X}$$

where $\alpha_0 = 5$ and $\alpha_1 = 10^5$. The convolution integral is defined by

$$\int_0^\tau F_1(t)\ F_2(\tau-t)dt.$$

If $F_1(t)$ is the wavelength and time-dependent source term $S(\lambda,t)$ and $F_2(\tau-t)$ is the atmospheric transmission term $I(\lambda,\tau-t)$, then the convolution process becomes

$$M(\lambda,\tau) = \int_0^\tau S(\lambda,t)\ I(\lambda,\tau-t)dt$$

which for this comparison results in

$$M(\lambda,\tau) = \frac{a_0\alpha_0}{(\alpha_1-a_1)}\ \lambda^3 \left[e^{-a_1\tau} - e^{-\alpha_1\tau} \right].$$

Assuming a detector response $R(\lambda)$ such that

$$R(\lambda) = 1: \quad \lambda_1 \leq \lambda \leq \lambda_2$$

and $$R(\lambda) = 0: \quad \text{elsewhere,}$$

integration over wavelength yields the detected signal

$$D(\tau) = \frac{1}{4}\ \frac{\alpha_0 a_0}{(\alpha_1-a_1)} \left[\lambda_2^4 - \lambda_1^4 \right] \left[e^{-a_1\tau} - e^{-\alpha_1\tau} \right] .$$

For check-out purposes, $\lambda_1 \equiv .4278$ microns, $\lambda_2 \equiv 1.07$ microns, thus

$$D(\tau) \simeq 5.322\text{X}10^{-5} \left[e^{-10^4\tau} - e^{-10^5\tau} \right]$$

which has a maximum of $3.71\text{X}10^{-5}$ at 25.6 μsec. The results of the analytic solution are shown as a continuous curve in Fig. 20. The discrete results

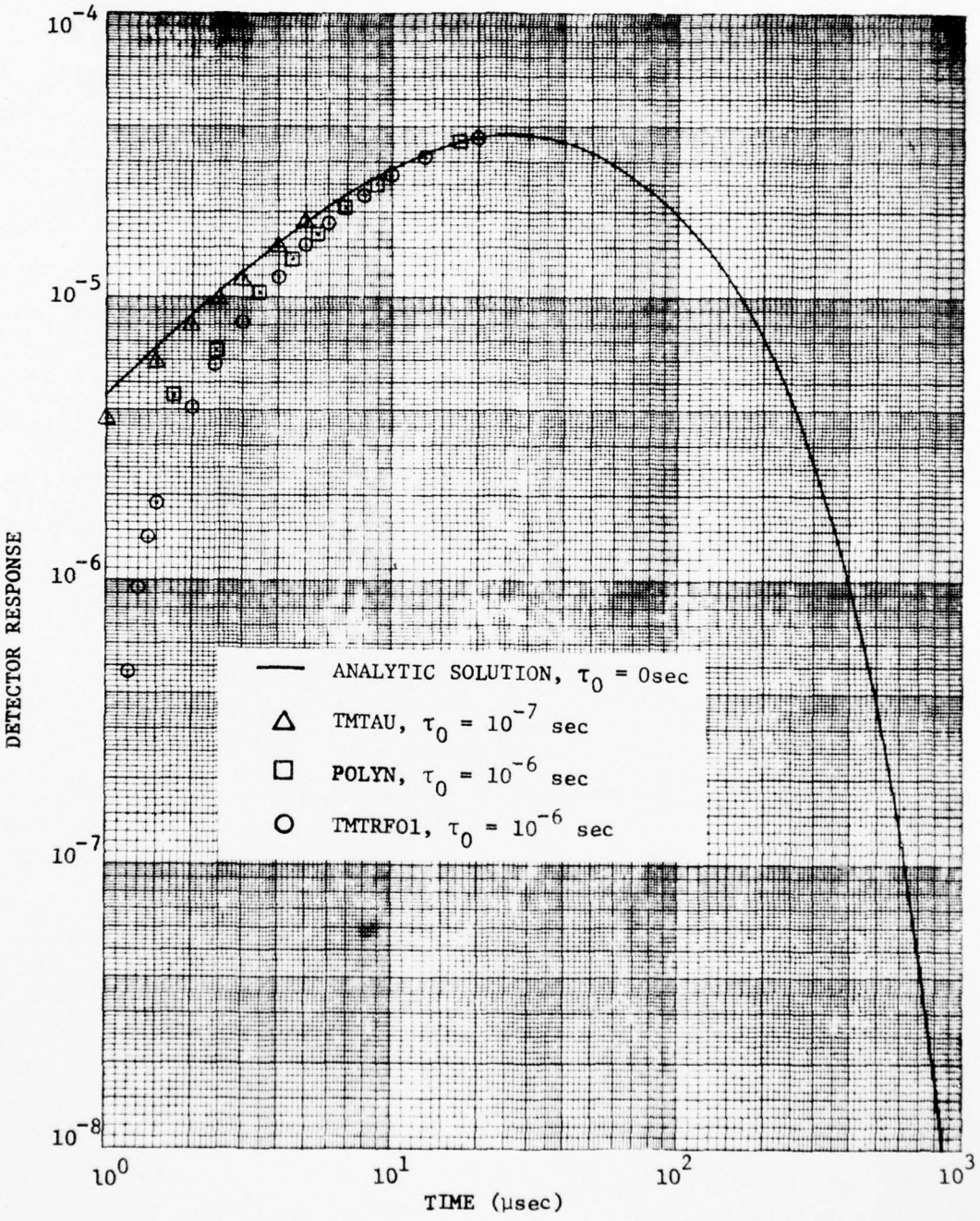

Fig. 20. Comparison of TMTAU, POLYN, and TMTRF01 Calculations for Check-Out Problem Using an Analytic Source Term and an Analytic Transmission Function

of TMTAU and TMTRF01 are plotted at the evaluated times; POLYN results are plotted at the logarithmic mean times on the same graph. No direct radiation contribution was assumed in the calculations. Results from each of the three computer procedures are shown only where the discrepancy between the analytic solution and the results from each procedure were noticeable. Apparent errors in the results from TMTAU, TMTRF01, and POLYN for early times can be explained by the differences in input data for those codes. TMTAU was run with the source defined for times $10^{-7} \leq t \leq 10^{-3}$. TMTRF01 and POLYN were run with the source defined for times $10^{-6} \leq t \leq 10^{-3}$. Since the convolution integral as evaluated above had a lower time limit of zero, any other lower bound will introduce an error. That error is apparent when the integral

$$M'(\lambda,\tau) \equiv \int_{\tau_0}^{\tau} S(\lambda,t)\ I\ (\lambda,\tau-t)dt$$

is evaluated and compared to the convolution solution for a lower time bound of 0.0. The results are:

$$M(\lambda,\tau) = \frac{a_0\alpha_0}{(\alpha_1-a_1)}\ \lambda^3 \left[e^{-a_1\tau} - e^{-\alpha_1\tau}\right]$$

$$M'(\lambda,\tau) = \frac{a_0\alpha_0}{(\alpha_1-a_1)}\ \lambda^3 \left[e^{-a_1\tau} - e^{-\alpha_1\tau}\ e^{(\alpha_1-a_1)\tau_0}\right]$$

where the vanishing error is $e^{(\alpha_1-a_1)\tau_0}$. The error is vanishing since

$$e^{-a_1\tau} - e^{-\alpha_1\tau} \simeq e^{-a_1\tau} - e^{-\alpha_1\tau}\ e^{(\alpha_1-a_1)\tau_0} \simeq e^{-a_1\tau} \quad \text{for} \quad \frac{\alpha_1}{a_1} = 10,$$

$\tau_0 < \tau$ and $\alpha_1\tau > 5$. A run of TMTRF01 for times $10^{-8} \leq t \leq 10^{-3}$ resulted in an absolute error of less than .05% at one microsecond. A comparison of the POLYN and TMTRF01 results for times $10^{-6} \leq t \leq 10^{-3}$ and the analytic formula

$$M'(\lambda,\tau) = \int_{\tau_0}^{\tau} S(\lambda,t)\ I(\lambda,\tau-t)dt,$$

where $\tau_0 \equiv 10^{-6}$, is shown in Fig. 21. The variance between the TMTAU, TMTRF01 and POLYN results and the analytic results is only aesthetically unpleasing since it will only be apparent in sources which have significant values at zero source time. This, of course, does not occur in realistic sources and, as evidenced by the TMTRF01 results where the times were $10^{-8} \leq t \leq 10^{-3}$; the procedure results can adequately define the convolution process if the parametric data adequately defines the source and transmission.

One of the basic uncertainties in the use of TMTAU has been in the results of the integration over wavelength at a given time which was based on the use of source and atmospheric transport data for only three wavelengths, 0.4278 μm, 0.75 μm, and 1.07 μm. This uncertainty resulted in the development of the TMTRF01 procedure which uses curve-fit coefficients data for more than three wavelengths in the convolution integral. The uncertainty in the TMTAU data has also resulted in a renewed interest in the POLYN procedure which also has the capability of doing the convolution integral for more than three wavelengths.

The TMTRF01 procedure differs from TMTAU only in that it provides for the use of more than three wavelengths. The wavelength dependence of the power at the detector at a given time is expressed in terms of the function

$$P(t,\lambda) = e^{(a_1(t) + a_2(t)\ \lambda + a_3(t)\ \lambda^2 \cdot\cdot + a_n\lambda^n)}$$

in TMTRF01 where n is the number of wavelengths for which the source and atmospheric transmission data are defined. The integral over wavelength is then evaluated numerically with use of the equation

$$P(t) = \sum_{i=1}^{28} P(t,\lambda_i)\ R(\lambda_i)\Delta\lambda$$

in both codes with an integration interval of $\Delta\lambda = (\lambda_u - \lambda_\ell)/28$ where λ_u

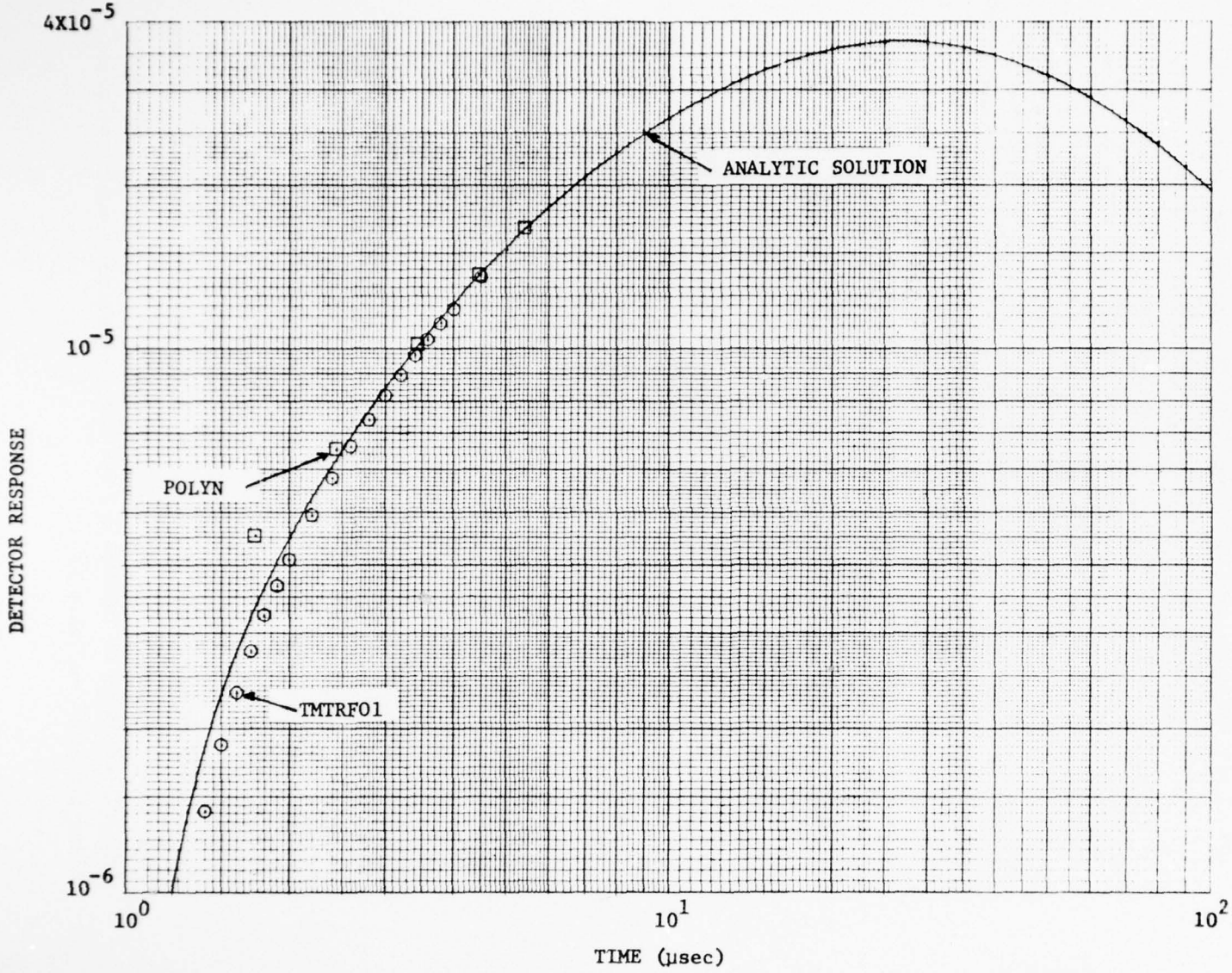

Fig. 21. Comparison of POLYN and TMTRF01 Results for Test Problem, Lower Time Value for Source Function = 10^{-6} sec in all Solutions

and λ_ℓ are the upper and lower bounds of the wavelength range (λ_u = 1.1 μm and λ_ℓ = 0.40 μm) and the λ_i are the midpoints of each of the 28 subintervals in wavelength into which the interval $\lambda_u - \lambda_\ell$ is divided. In POLYN the integration is performed over wavelength using $\Delta\lambda$ values input for each wavelength for which the receiver response data are input.

A test problem was run the POLYN and TMTRF01 codes using transmission data obtained by interpolation for 14 wavelengths from the curve-fit coefficient data for the 40-km meteorological range atmosphere at λ = 0.4278 μm, 0.75 μm, and 1.07 μm. The RADFLO source term for a 2-KT source at 0.1-km altitude with the silicon response function (Fig. 9) for the detector response was also used. The wavelength dependence of the power at the detector at satellite altitude (35800 km) for a look angle of 0° as computed by each of the convolution codes is given in Tables XVII, XVIII, and XIX for retarded times of 128.6 μsec, 5.984 msec, and 52.64 msec, respectively. The data given in Tables XVII, XVIII, and XIX for the TMTAU procedure were obtained from evaluation of the equation

$$P(t) = e^{(a_1(t) + a_2(t)\lambda + a_3(t)\lambda^2)}$$

where the a_i coefficients were obtained from the TMTAU output for the indicated times. The a_i coefficients were fitted to the TMTAU results for wavelengths of 0.4278, 0.75, and 1.07 μ. Also shown in the tables is the integral over wavelengths for each of these times. It is noted that POLYN and TMTRF01 produce results as a function of wavelength that differ mainly only in the second digit at the times shown. It is noted that the wavelength dependence of the power as given by TMTAU differs significantly from that given by POLYN and TMTRF01. The times used in Tables XVII, XVIII, and XIX represent times near first maximum, minimum, and second maximum of the power history curve. The ratios of POLYN to TMTRF01 and TMTAU to TMTRF01 for the integral over wavelength at these times are shown in Table XX.

AD-A042 769 RADIATION RESEARCH ASSOCIATES INC FORT WORTH TEX F/G 4/1
MONTE CARLO STUDIES ON THE TIME-DEPENDENT TRANSPORT OF OPTICAL --ETC(U)
MAR 77 D G COLLINS, M B WELLS F08606-74-C-0011
UNCLASSIFIED RRA-T7608-VOL-2 AFTAC-TR-77-6-VOL-2 NL

2 OF 2
ADA042 769

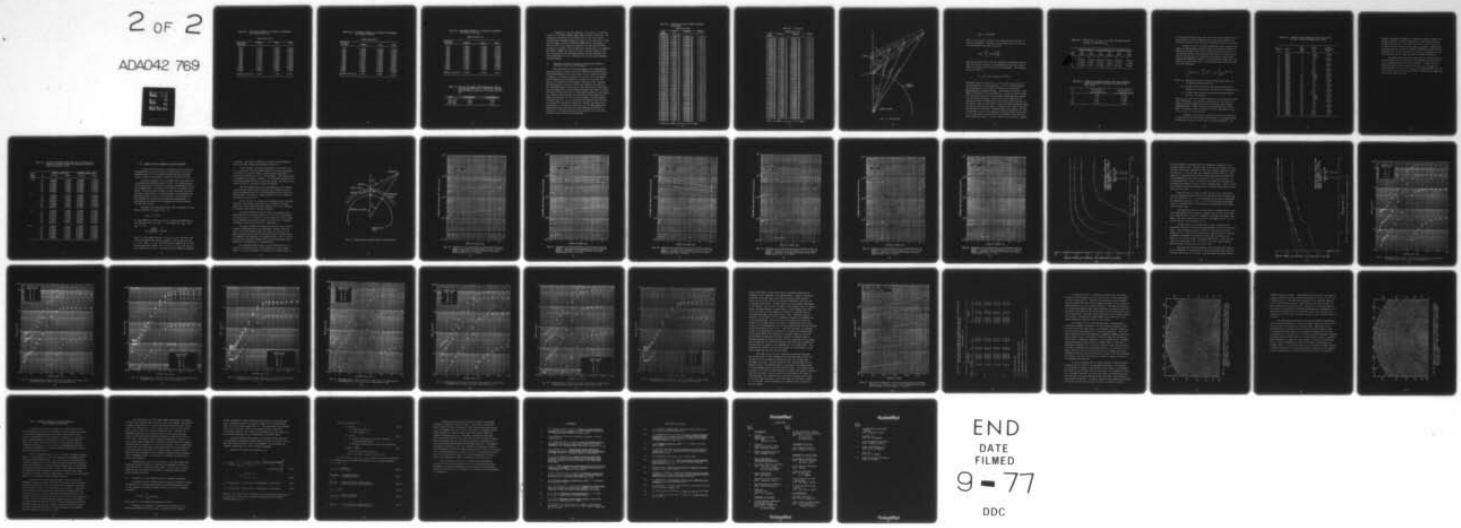

END
DATE FILMED
9-77
DDC

TABLE XVII. CONVOLUTION INTEGRAL AS A FUNCTION OF WAVELENGTH AT A TIME OF 128.6 μsec

POWER (watts/cm^2-μ)

Wavelength (microns)	TMTRF01	POLYN	TMTAU
.4278	1.847+2	1.860+2	1.793+2
.4675	4.156+2	4.249+2	2.400+2
.5052	5.497+2	5.660+2	2.998+2
.5476	3.792+2	3.915+2	3.617+2
.5983	4.525+2	4.654+2	4.144+2
.6539	3.213+2	3.278+2	4.311+2
.7085	3.609+2	3.648+2	4.007+2
.7693	2.239+2	2.243+2	3.241+2
.8364	2.463+2	2.453+2	2.187+2
.9004	9.058+1	8.988+1	1.285+2
.9613	9.112+1	9.066+1	6.728+1
1.0059	6.638+1	6.626+1	3.837+1
1.0400	3.803+1	3.816+1	2.376+1
1.0700	1.555+1	1.568+1	1.504+1
Integral (watts/cm^2)	1.651+2	1.752+2	1.70+2

TABLE XVIII. CONVOLUTION INTEGRAL AS A FUNCTION OF WAVELENGTH AT A TIME OF 5.984 msec

Wavelength (microns)	POWER (watts/cm^2-μ) TMTRFO1	POLYN	TMTAU
.4278	3.715+0	3.812+0	3.572+0
.4675	8.309+0	8.663+0	5.760+0
.5052	1.093+1	1.148+1	8.614+0
.5476	1.950+1	1.978+1	1.277+1
.5983	2.312+1	2.336+1	1.881+1
.6539	3.234+1	3.172+1	2.595+1
.7085	3.615+1	3.502+1	3.203+1
.7693	4.745+1	4.469+1	3.582+1
.8364	5.204+1	4.872+1	3.487+1
.9004	2.823+1	2.618+1	2.935+1
.9613	2.836+1	2.634+1	2.181+1
1.0059	4.050+1	3.760+1	1.615+1
1.0400	2.318+1	2.162+1	1.225+1
1.0700	9.466+0	8.874+0	9.291+0
Integral (watts/cm^2)	1.941+1	1.855+1	1.51+1

TABLE XIX. CONVOLUTION INTEGRAL AS A FUNCTION OF WAVELENGTH AT A TIME OF 52.64 msec

POWER (watts/cm^2-μ)

Wavelength (microns)	TMTRFO1	POLYN	TMTAU
.4278	3.368+2	3.315+2	3.279+2
.4675	7.534+2	7.535+2	4.433+2
.5052	9.912+2	9.990+2	5.615+2
.5476	8.032+2	8.137+2	6.910+2
.5983	9.524+2	9.609+2	8.171+2
.6539	7.164+2	7.155+2	8.875+2
.7085	8.007+2	7.899+2	8.685+2
.7693	4.882+2	4.760+2	7.519+2
.8364	5.352+2	5.189+2	5.538+2
.9004	2.402+2	2.323+2	3.584+2
.9613	2.412+2	2.337+2	2.080+2
1.0059	2.414+2	2.358+2	1.288+2
1.0400	1.382+2	1.356+2	8.533+1
1.0700	5.641+1	5.565+1	5.746+1
Integral (watts/cm^2)	3.540+2	3.656+2	3.62+2

TABLE XX. RATIO OF THE INTEGRAL OVER WAVELENGTH AS GIVEN BY THE POLYN AND TMTAU CODES TO THAT GIVEN BY TMTRFO1 CODE FOR TIMES OF 128.6 μsec, 5.984 msec, and 52.64 msec

TIME	POLYN/TMTRFO1	TMTAU/TMTRFO1
128.6 μsec	1.061	1.030
5.984 msec	.9557	.778
52.64 msec	1.033	1.022

A comparison of the time histories of the power at the detector as given by the POLYN, TMTRF01, TMTAU codes is given in Table XXI. Considering the differences in the methods used in each code, there is reasonably good agreement between the results of the three codes. (Note that the powers as given by POLYN and TMTRF01 have to be divided by a factor of 10^{10} to put them in the same units as that given by TMTAU.) In light of the results given in Tables XVII through XXI, it is suggested that POLYN or TMTRF01 be used in the future instead of TMTAU to avoid the uncertainties in the wavelength integral for each time when only three wavelengths are used to represent both the source and atmosphere transmission data.

6.3 Conversion of TMTAU Calculations for Synchronous Satellite Altitude to Other Satellite Altitudes

POLO calculations were run to determine if the time-dependent scattered fluxes at receiver altitudes of 20186.8 km and 93621.626 km could be determined from the calculations run for a detector altitude of 35800 km. The POLO calculations were run for a 0.75 μ wavelength point isotropic source positioned at a height of 0.5 km above the ground. The ground-level meteorological range was 25 km. Receivers were positioned at altitudes of 20186.8 km, 35800 km, and 93621.626 km. Scattered fluxes as a function of time after arrival of the direct flux were computed for 50 time intervals between 0 and 1.0×10^{-3} seconds. The detectors were positioned for each detector altitude at polar angles, θ_{SL}, between a radial through the source and the line connecting the source and receiver, of 0, 30, 60, and 90 degrees. The POLO geometry is shown in Fig. 22. R_L, R_S, and R_V are the distances from the source to the satellite altitudes of 20186.8 km, 35800 km, and 93621.626 km, respectively, in the direction denoted by θ_{SL}. The angle between the source-receiver axis and the earth radial through the satellite is denoted as β. The uncollided flux at each receiver for a unit point isotropic source is given by the expression,

TABLE XXI. COMPARISON OF POLYN, TMTRFO1 AND TMTAU CALCULATIONS

POWER (watts/cm^2)

TIME SECONDS	POLYN*	TMTRFO1*	TMTAU
3.260E-06	.000E 00		
6.392E-06	1.319E 00	1.173E 00	1.16E-10
7.870E-06	1.320E 00	1.230E 00	1.21E-10
1.292E-05	1.275E 00	1.191E 00	1.18E-10
1.885E-05	1.562E 00	1.860E 00	1.90E-10
2.140E-05	2.236E 00	2.440E 00	2.53E-10
3.006E-05	4.495E 00	6.858E 00	6.78E-10
3.289E-05	7.421E 00	7.463E 00	7.49E-10
3.741E-05	1.002E 01	1.271E 01	1.11E-09
4.304E-05	2.091E 01	3.268E 01	2.96E-09
4.748E-05	3.909E 01	4.724E 01	4.87E-09
4.930E-05	5.822E 01	7.066E 01	7.82E-09
5.420E-05	8.588E 01	9.846E 01	1.11E-08
5.941E-05	1.191E 02	1.341E 02	1.44E-08
7.076E-05	1.601E 02	1.748E 02	1.82E-08
7.698E-05	1.836E 02	1.777E 02	1.84E-08
8.366E-05	1.858E 02	1.784E 02	1.84E-08
9.082E-05	1.858E 02	1.769E 02	1.83E-08
1.101E-04	1.818E 02	1.700E 02	1.76E-08
1.191E-04	1.776E 02	1.683E 02	1.74E-08
1.286E-04	1.752E 02	1.651E 02	1.70E-08
1.559E-04	1.685E 02	1.557E 02	1.60E-08
1.847E-04	1.581E 02	1.463E 02	1.51E-08
2.141E-04	1.453E 02	1.303E 02	1.34E-08
2.408E-04	1.340E 02	1.223E 02	1.26E-08
2.676E-04	1.250E 02	1.144E 02	1.17E-08
2.939E-04	1.170E 02	1.078E 02	1.11E-08
3.206E-04	1.127E 02	1.052E 02	1.08E-08
3.473E-04	1.106E 02	1.035E 02	1.06E-08
3.740E-04	1.032E 02	9.200E 01	9.41E-09
4.007E-04	9.704E 01	9.217E 01	9.43E-09
4.407E-04	9.186E 01	8.135E 01	8.31E-09
4.674E-04	8.362E 01	7.693E 01	7.85E-09
5.341E-04	7.667E 01	6.851E 01	6.98E-09
6.008E-04	6.486E 01	5.497E 01	5.58E-09
6.675E-04	5.687E 01	5.310E 01	5.38E-09
7.342E-04	5.267E 01	4.709E 01	4.76E-09
8.008E-04	4.854E 01	4.544E 01	4.58E-09
9.341E-04	4.550E 01	4.147E 01	4.16E-09
1.067E-03	4.331E 01	4.139E 01	4.14E-09
1.201E-03	4.381E 01	4.254E 01	4.25E-09
1.334E-03	4.314E 01	4.017E 01	4.01E-09
1.600E-03	4.035E 01	3.737E 01	3.71E-09
1.866E-03	3.695E 01	3.363E 01	3.31E-09
2.133E-03	3.278E 01	2.959E 01	2.89E-09
2.399E-03	2.870E 01	2.596E 01	2.48E-09
2.665E-03	2.509E 01	2.278E 01	2.13E-09
2.931E-03	2.259E 01	2.121E 01	1.95E-09
3.197E-03	2.130E 01	2.036E 01	1.84E-09
3.462E-03	2.031E 01	1.941E 01	1.73E-09
3.728E-03	1.954E 01	1.896E 01	1.66E-09

* POLYN and TMTRFO1 results are 10^{10} X POWER

TABLE XXI. (Continued)

POWER (watts/cm^2)

TIME SECONDS	POLYN*	TMTRFO1*	TMTAU
3.994E-03	1.897E 01	1.839E 01	1.59E-09
4.392E-03	1.849E 01	1.814E 01	1.54E-09
4.658E-03	1.833E 01	1.816E 01	1.52E-09
5.321E-03	1.802E 01	1.774E 01	1.41E-09
5.984E-03	1.855E 01	1.941E 01	1.51E-09
6.647E-03	2.068E 01	2.207E 01	1.71E-09
7.310E-03	2.288E 01	2.376E 01	1.86E-09
7.972E-03	2.791E 01	3.240E 01	2.69E-09
9.296E-03	3.619E 01	3.943E 01	3.27E-09
1.062E-02	4.627E 01	5.252E 01	4.61E-09
1.194E-02	6.187E 01	6.953E 01	6.39E-09
1.326E-02	8.086E 01	8.866E 01	8.46E-09
1.590E-02	1.066E 02	1.184E 02	1.15E-08
1.854E-02	1.426E 02	1.570E 02	1.56E-08
2.118E-02	1.815E 02	1.912E 02	1.93E-08
2.381E-02	2.152E 02	2.209E 02	2.23E-08
2.644E-02	2.436E 02	2.451E 02	2.50E-08
3.169E-02	2.767E 02	2.832E 02	2.89E-08
3.432E-02	3.056E 02	2.999E 02	3.07E-08
3.694E-02	3.225E 02	3.153E 02	3.23E-08
3.956E-02	3.364E 02	3.261E 02	3.34E-08
4.349E-02	3.485E 02	3.381E 02	3.46E-08
4.611E-02	3.572E 02	3.427E 02	3.51E-08
5.264E-02	3.656E 02	3.540E 02	3.62E-08
5.917E-02	3.745E 02	3.598E 02	3.68E-08
6.569E-02	3.755E 02	3.564E 02	3.64E-08
7.220E-02	3.651E 02	3.414E 02	3.48E-08
7.870E-02	3.424E 02	3.142E 02	3.20E-08
9.168E-02	2.849E 02	2.412E 02	2.35E-08
1.046E-01	2.130E 02	1.799E 02	1.60E-08
1.176E-01	1.638E 02	1.469E 02	1.15E-08
1.305E-01	1.346E 02	1.244E 02	9.09E-09
1.566E-01	1.058E 02	9.146E 01	6.35E-09
1.696E-01	8.440E 01	7.915E 01	5.51E-09
1.827E-01	7.364E 01	6.972E 01	4.87E-09
1.957E-01	6.495E 01	6.159E 01	4.35E-09
2.218E-01	5.495E 01	4.960E 01	3.60E-09
2.610E-01	4.356E 01	3.786E 01	2.91E-09
2.870E-01	3.579E 01	3.365E 01	2.58E-09
3.131E-01	3.119E 01	2.878E 01	2.31E-09
3.392E-01	2.775E 01	2.597E 01	2.13E-09
3.653E-01	2.491E 01	2.316E 01	1.95E-09
3.914E-01	2.266E 01	2.146E 01	1.83E-09
4.306E-01	2.051E 01	1.924E 01	1.66E-09
4.697E-01	1.812E 01	1.670E 01	1.50E-09
5.219E-01	1.605E 01	1.486E 01	1.36E-09
5.871E-01	1.427E 01	1.318E 01	1.24E-09

*POLYN and TMTRFO1 results are 10^{10} X POWER

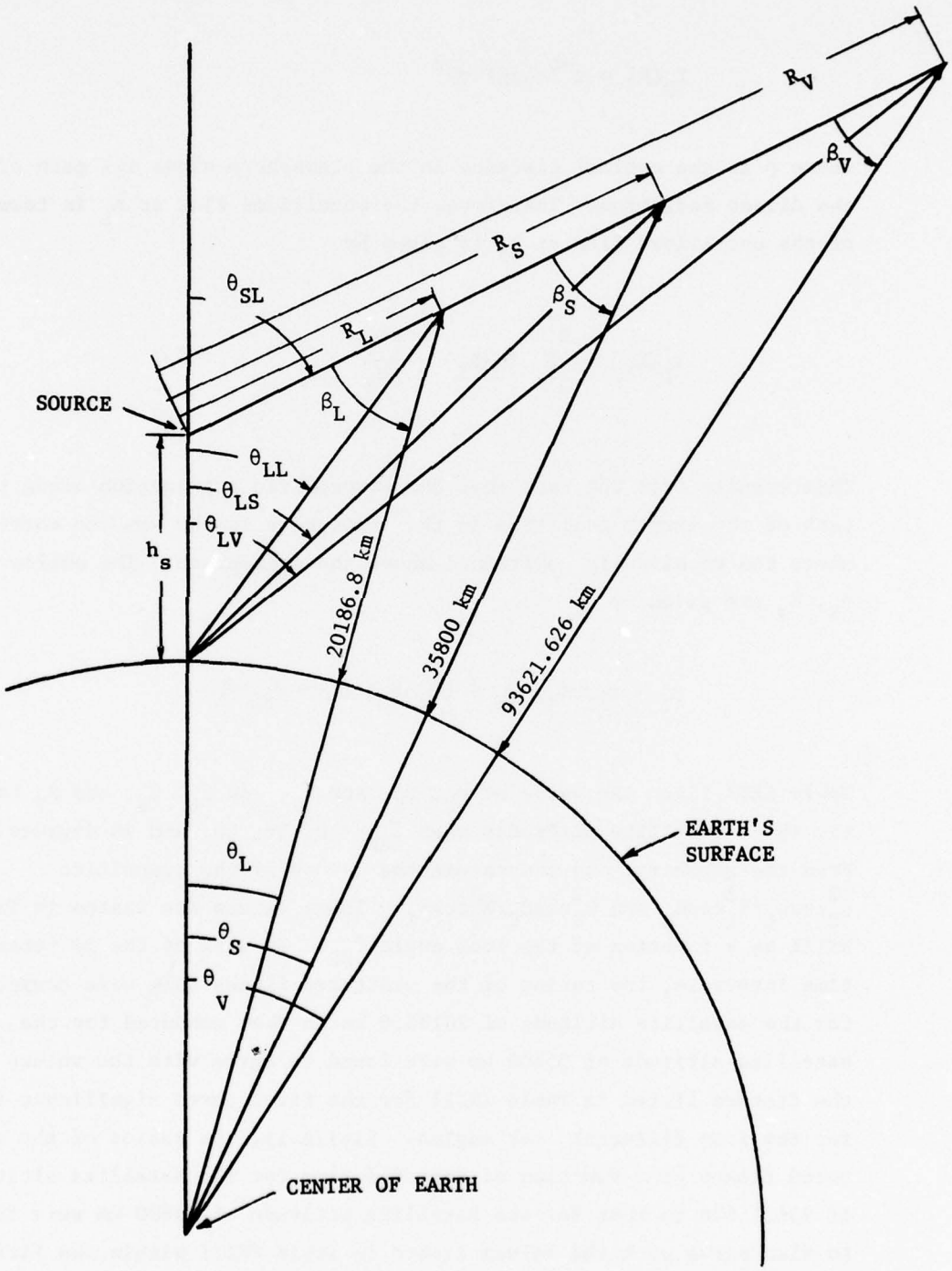

Fig. 22. POLO Geometry

$$I_D(R) = e^{-\rho}\cos\beta/4\pi R^2$$

where ρ is the optical distance in the atmosphere along the path of the direct radiation. Therefore, the uncollided flux at R_L in terms of the uncollided flux at R_S is given by

$$I_D(R_L) = \frac{R_S^2}{R_L^2} I_D(R_S) \frac{\cos\beta_L}{\cos\beta_S} \quad .$$

This results from the fact that the atmospheric attenuation along the path of the direct radiation in the atmosphere is the same no matter where the receiver is positioned above the atmosphere. The angles β_L, β_S, β_V are given by

$$\beta_L = \theta_{SL}-\theta_L, \ \beta_S = \theta_{SL}-\theta_S, \ \beta_V = \theta_{SL}-\theta_V \ .$$

Table XXII lists the value of θ_L, θ_S, and θ_V, and β_L, β_S, and β_V for the three satellite altitudes when θ_{SL} = 0, 30, 60, and 90 degrees. From the geometry, one can obtain the values of the quantities $R_S^2\cos\beta_L/R_L^2\cos\beta_S$ and $R_S^2\cos\beta_V/R_V^2\cos\beta_S$. These values are listed in Table XXIII as a function of the look angle θ_{SL}. In each of the 50 retarded time intervals, the ratios of the scattered fluxes that were computed for the satellite altitude of 20186.8 km to that computed for the satellite altitude of 35800 km were found to agree with the values of the factors listed in Table XXIII for the first three significant digits for the four different look angles. Similarly, the ratios of the scattered fluxes as a function of retarded time for the satellite altitude of 93621.626 to that for the satellite altitude of 35800 km were found to also agree with the values listed in Table XXIII within the first three significant figures. In fact, nearly all of the ratios computed

TABLE XXII. VALUES OF θ_L, θ_V, θ_S, β_L, β_V, AND β_S FOR EACH SATELLITE ALTITUDE AS A FUNCTION OF θ_{SL}

θ_{SL} (deg)	Altitude=20186.8 km		Altitude=93621.626 km		Altitude=35800 km	
	θ_L (deg)	β_L (deg)	θ_V (deg)	β_V (deg)	θ_S (deg)	β_S (deg)
0	0	0	0	0	0	0
30	23.10437	6.89563	28.17228	1.82772	25.66327	4.33673
60	47.99766	12.0023	56.83321	3.16679	52.47412	7.52588
90	76.10626	13.8937	86.34269	3.65731	81.30145	8.69855

TABLE XXIII. FACTORS FOR CONVERTING DIRECT FLUXES FROM SYNCHRONOUS SATELLITE ALTITUDE TO ALTITUDES OF 20186.8 KM AND 93621.626 KM

θ_{SL}	$R_S^2\cos\beta_L/R_L^2\cos\beta_S$ Altitude=20186.8 km	$R_S^2\cos\beta_V/R_V^2\cos\beta_S$ Altitude=93621.626 km
0	3.145	0.1462
30	3.057	0.1500
60	2.833	0.1608
90	2.567	0.1762

for the scattered fluxes were found to differ by no more than 0.005 for the satellite altitude of 20186.8 km and no more than 0.0005 for the satellite altitude of 93621.626 km from the values listed in Table XXIII.

From the results of the POLO calculations, it is concluded that direct and time-dependent scattered fluxes for satellite altitudes of 20186.8 km and 93621.626 km can be obtained with an error of less than 1.0% from the data previously generated with POLO for a satellite altitude of 35800 km (Ref. 14). These data are stored on Tape No. 2696 (labeled POLODCBINE,DSN = POLOD) in the order shown in Table XXIV. The cumulative distributions of the scattered fluxes were curve-fitted with use of the expression,

$$\int_0^{\tau} I_S(t)dt = K_1 - \sum_{i=1}^{i\leq 6} a_i e^{-b_i \tau} + K_2 - \sum_{j=1}^{j\leq 3} a_j e^{-b_j(\tau-\tau_0)}$$

where K_1 = maximum cumulated scattered flux from photons that have not undergone ground reflection,

K_2 = maximum cumulated scattered flux from photons that have undergone both ground reflection and air scattering minus K_1,

τ_0 = retarded time at which ground-reflected photons begin to arrive at the receiver,

and a_i, b_i, a_j, and b_j are constants obtained by curve-fitting the cumulative flux values. The curve-fit coefficients for the synchronous satellite altitude (35800 km) are stored on Tape No. 801 (labeled POLODCVFITSC,DSN = POLOFT) according to the sequence shown in Table XXIV. The curve-fit data on Tape No. 801 are for look angles of θ_{LS} = 0, 30, 45, 60, 70, 75, 80, and 90°.

To obtain a power history at satellite altitudes of 20186.8 km or 93621.626 km for a given source power history, it is suggested that the POLO data on Tape No. 801 be used in the TMTAU procedure. The

TABLE XXIV. SEQUENCE OF POLO OUTPUT DATA SETS STORED ON TAPE NO. 2696 (LABELED POLODCBINE, DSN = POLOD)

Sequence No.	Problem No.	Met. Range (km)	Source Alt. (km)	Source Wavelength (μm)
1	43031	3	0.001	0.4278
2	75031	3	0.001	0.75
3	107031	3	0.001	1.07
4	43032	3	0.5	0.4278
5	75032	3	0.5	0.75
6	107032	3	0.5	1.07
7	43033	3	3.0	0.4278
8	75033	3	3.0	0.75
9	107033	3	3.0	1.07
10	43034	3	10.0	0.4278
11	75034	3	10.0	0.75
12	107034	3	10.0	1.07
13	43101	10	0.001	0.4278
14	75101	10	0.001	0.75
15	107101	10	0.001	1.07
16	43102	10	0.5	0.4278
17	75102	10	0.5	0.75
18	107102	10	0.5	1.07
19	43103	10	3.0	0.4278
20	75103	10	3.0	0.75
21	107103	10	3.0	1.07
22	43104	10	10.0	0.4278
23	75104	10	10.0	0.75
24	107104	10	10.0	1.07
25	43251	25	0.001	0.4278
26	75251	25	0.001	0.75
27	107251	25	0.001	1.07
28	43252	25	0.5	0.4278
29	75252	25	0.5	0.75
30	107252	25	0.5	1.07
31	43253	25	3.0	0.4278
32	75253	25	3.0	0.75
33	107253	25	3.0	1.07
34	43254	25	10.0	0.4278
35	75254	25	10.0	0.75
36	107254	25	10.0	1.07

results so obtained from TMTAU for a satellite altitude of 35800 km can then be converted to either the 20186.8 km or 93621.626 km satellite altitudes with the use of the correction factors listed in Table XXV. It must be pointed out that only the angle θ_{SL} remains a constant when converting data for a satellite altitude of 35800 km to other satellite altitudes; that is, the look angles θ_{LL} and θ_{LV} are different for each source altitude and look angle θ_{LS} used in the POLO calculations.

An examination of Table XXV reveals that the correction factors and look angles for each satellite altitude (20186.8 and 93621.626 km) do not vary significantly with source altitude. It appears for all source altitudes that one can assume that $\theta_{LS} = \theta_{LL} = \theta_{LV}$ and the correction factors as a function of θ_{LS} for a source altitude of 3.0 km can be used for all source altitudes without introducing any significant error in the results obtained.

TABLE XXV. FACTORS FOR CONVERTING TMTAU AND POLO CALCULATIONS FOR A SATELLITE ALTITUDE OF 35800 KM TO SATELLITE ALTITUDES OF 20186.8 KM AND 93621.626 KM

Source Height (km)	θ_{LS}	35800km to 20186.8km		35800km to 93621.626km	
		θ_{LL}(deg)	FACTOR	θ_{LV}(deg)	FACTOR
0.001	0	0.00000	3.14520	0.00000	0.146224
	30	29.99999	3.05705	30.00000	0.150050
	45	44.99999	2.95672	45.00000	0.154675
	60	59.99999	2.83285	60.00000	0.160832
	70	69.99999	2.74374	70.00000	0.165619
	75	74.99999	2.69870	75.00000	0.168169
	80	79.99999	2.65396	80.00000	0.170798
	90	89.99999	2.56699	90.00000	0.176214
0.5	0	0.00000	3.14527	0.00000	0.146216
	30	29.99971	3.05711	30.00024	0.150048
	45	44.99960	2.95676	45.00033	0.154674
	60	59.99955	2.83288	60.00038	0.160831
	70	69.99954	2.74376	70.00040	0.165618
	75	74.99954	2.69872	75.00041	0.168168
	80	79.99955	2.65397	80.00041	0.170798
	90	89.99820	2.56702	90.00097	0.176215
3.0	0	0.00000	3.14560	0.00000	0.146209
	30	29.99823	3.05738	30.00144	0.150037
	45	44.99764	2.95698	45.00197	0.154665
	60	59.99732	2.83302	60.00231	0.160825
	70	69.99727	2.74385	70.00243	0.165614
	75	74.99728	2.69879	75.00245	0.168166
	80	79.99732	2.65402	80.00245	0.170796
	90	89.98921	2.65672	90.00584	0.176218
10.0	0	0.00000	3.14656	0.00000	0.146174
	30	29.99410	3.05817	30.00481	0.150007
	45	44.99213	2.95758	45.00658	0.154641
	60	59.99108	2.83342	60.00771	0.160809
	70	69.99089	2.74411	70.00809	0.165604
	75	74.99093	2.69890	75.00817	0.168158
	80	79.99106	2.65415	80.00818	0.170792
	90	89.96404	2.56764	90.01948	0.176227

VII. THERMAL RADIATION TRANSPORT IN CLOUDY ATMOSPHERES

A series of POLO Monte Carlo calculations were run during the reporting period to study the effects of cloud layers on the time-dependent transport of the radiation emitted from point isotropic sources to detectors positioned at synchronous satellite altitude.

The model atmosphere used in the Monte Carlo calculations had a ground-level meteorological range of 10 km. The size distribution used to characterize the aerosols was the Haze C distribution (Ref. 17) for continental haze. POLO problems were run for two different cloud models. In the first POLO problems, a stratus cloud with an optical thickness of approximately 14 mean-free-paths at all wavelengths was positioned between 0.5 km and 1.0 km altitude. In the next set of POLO problems, an altostratus cloud layer with approximately a 20 mean-free-path thickness at all wavelengths was positioned between 3 km and 4 km altitude.

The particle size distribution N(r) used to describe the cloud models is given by the equation (Ref. 21)

$$N(r) = A\, r^{\alpha}\, e^{-Br^{\gamma}} .$$

The total number N_0 of particles per cm^3 is given by integrating the size distribution over all radii. If one assumes that $r_{min} = 0$ and $r_{max} = \infty$, then

$$N_0 = \frac{A\Gamma\left(\frac{\alpha+1}{\gamma}\right)}{\gamma B^{(\alpha+1)/\gamma}} = \int_0^{\infty} N(r)dr \quad .$$

where $\Gamma(x)$ is the gamma function. If N_0, α, B, and γ are known, then A can be determined from the above equation. For the stratus cloud: $\alpha = 3$, $B = 0.666$, $\gamma = 1$, $N_0 = 250$, and the size range was 0.4 to 30 μm. For the altostratus cloud: $\alpha = 5$, $B = 1.111$, $\gamma = 1$, $N_0 = 400$, and the size range was 0.2 to 18 μm. The droplets for each model were assumed

to be water. The index of refraction for water at the wavelengths used in the POLO calculations was taken from Ref. 22.

Point isotropic sources were positioned at altitudes of 0.1, 0.5, 3, and 10 km. The POLO problems were run for source wavelengths of 0.4278, 0.75, and 1.07 microns. Detectors were positioned at satellite look angles of 0, 45, 75, and 90 degrees. The ground surface was assumed to be a Lambert reflector. The cloud layer was taken to be a scattering medium and not as a reflection surface. The POLO calculations were run for a satellite altitude of 35800 km.

The POLO-computed direct and time-dependent scattered fluxes at each detector position were convoluted with a RADFLO-calculated time and wavelength source for a wide-band silicon detector using the POLY procedure. The detector response function used in the POLY calculations is shown in Fig. 9.

Figure 23 shows the source-receiver geometry used in the POLO procedure. The satellite look angle, θ_L, is defined as the angle between the radial through the source position and a line connecting the subsource point and the satellite position.

The time-integrated scattered fluxes at the satellite for a ground albedo of 0.8 and look angles θ_L of 0, 45, 75, and 90 degrees are shown in Figs. 24 - 26 and 27 - 29 as a function of source height for an atmosphere containing a stratus cloud layer and an atmosphere containing an altostratus cloud layer, respectively.

For source altitudes both below and above the cloud, the POLO procedure followed photons as they underwent collisions within the cloud. For source altitudes above the clouds, the results of the POLO calculations showed that the scattered flux at the satellite was not dependent on the magnitude of the ground albedo. When the source was below the cloud, the scattered flux at the satellite was highly dependent on the magnitude of the ground albedo.

The cumulated scattered flux at the satellite position as a function of retarded time for a source height of 0.1 km, a ground albedo of 0.0 and a wavelength of 0.4278 microns is shown in Fig. 30

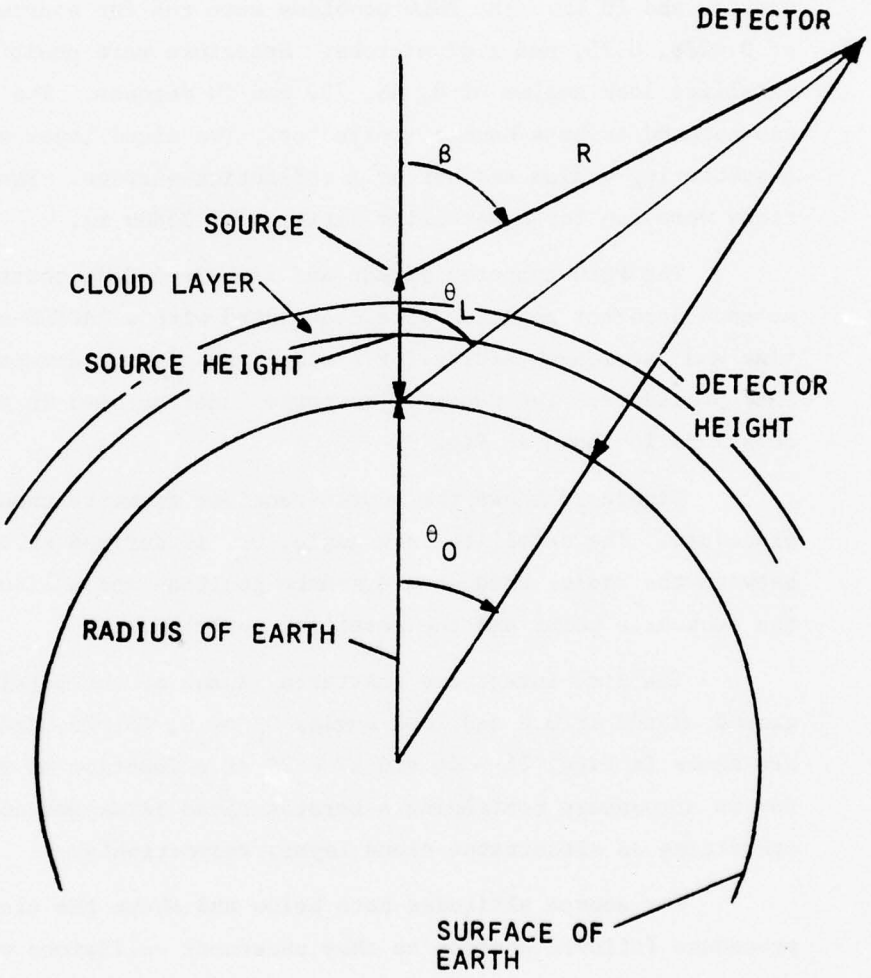

Fig. 23. Source-Receiver Geometry Used in Cloud Problems

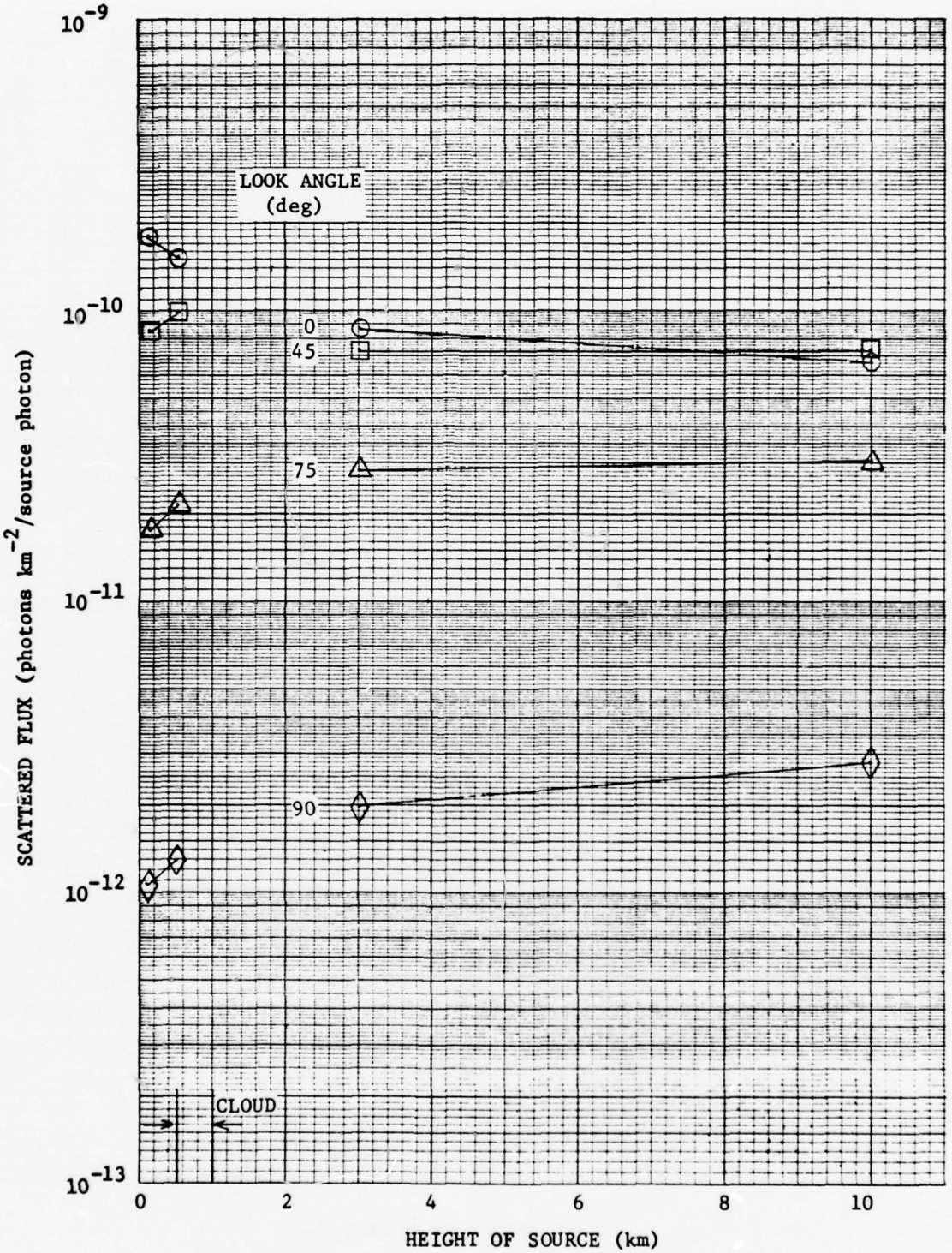

Fig. 24. Variation of the Scattered Flux at the Satellite with the Height of the Source for Look Angles of 0, 45, 75, and 90 Degrees: Atmosphere Containing a Stratus Cloud Layer, Ground Albedo = 0.8, λ = 0.4278 μ

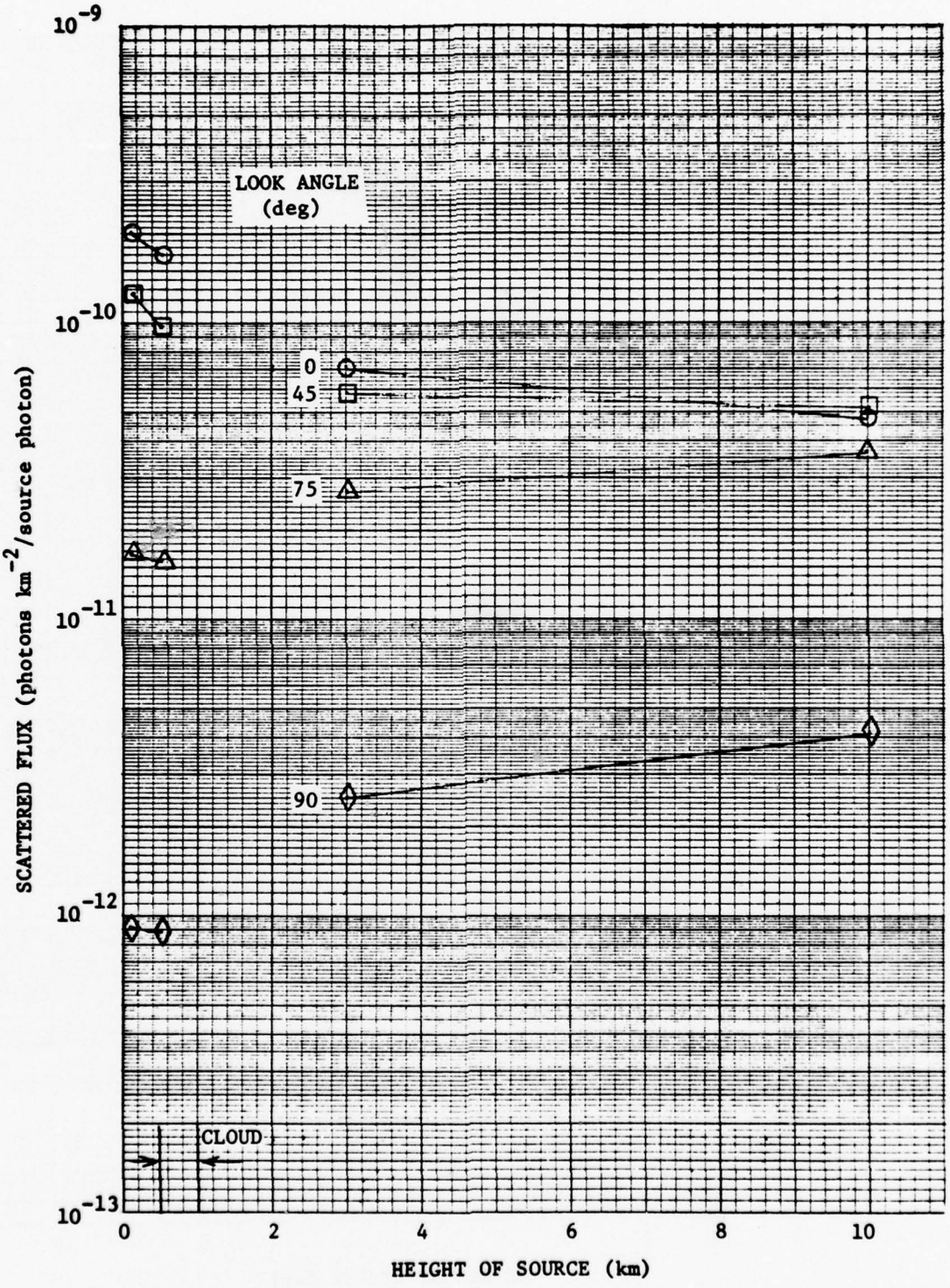

Fig. 25. Variation of the Scattered Flux at the Satellite with the Height of the Source for Look Angles of 0, 45, 75, and 90 Degrees: Atmosphere Containing a Stratus Cloud Layer, Ground Albedo = 0.8, λ = 0.75 μ

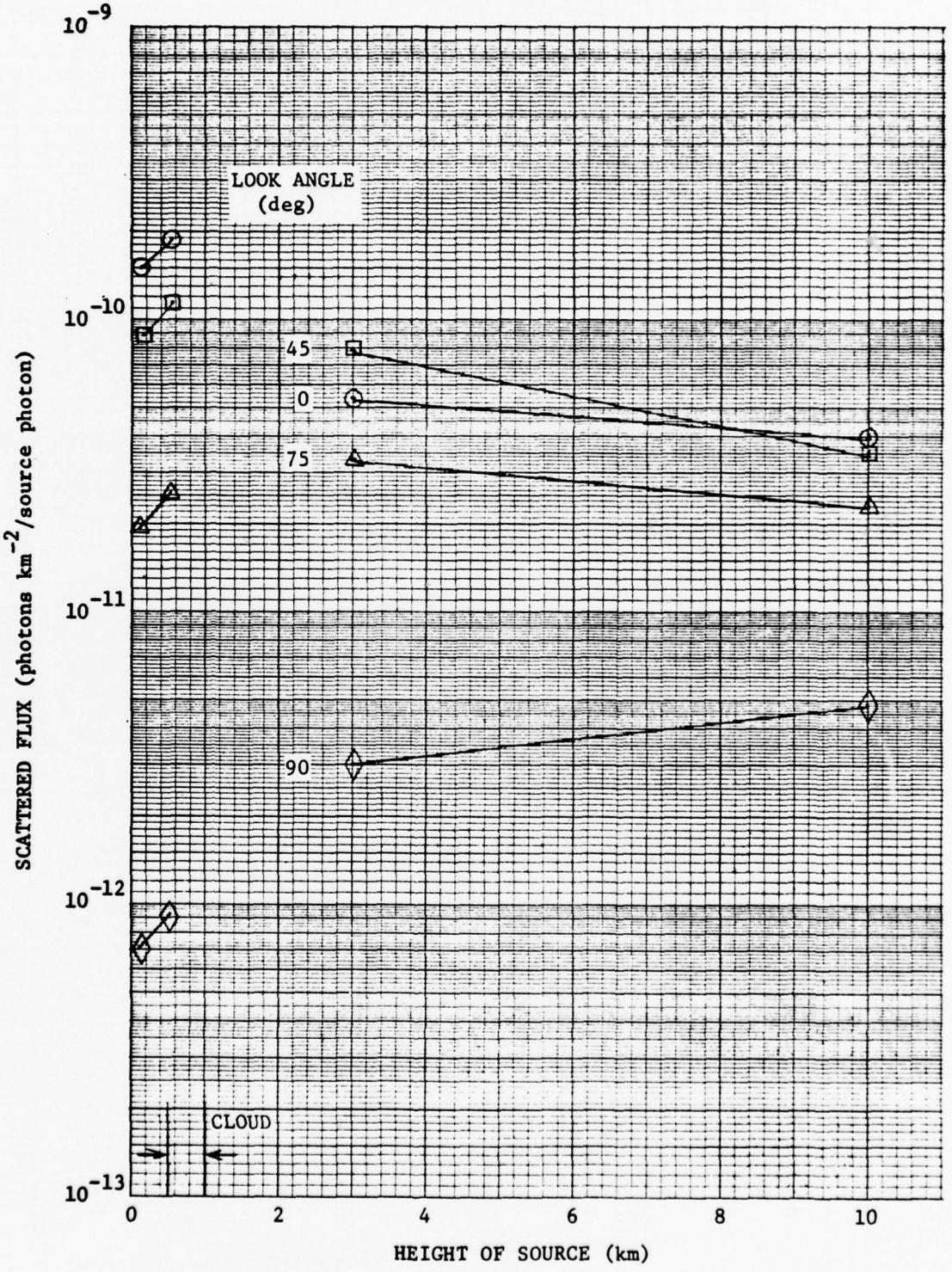

Fig. 26. Variation of the Scattered Flux at the Satellite with the Height of the Source for Look Angles of 0, 45, 75, and 90 Degrees: Atmosphere Containing a Stratus Cloud Layer, Ground Albedo = 0.8, λ = 1.07 μ

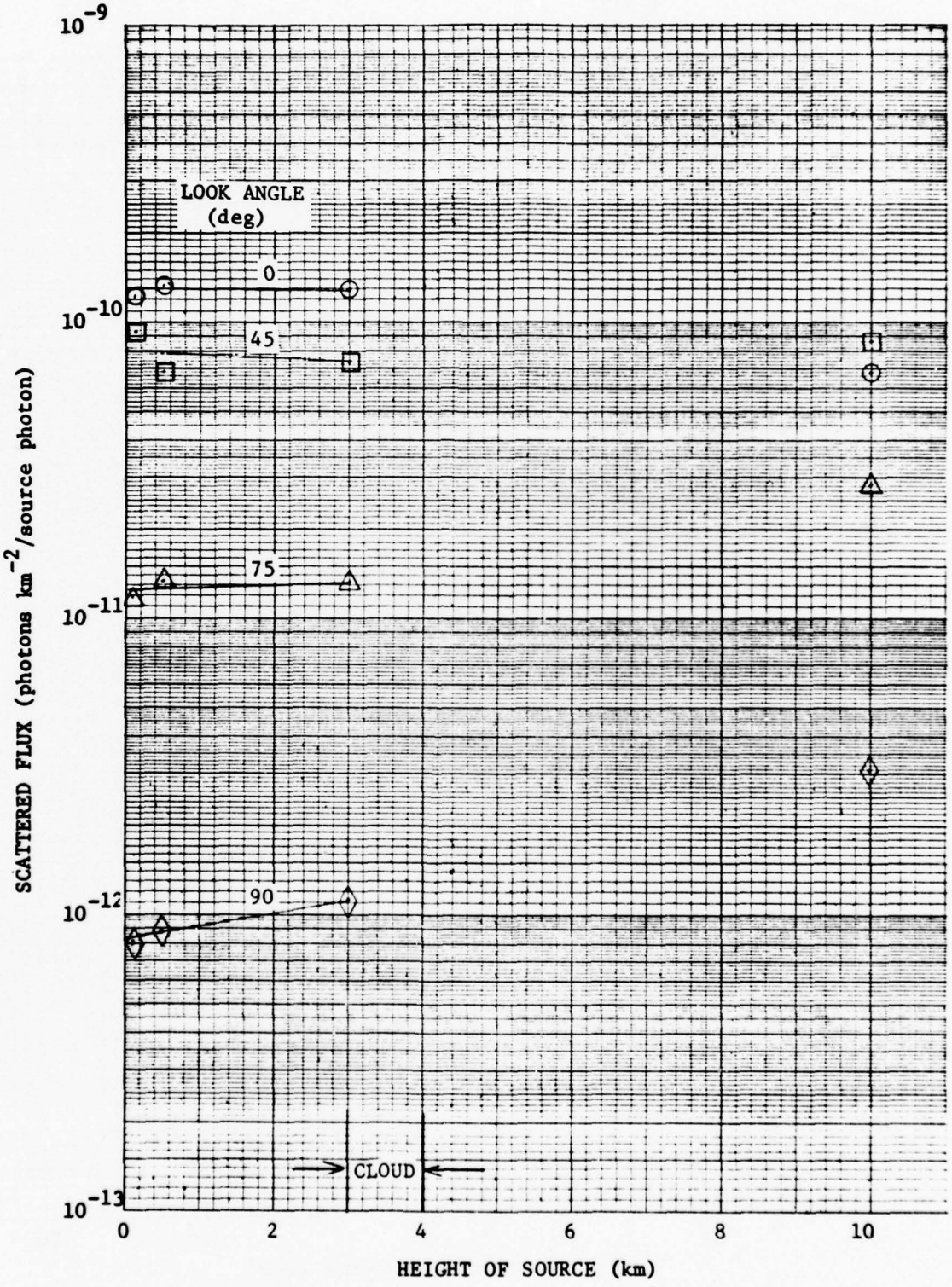

Fig. 27. Variation of the Scattered Flux at the Satellite with the Height of the Source for Look Angles of 0, 45, 75, and 90 Degrees: Atmosphere Containing Altostratus Cloud Layer, Ground Albedo = 0.8, λ = 0.4278 μ

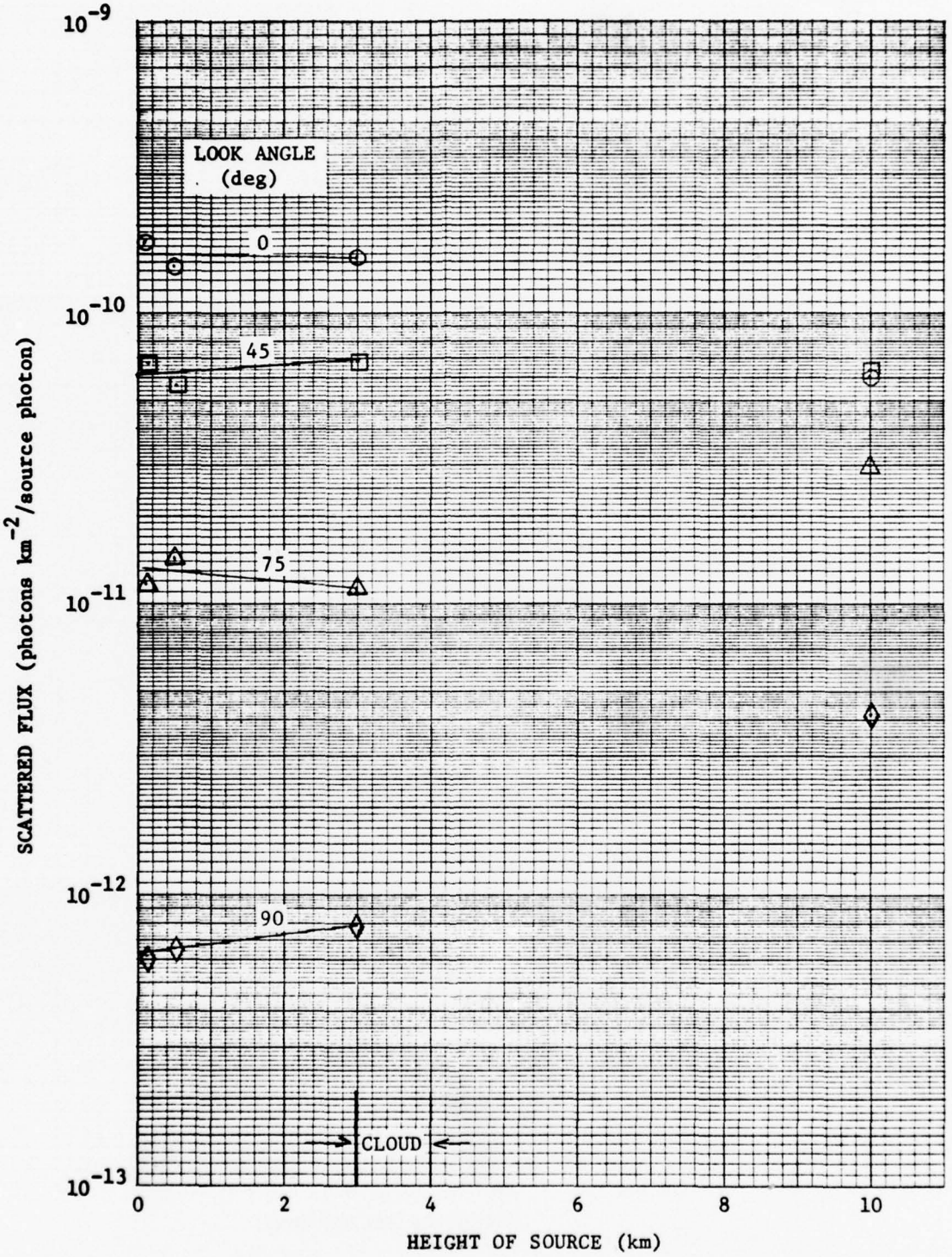

Fig. 28. Variation of the Scattered Flux at the Satellite with the Height of the Source for Look Angles of 0, 45, 75, and 90 Degrees: Atmosphere Containing Altostratus Cloud Layer, Ground Albedo = 0.8, λ = 0.75 μ

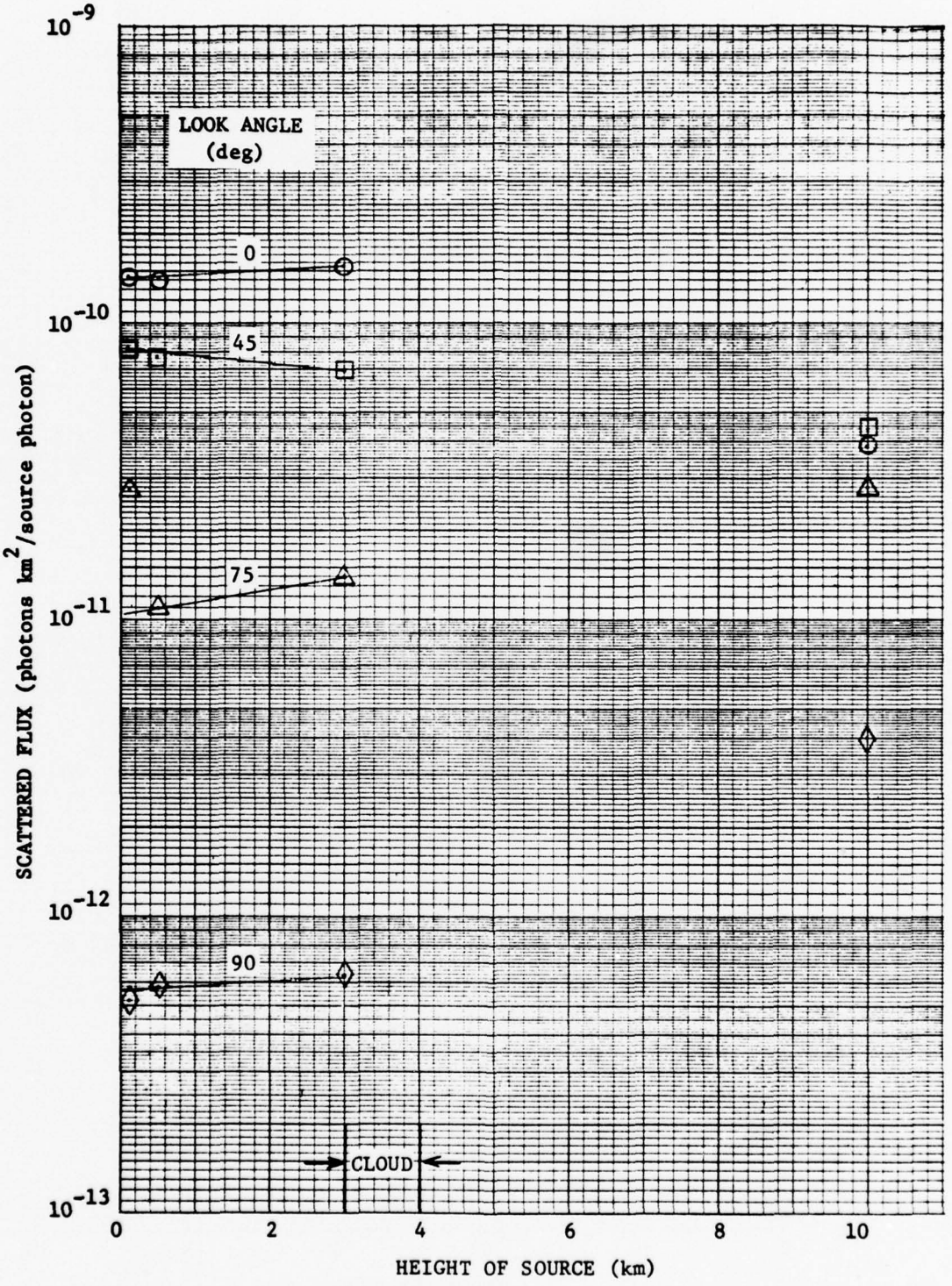

Fig. 29. Variation of the Scattered Flux at the Satellite with the Height of the Source for Look Angles of 0, 45, 75, and 90 Degrees: Atmosphere Containing Altostratus Cloud Layer, Ground Albedo = 0.8, λ = 1.07 μ

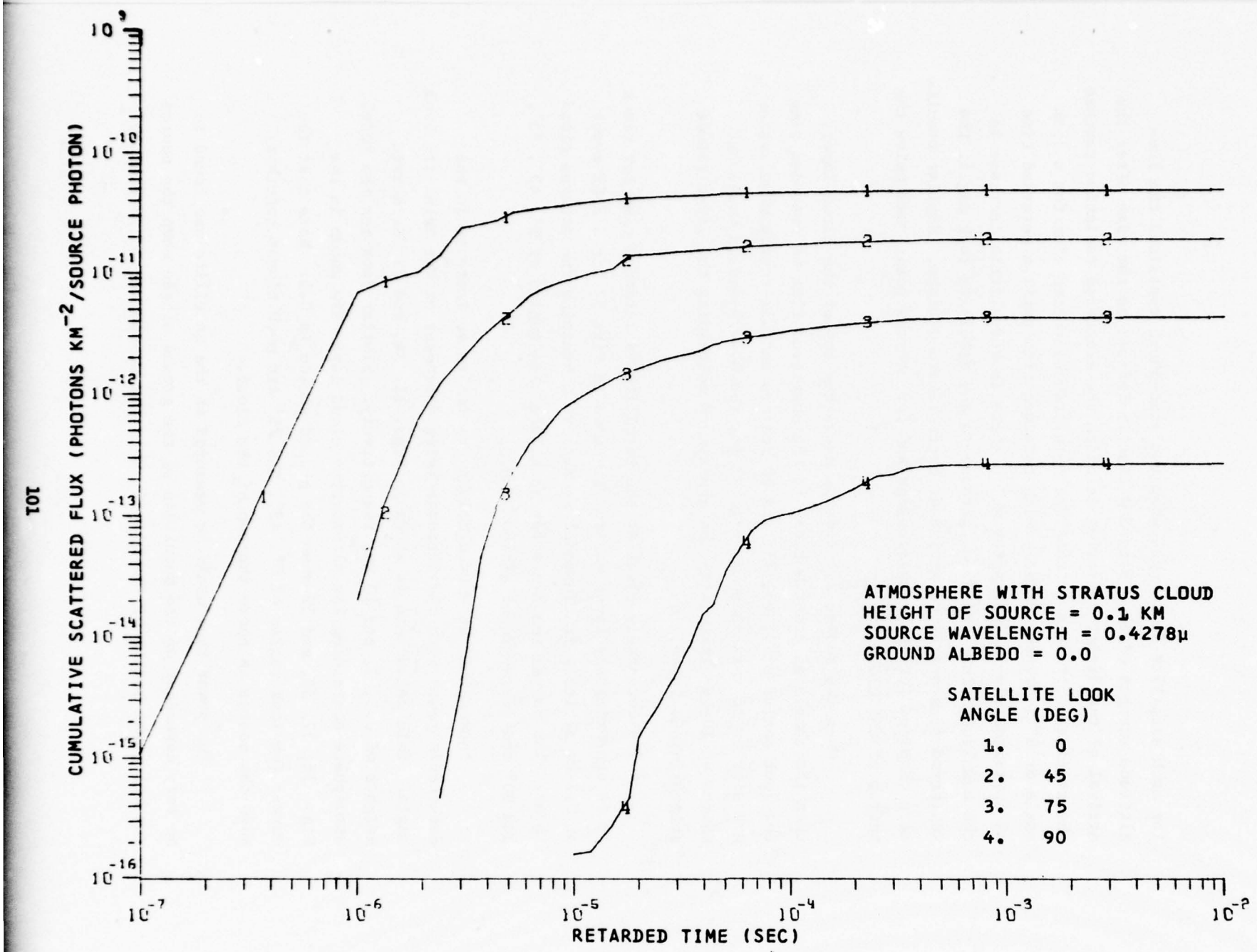

Fig. 30. Cumulative Scattered Flux at Satellite vs Time, Source Height = 0.1 km

for each satellite look angle when the atmosphere contained the low-altitude stratus cloud. Retarded time is defined as the time after the arrival of the direct radiation at which the scattered radiation reaches the receiver. It is seen that the cumulated scattered flux for a look angle of 0° increases rapidly with retarded time until a retarded time of approximately 10 μsec after which there is very little increase in the cumulated flux. With an increase in the satellite look angle, the scattered flux starts to arrive at later retarded times. Similar results were obtained for other wavelengths and for sources positioned below the bottom of the cloud.

When the source altitude is above the top of the cloud layer, then the cumulated distributions of the scattered flux vs retarded time for look angles of 0, 45, 75, and 90 degrees and all source wavelengths are similar to that shown in Fig. 31 for the 0.4278-micron wavelength source at 10-km altitude in the atmosphere containing the low-altitude stratus cloud layer.

The detectable power at the satellite vs retarded time for times up to approximately first maximum is shown in Fig. 32 for a 2-KT event at 0.1-km altitude in the model atmosphere containing the stratus cloud layer. The curves shown are for satellite view angles of 0°, 45°, 75°, and 90° and for a ground albedo of 0.0.

Increasing the source height results in an increase in the detectable power with the increase being dependent on the satellite look angle. This dependence is shown in Figs. 33, 34, and 35 for source heights of 0.5, 3, and 10 km, respectively. Similar data for the model atmosphere containing the altostratus cloud layer are shown in the Figs. 36, 37, 38, and 39 when the ground albedo is 0.0. Note that the curves for look angles of 0°, 45°, and 75° are much closer together when the source is above the top of the cloud.

The power that would be measured at the satellite was found to be very dependent on the magnitude of the ground albedo when the source was below the bottom of the cloud. When the source was above the top

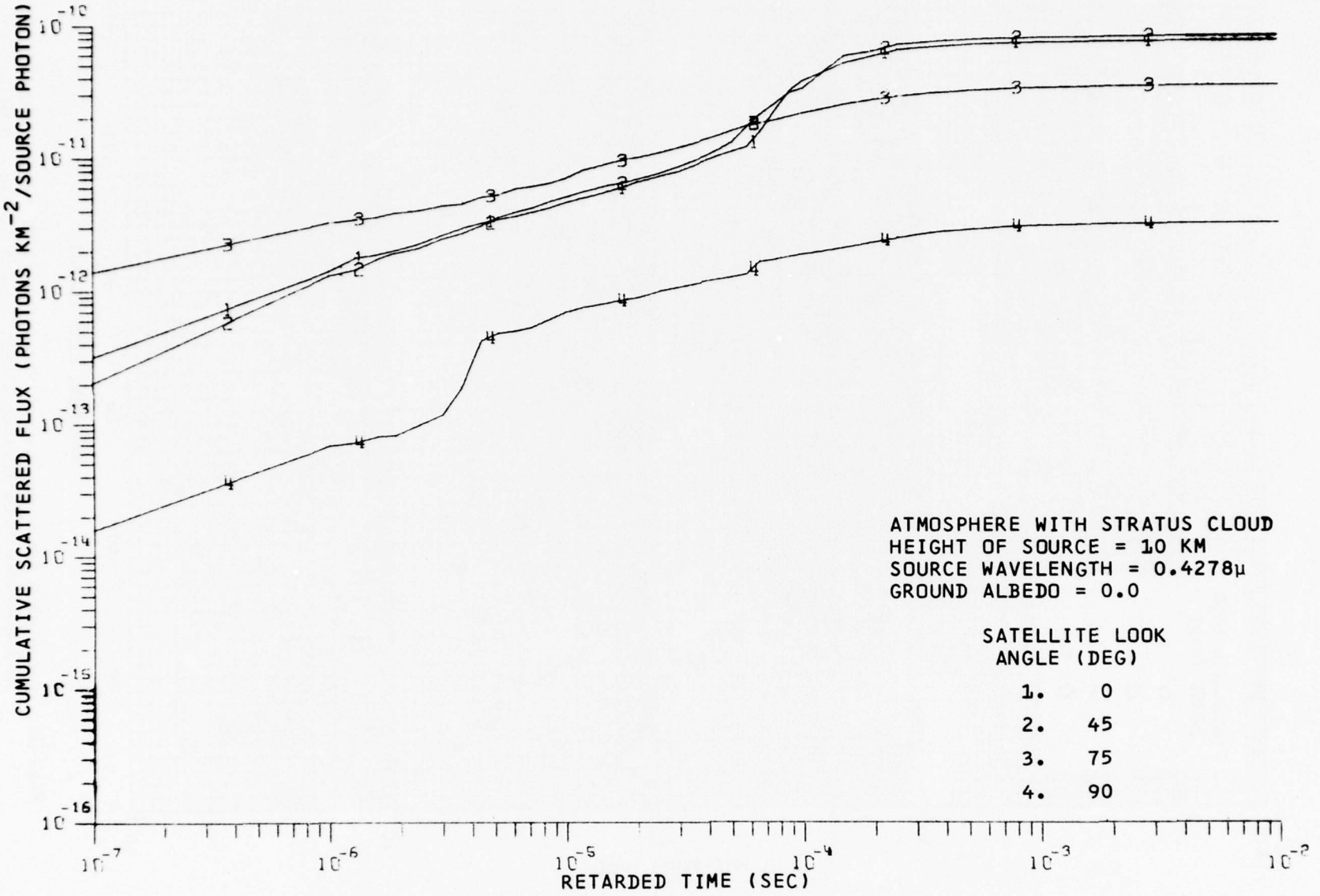

Fig. 31. Cumulative Scattered Flux at Satellite vs Time, Source Height = 10 km

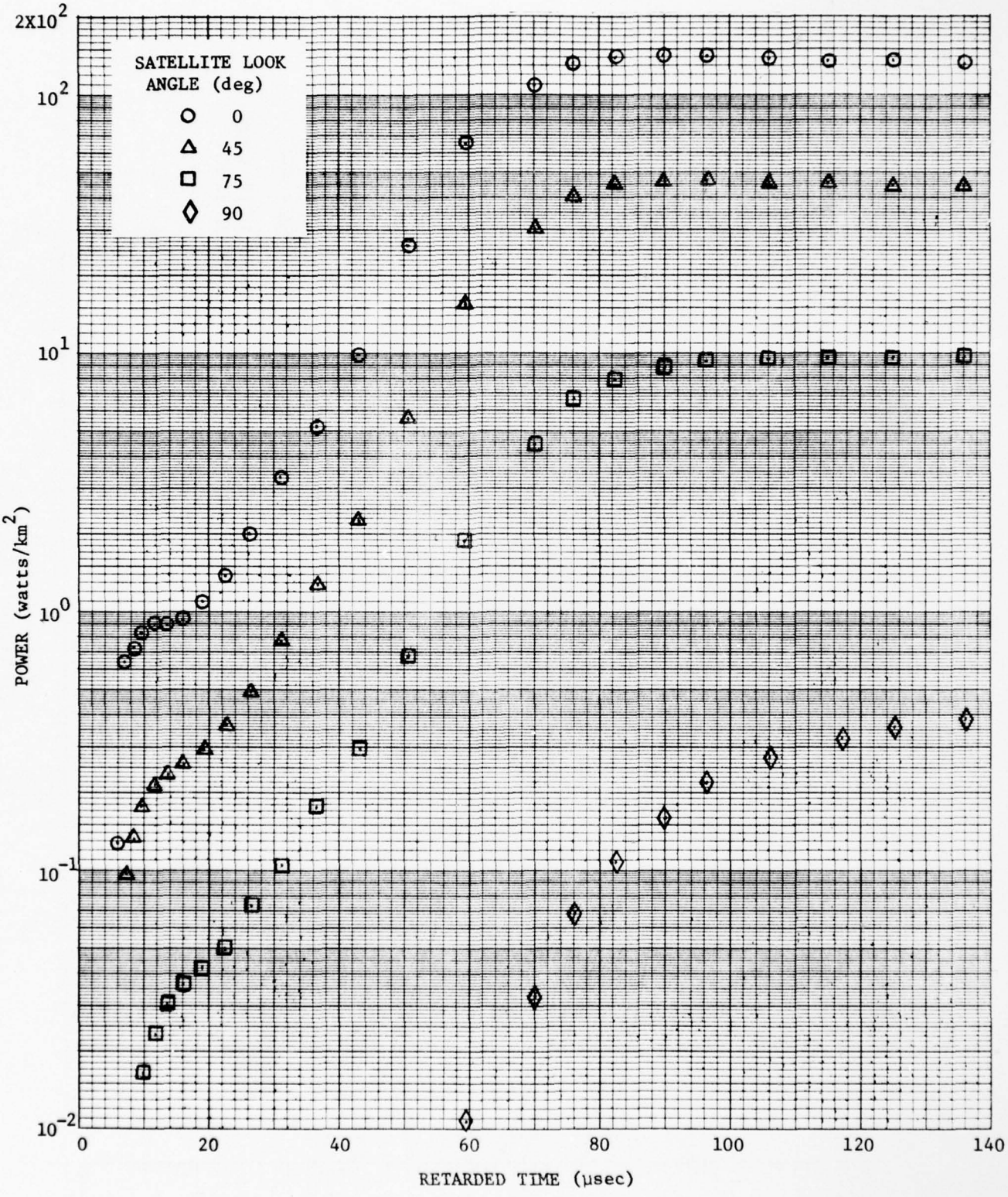

Fig. 32. Detectable Power vs Time at Satellite (2 KT Event at 0.1-km Altitude in Atmosphere with Stratus Cloud, Ground Albedo = 0.0)

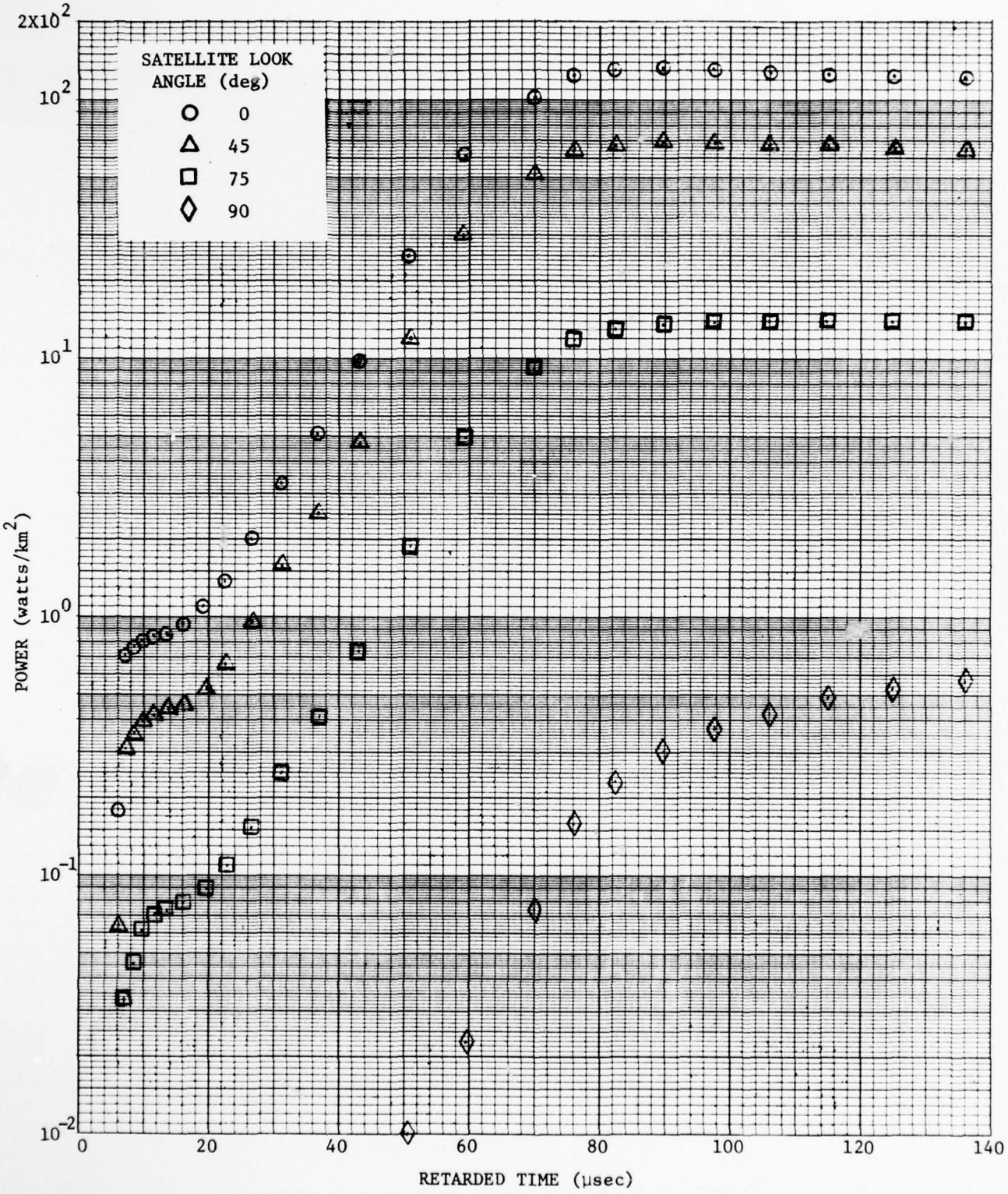

Fig. 33. Detectable Power vs Time at Satellite (2 KT Event at 0.5-km Altitude in Atmosphere with Stratus Cloud, Ground Albedo = 0.0)

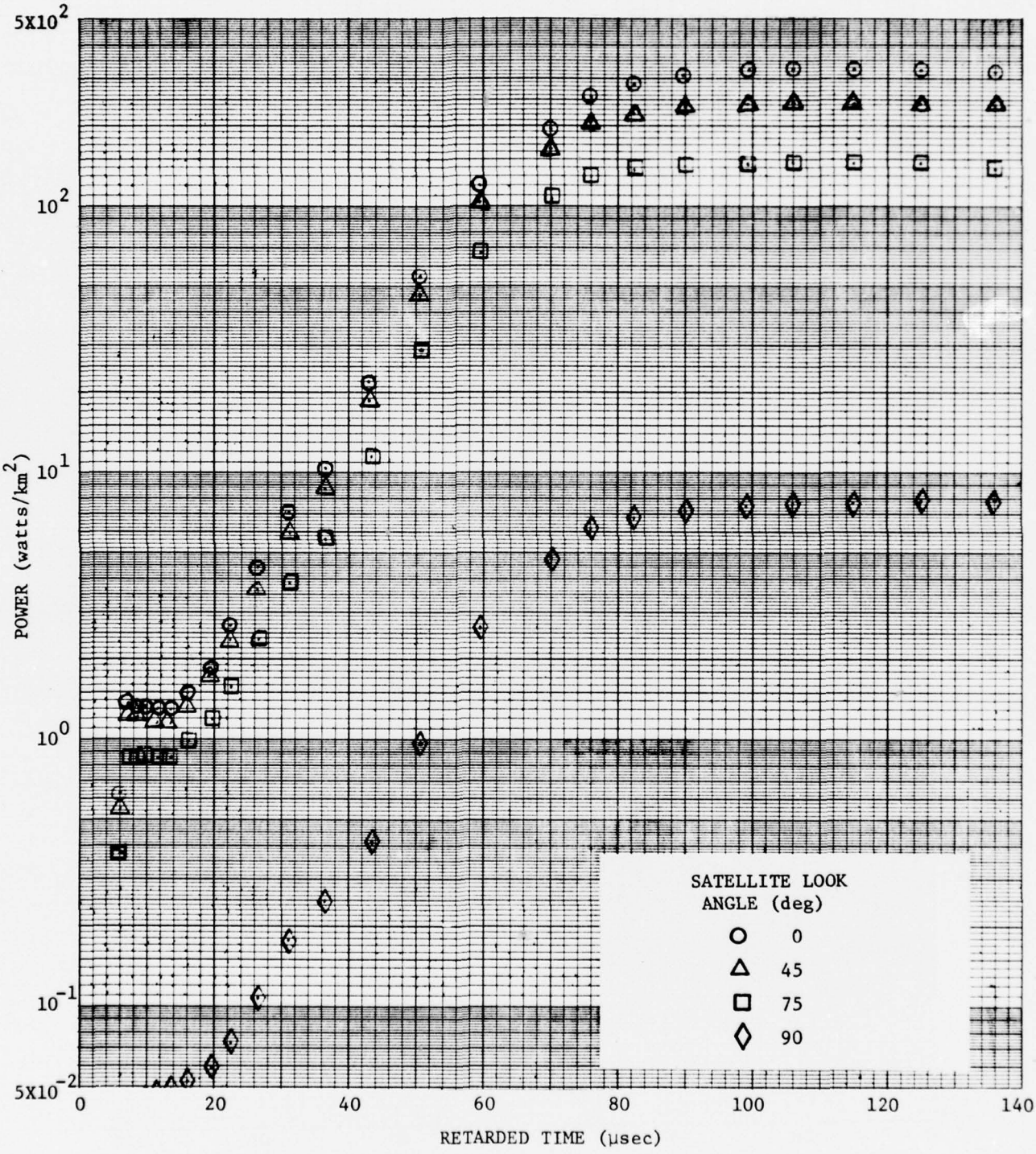

Fig. 34. Detectable Power vs Time at Satellite (2 KT Event at 3-km Altitude in Atmosphere with Stratus Cloud, Ground Albedo = 0.0)

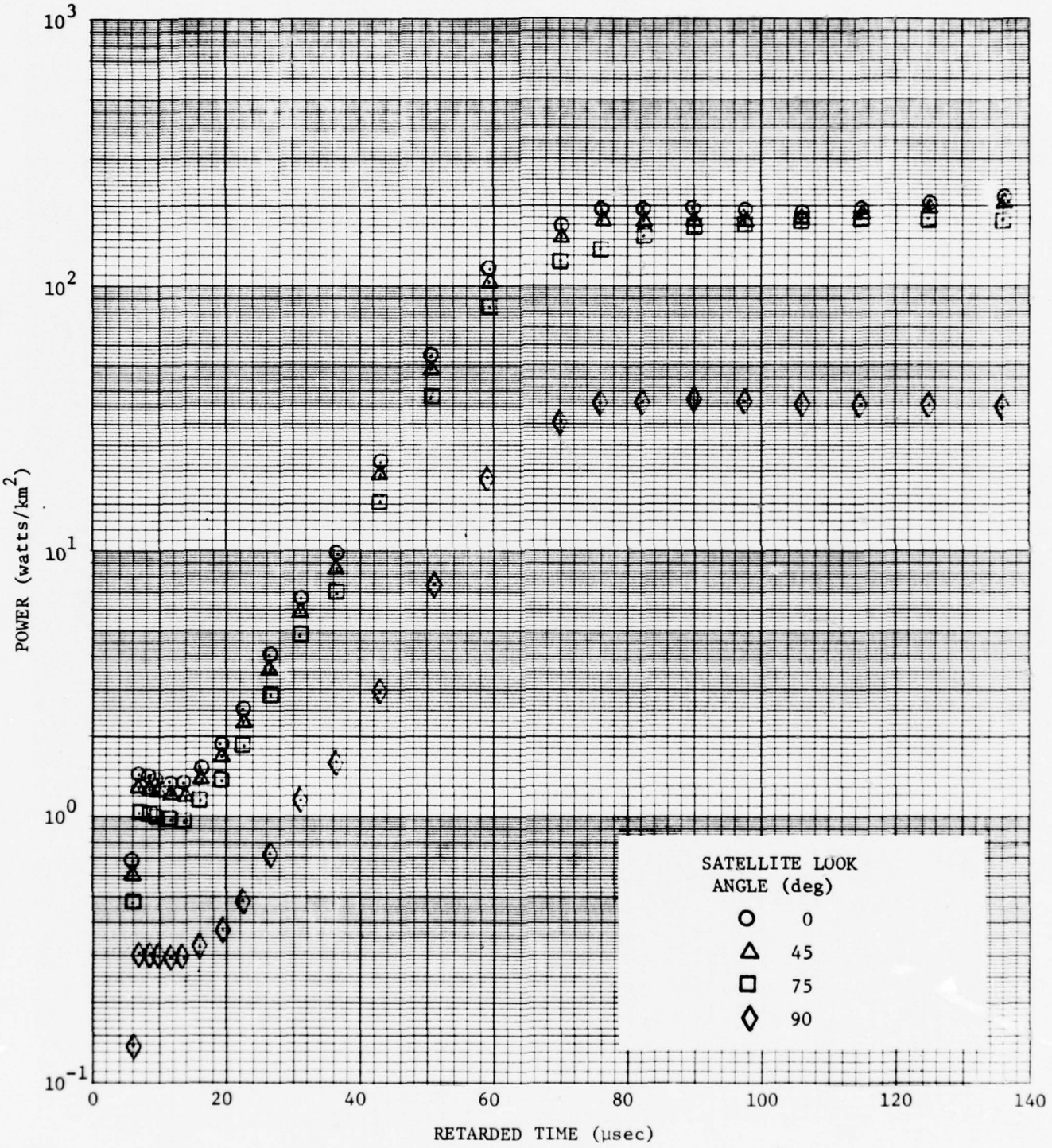

Fig. 35. Detectable Power vs Time at Satellite (2 KT Event at 10-km Altitude in Atmosphere with Stratus Cloud, Ground Albedo = 0.0)

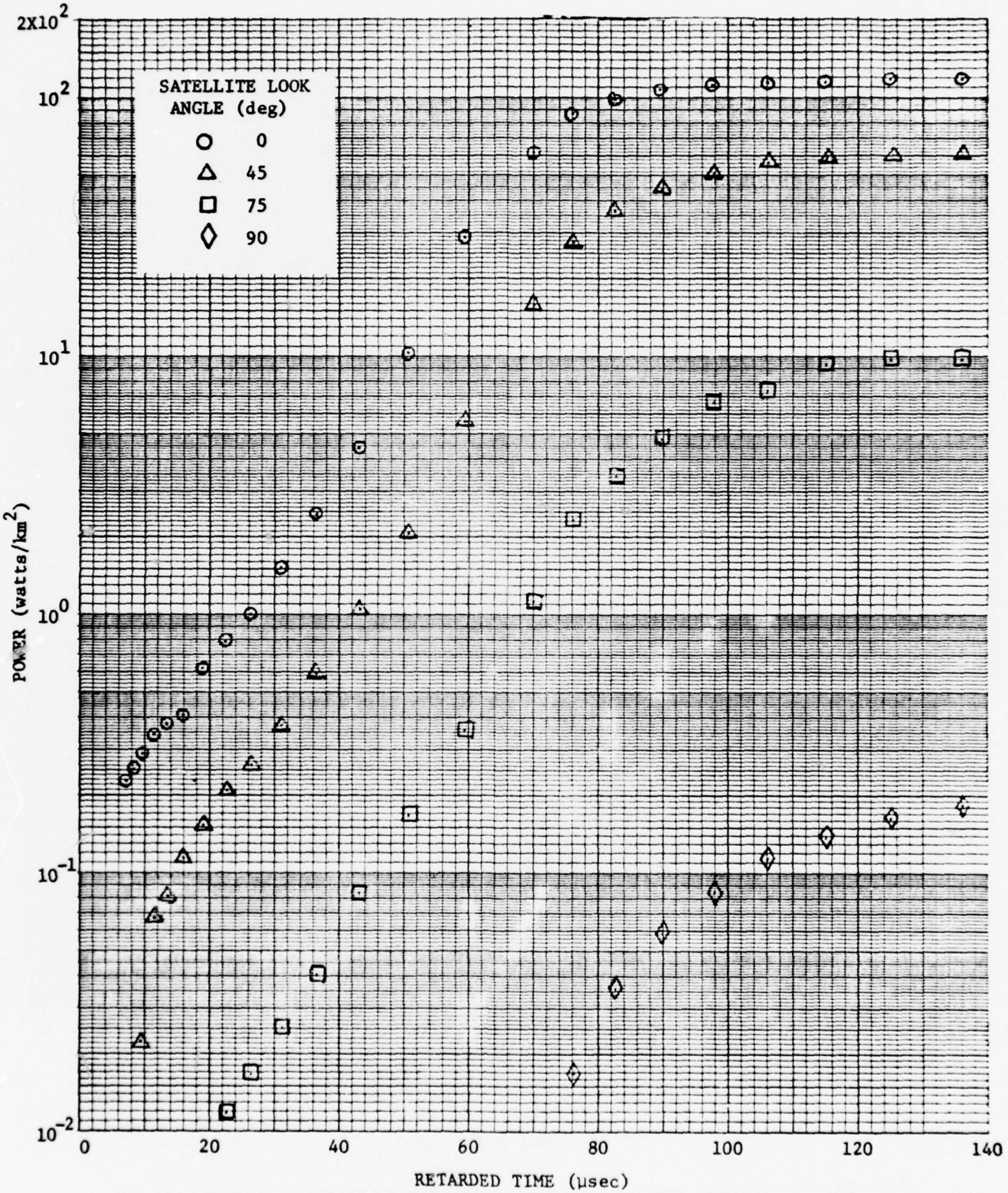

Fig. 36. Detectable Power vs Time at Satellite (2 KT Event at 0.1-km Altitude in Atmosphere with Altostratus Cloud, Ground Albedo = 0.0)

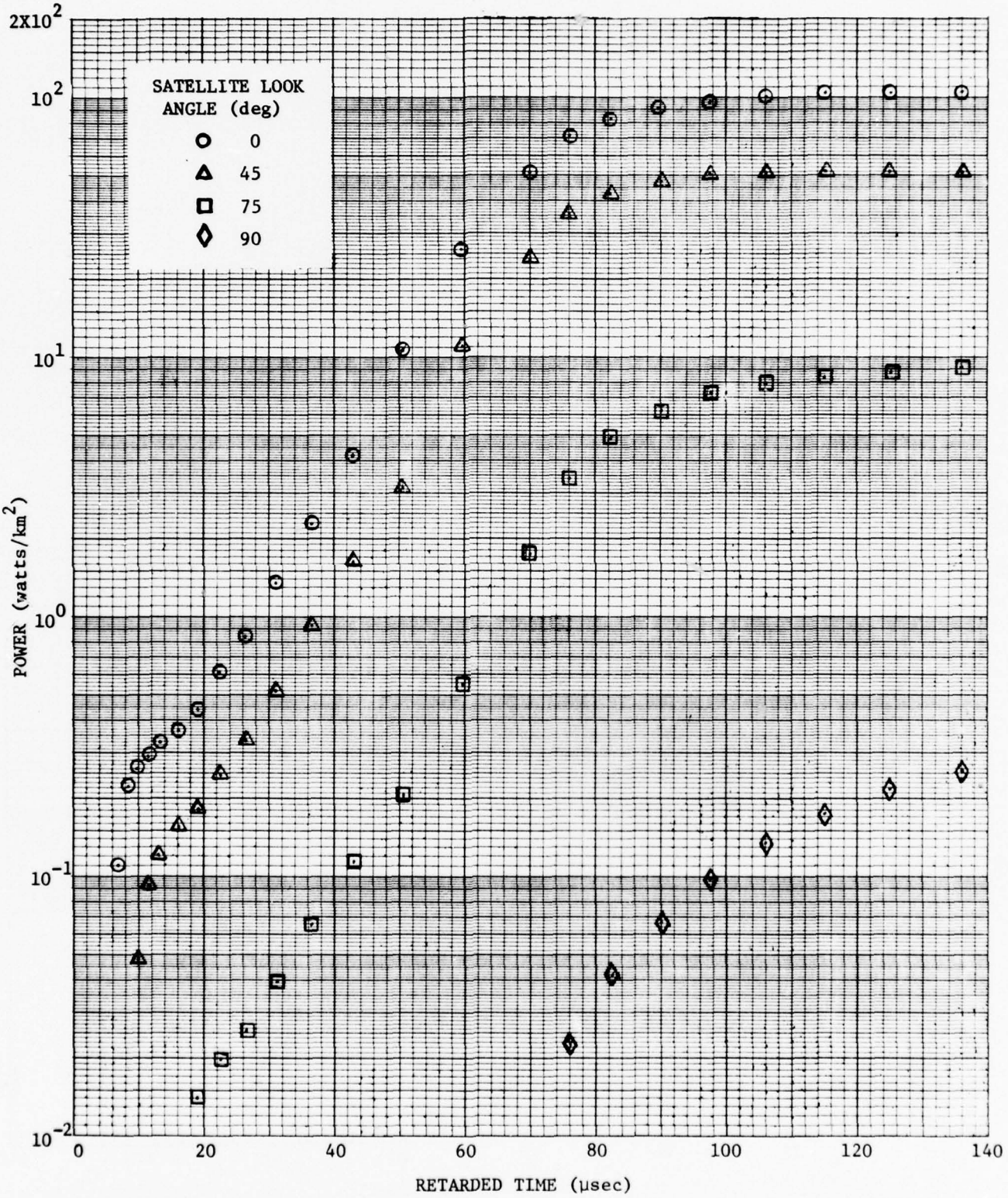

Fig. 37. Detectable Power vs Time at Satellite (2 KT Event at 0.5-km Altitude in Atmosphere with Altostratus Cloud, Ground Albedo = 0.0)

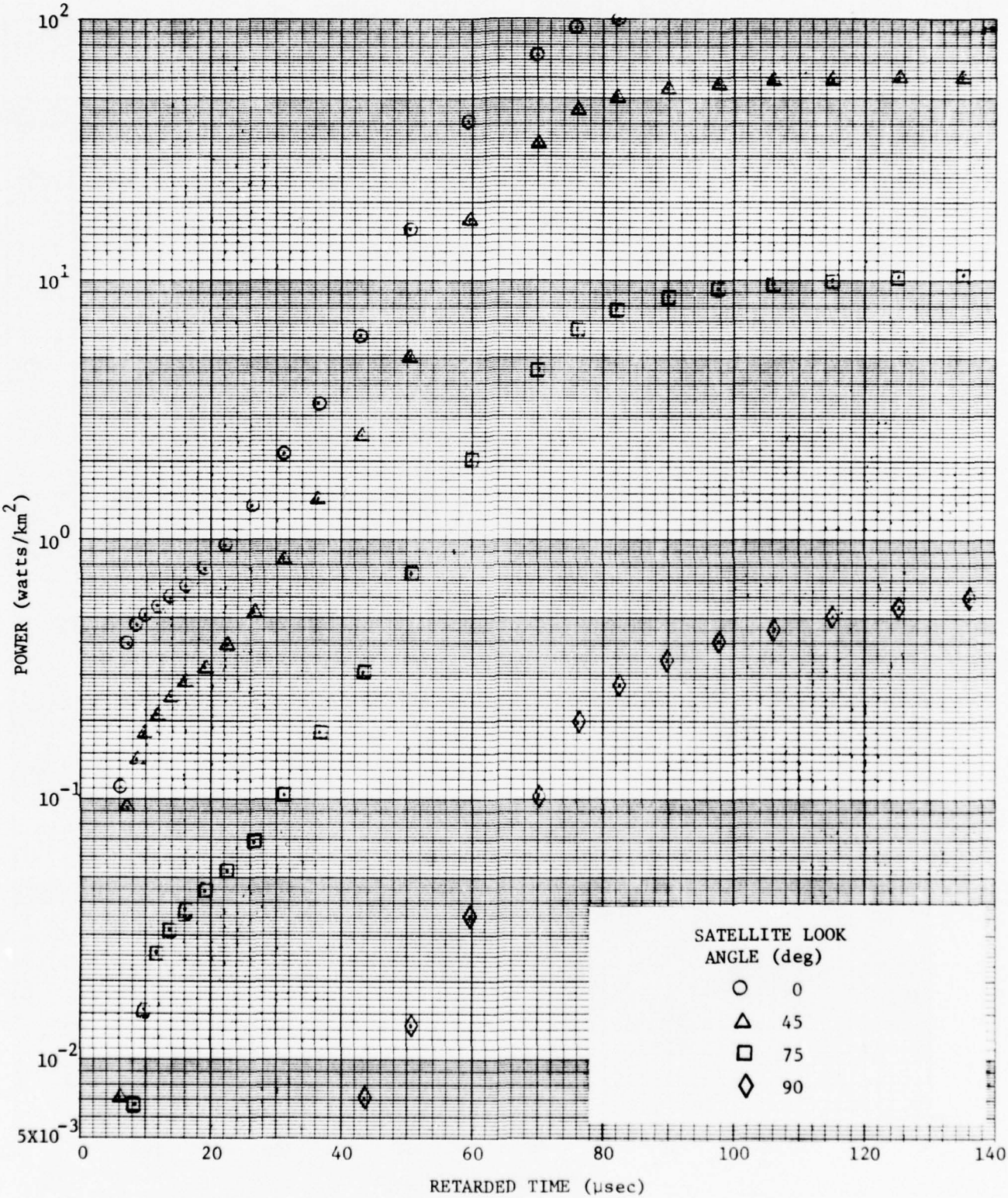

Fig. 38. Detectable Power vs Time at Satellite (2 KT Event at 3-km Altitude in Atmosphere with Altostratus Cloud, Ground Albedo = 0.0)

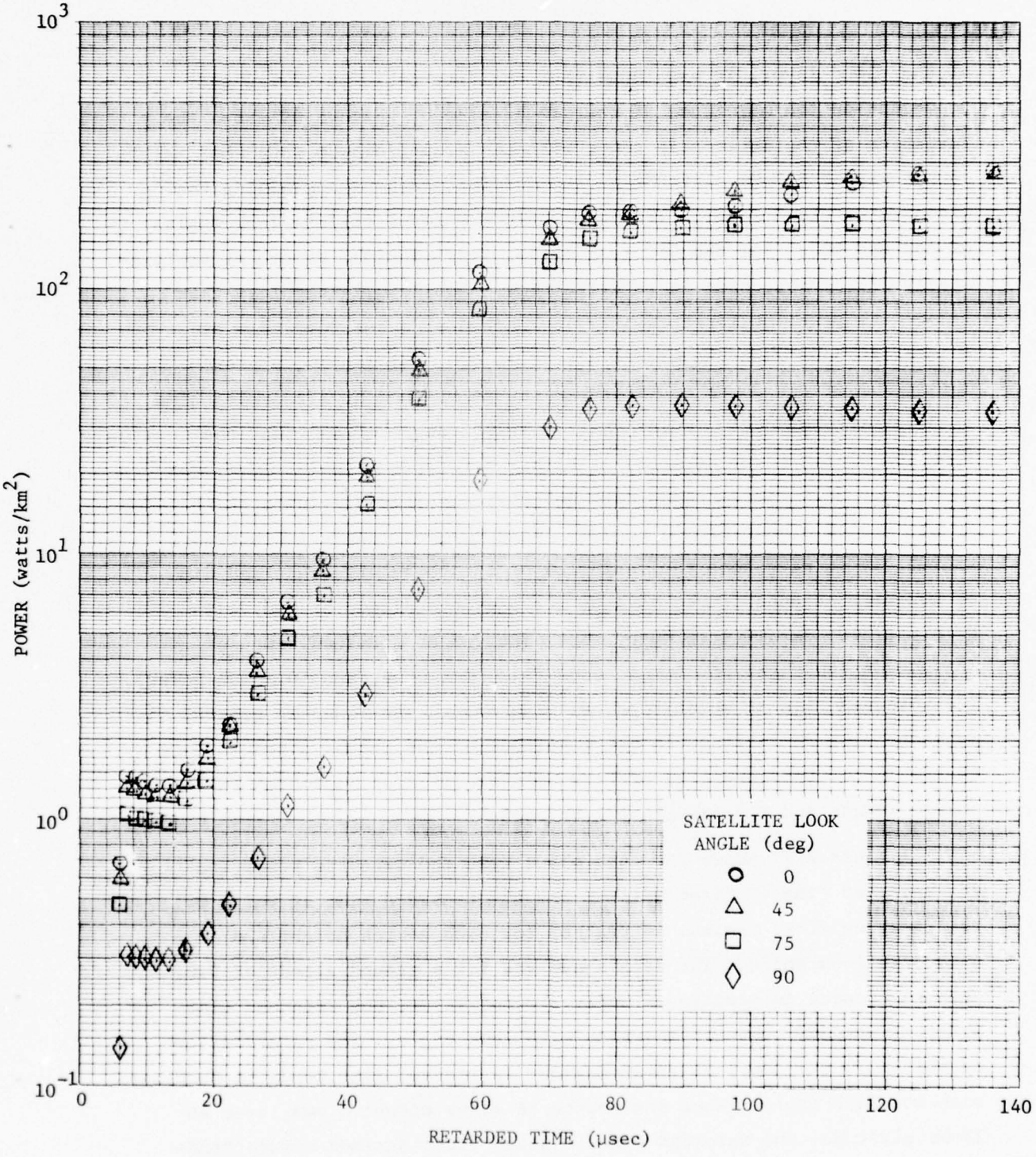

Fig. 39. Detectable Power vs Time at Satellite (2 KT Event at 10-km Altitude in Atmosphere with Altostratus Cloud, Ground Albedo = 0.0)

of the cloud layer, it was found that the detectable power was not dependent on the magnitude of the ground albedo. Figure 40 shows the variation of the detectable power with the ground albedo when the source was at 0.1-km altitude in the model atmosphere containing the altostratus cloud layer. The data shown are for satellite look angles of 45° and 90°. For the 45° look angle, first maximum occurs at approximately 136 microseconds in retarded time. Justly slightly less than 1/2 of the power at first maximum is reached at a retarded time of 70 microseconds when the ground albedo is 0.0. Similarly, approximately 0.1 of the power at first maximum is reached at a retarded time of 36.4 microseconds. It is seen for a look angle of 45° that the fraction of the power detected at either a retarded time of 70 microseconds or 36.4 microseconds does not vary significantly with an increase in the ground albedo from 0 to 1.0. When the look angle is increased to 90°, it is seen that the variation of the power at a retarded time of 192 microseconds (first maximum for a ground albedo of 0.0) with ground albedo is different from that observed at retarded times of 106 microseconds and 76 microseconds ($\sim$1/2 max power and $\sim$0.1 max power). The retarded time at which first maximum occurs was found in general to increase with an increase in the magnitude of the ground albedo. This change in the retarded time of first maximum is also dependent on the source height and the satellite look angle.

Table XXVI shows for each cloud type the detected power and the retarded time at first maximum and the retarded time at which 0.1 the power at first maximum is reached for each source height and satellite look angle. The data shown are for a ground albedo of 0.0. When the source is positioned under a cloud layer, the retarded time of first maximum tends to increase with look angle. The retarded time at which 0.1 the power at first maximum is reached also tends to increase with the look angle. When the source is above either cloud layer at 10-km altitude, the retarded time at which first maximum occurs tends to decrease with an increase in the look angle and the time at which 0.1 of the power at first maximum occurs remains nearly constant for all look angles.

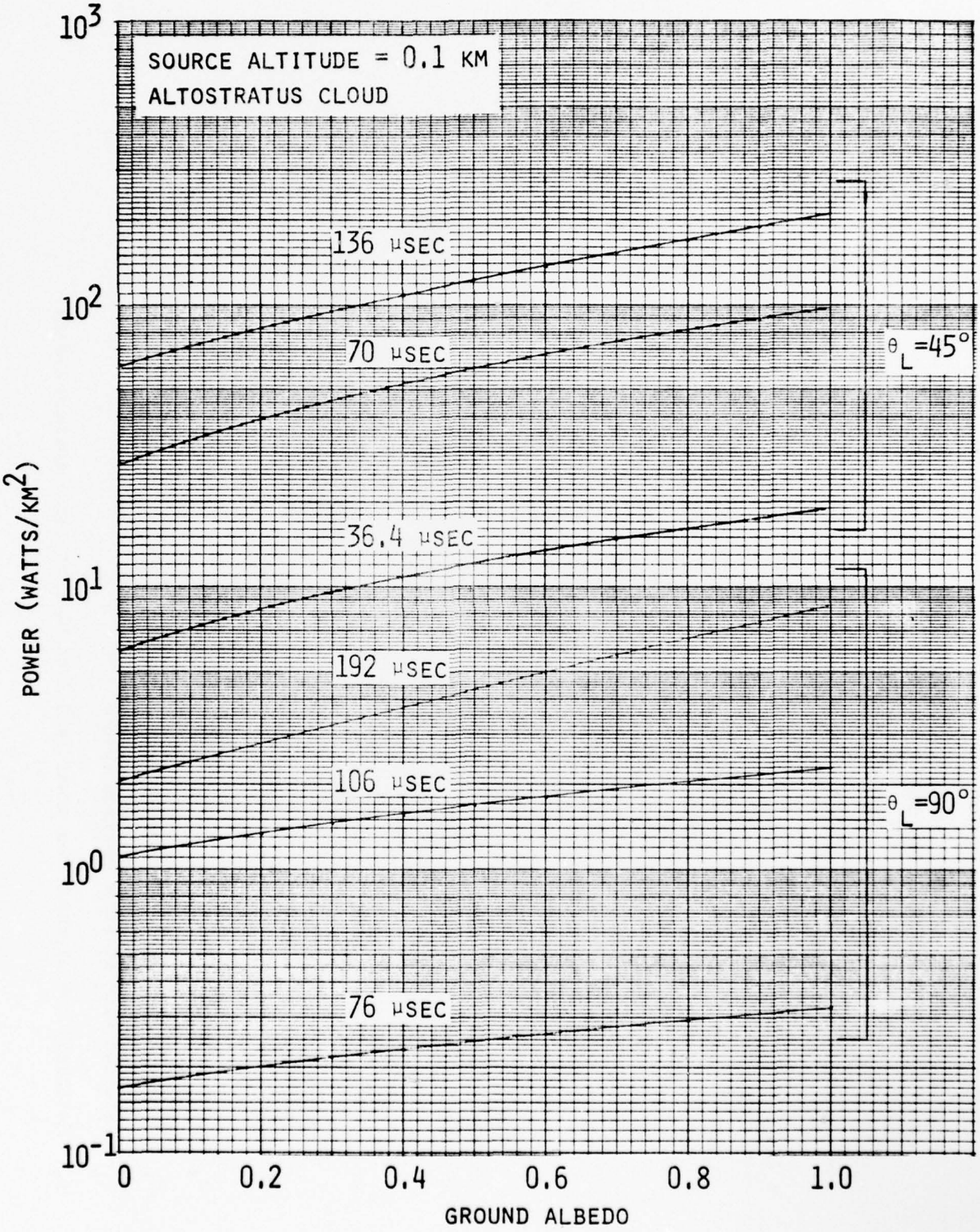

Fig. 40. Variation of Detectable Power with Ground Albedo for Retarded Times of First Maximum, One-Half First Maximum and One-Tenth First Maximum, and Look Angles of 0° and 90°

TABLE XXVI. POWER AT FIRST MAXIMUM AND RETARDED TIMES FOR FIRST MAXIMUM AND WHEN THE POWER IS ONE-TENTH THE POWER AT FIRST MAXIMUM

Ground Albedo = 0.0

		ALTOSTRATUS			STRATUS		
h_s (km)	θ_L (deg)	P_1	t_1	t_2	P_1	t_1	t_2
0.1	0	1.187+2	136	52.0	1.387+2	106	45.0
	45	6.123+1	136	60.0	4.623+1	97.4	49.0
	75	9.765+0	136	69.0	9.615+0	125	53.0
	90	2.020-1	192	77.0	4.544-1	304	72.5
0.5	0	1.051+2	136	50.5	1.319+2	89.7	45.5
	45	5.191+1	136	54.0	6.885+1	89.7	46.0
	75	9.258+0	147	63.5	1.400+1	106	48.5
	90	3.816-1	211	81.0	5.814-1	192	67.5
3	0	1.119+2	136	48.5	3.274+2	106	46.5
	45	6.145+1	160	52.0	2.434+2	106	45.5
	75	1.053+1	147	53.5	1.451+2	125	45.0
	90	6.705-1	192	65.5	7.822+0	136	48.5
10	0	2.878+2	160	45.0	2.429+2	192	44.0
	45	2.889+2	192	46.5	2.353+2	192	45.0
	75	1.733+2	106	44.5	1.801+2	115	44.0
	90	3.666+1	89.7	45.0	3.691+1	89.7	45.0

h_s = Source height (km)

P_1 = Power at first maximum (watts/km^2)

t_1 = Retarded time at first maximum (μsec)

t_2 = Retarded time at which the power is 0.1 of that at first maximum (μsec)

An attempt was made to evaluate the angular and time distributions of the scattered light as it exits from a cloud located above a point isotropic source. Computer runs were made using the TPOLOL procedure which gives the time and angular dependence of the scattered light intensity at a set of point receivers. These runs were made for the 10-km meteorological range model atmosphere containing a five mean-free-path thick stratus cloud located between 500 and 1000 meters above the ground surface. The point source was located at the lower boundary of the cloud. An analysis of these TPOLOL runs showed that a very large statistical variation exists in the results.

An example of the statistical variation is illustrated by observing the angular distribution of the scattered intensity at the receiver located at a look angle of zero degrees (detector located at the top of the cloud directly above the source position). Since the source emission and the atmosphere are azimuthally symmetric about the source receiver axis, the scattered radiation signal at the detector should also be azimuthally symmetric. Any variation in the calculated scattered radiation signal with the azimuthal angle is then due to statistical variations in the results. Figure 41 shows the scattered intensity, integrated over time and polar angle, as a function of azimuthal angle for the receiver located at the zero-degree look angle. Although 25,000 histories were run with an average of 37.769 collisions per history, there are variations by as much as a factor of three in the azimuthal distribution.

It was anticipated that the large statistical variations were caused by the $1/r^2$ factor in the estimating function. The estimate of the scattered intensity contributed by each collision is divided by the square of the distance from the collision to the receiver position. For a receiver located at the top of the cloud, a collision may occur near the top of the cloud and thus produce extremely high estimates of the scattered intensity. A problem, using the model atmosphere described above, was run with the receivers located at a satellite position

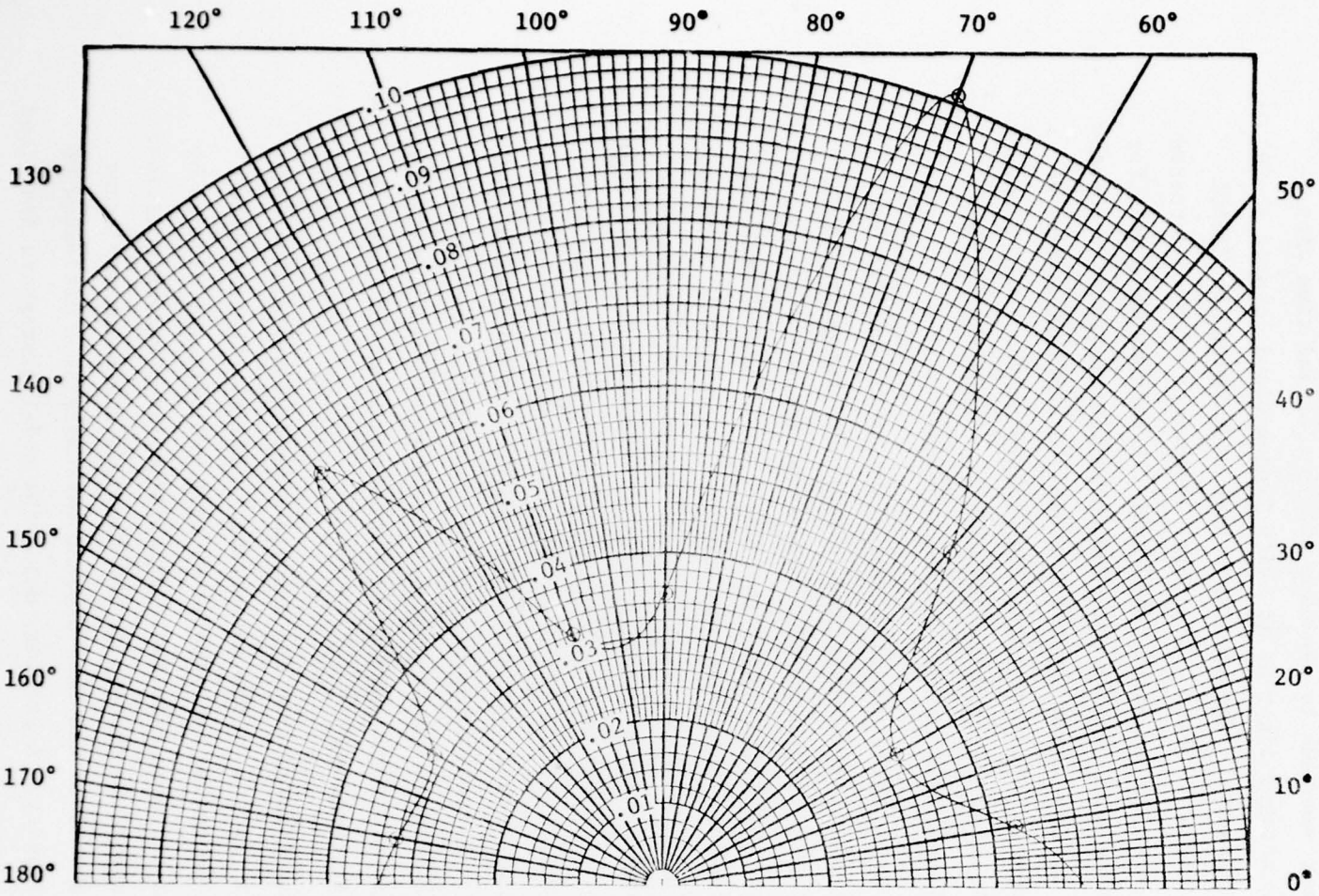

Fig. 41. Azimuthal Angle Dependence of Scattered Intensity at Cloud Top for a Detector Look Angle of 0°: Ground Albedo = 0.8, Source Height = 500 m, Detector Height = 1 km, λ = 0.4278 μ, 5 Mean-Free-Path Thick Stratus Cloud

(35800 kilometers altitude). The azimuthal distribution of the scattered intensity obtained from that problem (multiplied by a factor of 10^{10}) is plotted in Fig. 42. Note that the variation in the azimuthal distribution for the satellite receiver is much smaller than that computed for the receiver at the top of the cloud. This is due to the fact that all collisions in the cloud and surrounding atmosphere are approximately the same relative distance from the satellite receiver and, therefore, the variation in the $1/r^2$ factor for each estimate of the scattered intensity is small.

The statistical variations in the time and spatial distributions of the scattered intensities computed for point receivers located at the cloud top were also found to be extremely large. Therefore, it was decided that area receivers rather than point receiver should be used to determine the time, angular, and spatial distributions of the scattered intensity at the cloud top. An effort has been initiated to develop a modified version of POLO that will utilize surface receivers instead of point receivers to compute the time, angular, and spatial distributions of the scattered intensity for radiation transport in atmosphere containing clouds. It is believed that the use of surface receivers instead of point receivers will reduce the statistical variation in the computed scattered intensities for receivers positioned within the atmosphere.

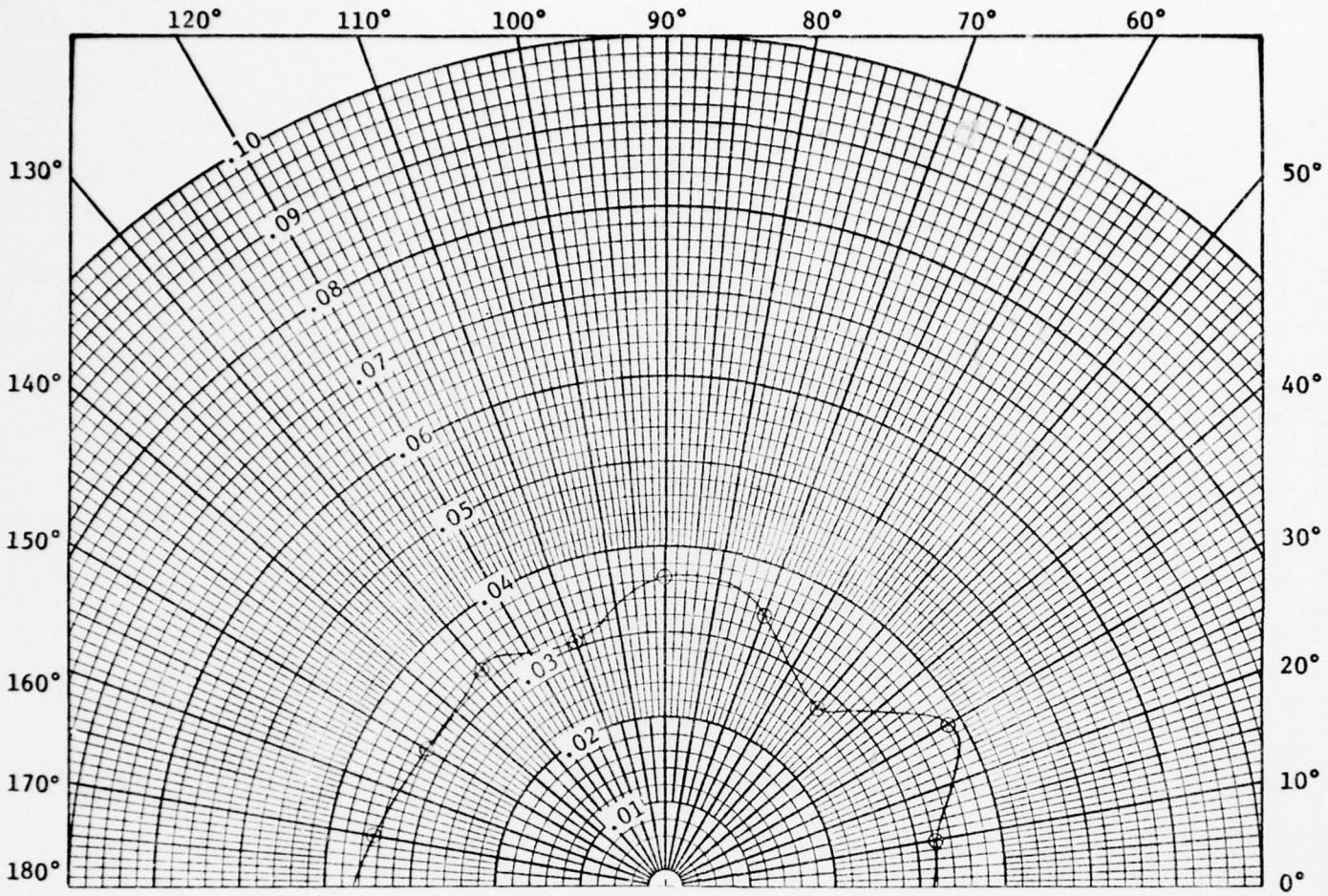

Fig. 42. Azimuthal Angle Dependence of the Scattered Intensity at a Satellite Detector for a Look Angle of 0°: Ground Albedo = 0.0, Source Height = 500 m, Detector Height = 35800 km, λ = 0.4278 μ, 5 Mean-Free-Path Thick Stratus Cloud

VIII. DISCRETE ORDINATES USE IN TIME-DEPENDENT LIGHT TRANSPORT CALCULATIONS

A study was initiated to determine the feasibility of using time-dependent discrete-ordinate methods for light transport in clouds. The extremely forward peaked phase functions encountered in cloud problems combined with the large optical thicknesses of clouds tend to produce large statistical fluctuations in results obtained with the Monte Carlo method. The initial effort to apply discrete ordinate methods was an attempt to utilize the TDA (Time Dependent ANISN) Ref. 4) program distributed by the Radiation Shielding Information Center at ORNL as code package CCC-180.

TDA is a one-dimensional code, i.e., plane or spherical geometry. While it is not possible to describe realistic cloudy atmospheres containing a point isotropic light source with TDA, it is believed that a successful application of TDA to light transport should precede applications of two-dimensional discrete ordinate methods such as the TWO-TIME code currently undergoing checkout at LASL. The attempt to utilize the TDA program for light transport has pinpointed several difficulties that must be overcome before discrete-ordinate methods can be successfully applied to time-dependent light transport problems.

In TDA it is essential that the spatial intervals and time boundaries coincide such that as the wave front passes from one spatial interval to the next, the age (time after source emission) of the wave front is such as to put it in the center of the interval. Otherwise, the wave front becomes smeared over distance (and possibly time) and resolution is lost. For an optimum discrete-ordinates solution, the spatial intervals are usually selected to be less than one mean-free-path in width. After the required spatial interval values are calculated, the time required for the wave front to reach each spatial boundary is calculated using the velocity of light. After the wave front leaves the cloud, the spatial interval and time boundaries can be changed (within reason) to suit the user's needs.

The coefficients of an nth order Legendre polynomial are required to define the scattering phase functions in the TDA program. The Legendre polynomial coefficients for a given sized aerosol particle may be determinted with combinations of the A_n and B_n scattering functions computed with Mie theory (Ref. 20) as will be discussed later. However, the expansion of the phase function for aerosols of the sizes typically found in clouds may require Legendre polynomials of the order of 200 to 300 or more. TDA requires that the angular quadrature set contain at least as many angle quadratures as there are coefficients in the Legendre polynomial used to represent the scattering function. Use of quadratures of this order in the TDA program introduces problems in allocating core space and requires large amounts of computer time. It has also been determined that no symmetric Gauss-Legendre quadrature would be adequate (with a reasonable number of directions) to represent the peak portion of the phase function.

Communications with one of the authors of the TDA program indicated that it may be feasible to modify the TDA program to read in a precalculated set of quadratures and weights. In that case, a smaller quadrature set can possibly be selected to adequately represent the scattering phase function.

8.1 Expansion of the MIE Phase Function in Legendre Polynomials

In applying results obtained from Mie theory to radiative transfer calculations, it is necessary when using calculational methods such as discrete ordinates to expand the phase function, $P(\cos\theta)$, in Legendre polynomials:

$$P(\cos\theta) = \sum_{n=0}^{\infty} a_n p_n(\cos\theta) \ ,$$

where $p_n(\cos\theta)$ is the Legendre polynomial of order n.

Although it is possible to calculate the coefficients a_n by numerical integration from the i_1 and i_2 functions of Mie theory, a

direct calculation of these coefficients from theory is more efficient. Such a calculation scheme is provided in papers by Chu and Churchill (Ref. 23), and by Clark et al. (Ref. 24). The calculations are effected by the use of the Mie A_n and B_n scattering functions, and involve coefficients labeled w and v which are functions only of the order n of the Legendre polynomial and are independent of any other input.

Without discussing the methods of converting the Mie equations to corresponding Legendre polynomial forms (see Refs. 23 and 24), we will show and discuss the final forms of the Legendre solution giving the Legendre coefficients a_n by use of computer programs.

Equation (8.1) gives the solution of a_n:

$$a_n = \frac{2}{\alpha^2 K(\alpha,\beta)} \sum_{j=1}^{\infty} \sum_{k=1}^{j} \left(\frac{2}{1+\delta_{jk}}\right) \left\{(2n+1) \left[\frac{j(j+1)+k(k+1)-n(n+1)}{2}\right]^2 w_{jkn} W_{jk} + v_{jkn} V_{jk}\right\} \tag{8.1}$$

$$\delta_{jk} = \begin{cases} 0 \text{ for } j \neq k \\ 1 \text{ for } j = k \end{cases} \tag{8.2}$$

$$W_{jk} = \mathrm{Re}(A_j)\mathrm{Re}(A_k) + \mathrm{Im}(A_j)\mathrm{Im}(A_k) + \mathrm{Re}(B_j)\mathrm{Re}(B_k) + \mathrm{Im}(B_j)\mathrm{Im}(B_k) \tag{8.3}$$

$$V_{jk} = \mathrm{Re}(A_j)\mathrm{Re}(B_k) + \mathrm{Im}(A_j)\mathrm{Im}(B_k) + \mathrm{Re}(B_j)\mathrm{Re}(A_k) + \mathrm{Im}(B_j)\mathrm{Im}(A_k) \tag{8.4}$$

where Re = real part of, Im = imaginary part of, and $A_n(\alpha,\beta)$ and $B_n(\alpha,\beta)$ or (A_j, A_k, B_k) are Mie scattering functions obtained with the MIE-2 computer code (Ref. 20).

The other variables are:

$$\alpha = 2\pi RI/\lambda \tag{8.5}$$

RI = particle radius (μ)

λ = wave length (μ)

$$\beta = \alpha(m-ik) \tag{8.6}$$

m = index of refraction of particle relative to the surrounding medium,

k = extinction coefficient of the particle material.

$$K(\alpha,\beta) = \frac{\sigma_{ST}}{\pi(RI)^2} \tag{8.7}$$

σ_{ST} = scattering cross section

$\pi(RI)^2$ = geometric geometric cross section

The definitions of w_{jkn} and v_{jkn} are given in terms of the recursion relationships used to calculate them rather than the original equations given in Ref. 23.

$$w_{n-1,1,n} = \frac{(n+1)}{(2n+1)(2n+3)}, \tag{8.8}$$

$$\frac{W_{j-1,k+1,n}}{W_{jkn}} = \frac{(j+k-n+1)(j+k+n+2)}{(j+k-n+2)(j+k+n+3)}, \tag{8.9}$$

$$\frac{W_{j-2,k,n}}{W_{jkn}} = \frac{(j+k+n+1)(j+k-n)(j-k+n)(k-j+n+1)}{(j+k+n)(j+k-n-1)(j-k+n-1)(k-j+n+2)}, \tag{8.10}$$

$$V_{n,1,n} = n(n+1), \tag{8.11}$$

$$\frac{V_{j+1,k+1,n}}{V_{jkn}} = \frac{(j+k-n+2)(j+k+n+3)}{(j-k-n+1)(j+k+n+2)}, \tag{8.12}$$

$$\frac{V_{j-2,k,n}}{V_{jkn}} = \frac{(j+k+n)(j+k-n-1)(j+k+n-1)(k-j+n+2)}{(j+k-n+1)(j+k-n)(j-k+n)(k-j+n+1)}. \tag{8.13}$$

A computer procedure was developed to evaluate the Legendre polynomial coefficients using Eq. (8.1). The portion of the MIE-II program (Ref. 20) which calculates the Mie scattering functions A_n and B_n was incorporated into the program. The Legendre polynomial coefficients computed for several aerosol sizes were used to expand the Legendre polynomials and those expansions compared with the phase functions computed for the same sized aerosols with the MIE-II program. These comparisons indicate the Legendre polynomial coefficients computed give an accurate definition of the phase function. The length of the Legendre coefficient array (a_n) necessary to represent the phase function appears to be on the order of $2\alpha+2$ where $\alpha = 2\pi r/\lambda$ is the aerosol size. Clouds typically have aerosols up to 20 to 30 microns in radius; thus, for 0.5-micron wavelength light the size parameter could be as large as 375 requiring a Legendre polynomial of the order of 752.

Since the phase function for an aerosol size distribution generally has less structure than those for the individual aerosols, the number of combined coefficients for an aerosol size distribution possibly will not need to be as high as that required for the individual size parameters.

REFERENCES

1. D. G. Collins and M. B. Wells, A Study of Thermal Radiation Propagation in the Atmosphere, Radiation Research Associates, Inc. Technical Report RRA-T7011 (August 1970)

2. R. M. McClatchey, Air Force Geophysics Laboratory, private communication

3. J. K. Warkentin and M. B. Wells, A Study of Thermal Radiation Propagation and Detection Capability, Radiation Research Associates, Inc. Technical Report RRA-T7301 (January 1973) (S)

4. S. A. Dupree, et al., Time-Dependent Neutron and Photon Transport Calculations Using the Method of Discrete Ordinates, Los Alamos Scientific Laboratory Report LA-4557 (1970)

5. M. B. Wells, The Effects of Gaseous Absorption and Ground Reflection on Infrared Radiation Fluxes at Satellite Based Receivers, Radiation Research Associates, Inc. Report RRA-M7501 (1975)

6. J. E. A. Selby, Atmospheric Transmittance from 0.25 to 28.5 μm: Computer Code LOWTRAN3, Air Force Cambridge Research Laboratories Report No. AFCRL-TR-75-0255 (1975)

7. W. G. M. Blättner and M. B. Wells, Sky Radiance Calculations in the 0.5 μm - 5.0 μm Wavelength Range, Radiation Research Associates, Inc. Technical Report RRA-T7501 (1975)

8. U. S. Standard Atmosphere Supplements, 1966, U. S. Government Printing Office (1966)

9. J. E. A. Selby and R. M. McClatchey, Atmospheric Transmittance from 0.25 to 28.5 μm: Computer Code LOWTRAN2, Air Force Cambridge Research Laboratory Report AFCRL-72-0745 (1972)

10. M. L. Vatsia, Atmospheric Optical Environment, U. S. Army Electronics Command Report ECOM-7023 (1972)

11. R. J. List, Smithsonian Meteorological Tables, Smithsonian Institution, Washington, D.C. (1966)

12. L. Elterman, R. B. Toolin, and J. D. Essex, "Stratospheric Measurements with Implications for Global Climate," Appl. Opt. 12, No. 2 (1973)

REFERENCES (Continued)

13. W. G. Blättner, FLASHI, 1975, Radiation Research Associates, Inc. Research Note RRA-N7505 (1975)

14. J. K. Warkentin and M. B. Wells, A Study of Thermal Radiation Propagation in the Atmosphere, Vol. I: Monte Carlo Transport Calculations (U), Radiation Research Associates, Inc. Technical Report RRA-T7401 (1974) (S)

15. U. S. Standard Atmosphere, 1962, U. S. Government Printing Office (1962)

16. L. Elterman, UV, Visible and IR Attenuation for Altitudes to 50 km, 1968, Air Force Cambridge Research Laboratory Report AFCRL-68-0153 (1968)

17. D. Deirmendjian, Am. Geophys. 15, 218-249 (1959)

18. R. M. McClatchey, et al., Optical Properties of the Atmosphere (Third Edition), Air Force Cambridge Research Laboratory Report AFCRL-72-0497 (1972)

19. Phillips Taylor, Theory and Application of Numerical Analysis, Academic Press, London (1973)

20. Wolfram G. M. Blättner, Utilization Instructions for the Downward Recursion Version of the MIE-2 Program, Radiation Research Associates, Inc. Research Note RRA-N7603 (1976)

21. D. Deirmendjian, Electromagnetic Scattering on Spherical Polydispersions, Elsevier, New York (1969)

22. W. Irvine and J. Pollack, "Infrared Optical Properties of Water and Ice Spheres," Icarus (1967)

23. C. M. Chu and S. W. Churchill, J. Opt. Soc. Am. 45, 958 (1955)

24. G. C. Clark, C. M. Chu, and S. W. Churchill, J. Opt. Soc. Am. 47, 81 (1957)

DISTRIBUTION

No of Copies	
	DOD AGENCIES
2	Director Defense Nuclear Agency ATTN: RAAE Technical Library
1	Director Defense Intelligence Agency ATTN: Technical Library
12	Defense Documentation Center ATTN: Document Control
	ENERGY RESEARCH AND DEVELOPMENT ADMINISTRATION
3	Los Alamos Scientific Laboratory ATTN: J-10 (Dr H. Horak) J-10 (Dr Guy Barasch) TD-3 (Dr Bob Henson)
1	Sandia Laboratories ATTN: Bob Bradley
1	Lawrence Livermore Laboratory ATTN: Technical Library
1	Oak Ridge National Laboratory ATTN: Technical Library
1	EG&G, Inc. Los Alamos NM ATTN: Dr C. Mitchell
	DEPARTMENT OF THE ARMY
2	US Army Waterways Experiment Station-Mobility and Environmental System Lab ATTN: Dr L. E. Link Dr Warren Grabau
3	US Army Electronics Command Atmospheric Sciences Laboratory ATTN: Dr M. L. Vatsia Dr Jerry Lentz Dr Richard Gomez
	DEPARTMENT OF THE NAVY
1	Naval Research Laboratory ATTN: Technical Library
	DEPARTMENT OF THE AIR FORCE
2	AF Geophysics Laboratories ATTN: OPR (Mr H. Gardiner) OPA (Dr R. Fenn)
1	AF Institute of Technology ATTN: Library
2	AF Weapons Laboratory ATTN: Dr Joe Janni Dr C. Needham
1	Space and Missile Systems Organization ATTN: SZS (Maj H. Hayden)
2	AF Technical Applications Center ATTN: TFR (Capt J. Lange)
	DOD CONTRACTORS
1	Aerospace Corporation ATTN: Dr R. D. Rawcliffe
1	General Electric Company-TEMPO ATTN: DNA Information and Analysis Center

No of Copies	
1	Lockheed Missiles and Space Company ATTN: Technical Library
1	Visidyne, Inc. ATTN: Dr J. Carpenter
1	Mission Research Corporation ATTN: Technical Library
1	Science Applications, Inc. ATTN: Dr R. Hillendahl
1	HSS, Inc. ATTN: Dr H. Stewart
10	Radiation Research Associates ATTN: M. B. Wells